# 博士論文

**Development of polymeric nanocarriers loading mRNA for *in situ* generation of chimeric receptors on immune cells against cancer**

**(**がんに対するキメラ抗原受容体を発現する免疫細胞の生体内創製に向けた mRNA 搭載高分子ナノキャリアの構築)

**Mixich Lucas**

**ミクスィヒ ルカス**

# Contents

# Chapter 1.

# General Introduction

## 1.1 Immunotherapy as a cancer treatment strategy

Cancer immunotherapy has emerged as a revolutionary approach in cancer treatment, shifting the focus from traditional methods such as surgery, chemotherapy, and radiotherapy (Shi et al. 2018). It has become a pivotal component in cancer care, spanning from metastatic stages to adjuvant and neoadjuvant settings across various cancer types(Esfahani et al. 2020). However, the broad implementation of immunotherapies faces challenges, as these therapeutics can lead to serious adverse effects, including autoimmunity and nonspecific inflammation (Riley et al. 2019). Despite these challenges, cancer immunotherapy has shown remarkable success in the treatment of different cancer types, particularly through checkpoint inhibitor-based immunotherapies targeting cytotoxic T lymphocyte antigen 4 (CTLA4) or the programmed cell death 1 (PD1) pathway (Havel, Chowell, and Chan 2019), or the use of adoptive T cell therapy with chimeric antigen receptors (CARs) targeting cancer antigens like CD19, that revolutionized the treatment of advanced acute lymphoblastic leukemia and diffuse large B-cell lymphoma (Kamel 2021).

CAR-T cell therapy has shown significant progress in hematological malignancies by harnessing the cytotoxic potential of T cells against cancer cells. The modification of T cells to express cancer-specific CARs involves the transduction of T cells with genes encoding the CAR construct. Upon binding to the cancer antigen, CAR T cells release a large number of cytokines, such as interferon-γ (IFN-γ), and tumor necrosis factor-α (TNF-α) This cytokine release is a crucial part of the immune response and contributes to the killing of cancer cells (Yu et al. 2019; Fitzgerald et al. 2017). However, the efficacy of CAR-T cells against solid tumors has been more limited (Sterner and Sterner 2021; Pan et al. 2022).

In addition to T cells, other immune cell types such as macrophages have been explored in cancer immunotherapy. CAR macrophages share many features and hurdles with CAR T cells, however, CAR macrophages possess unique advantages over CAR T cells on two other

major hurdles in solid tumors: immune cell trafficking and infiltration into the tumor microenvironment (TME), and the immunosuppressive nature of the TME (Pan et al. 2022). In contrast to T cells, infiltration of macrophages at the TME is common due to many cytokines secreted at the tumor sites. Hypoxia in solid tumors induces tumor cells and stroma to produce cytokines, such as CCL2 (C–C motif chemokine ligand 2), CXCL12 (C-X-C Motif Chemokine Ligand 12), CSF1 (Colony Stimulating Factor 1) and VEGF to recruit macrophages (Henze and Mazzone 2016).The tumor microenvironment plays a crucial role in cancer progression and response to therapy. Chemokines, in particular, are key players in the TME, regulating immune cell recruitment and affecting cancer immunity and tumorigenesis (Nagarsheth, Wicha, and Zou 2017). The expression and activity of chemokines within the TME have been associated with cancer outcomes, making them potential targets for cancer immunotherapy (Vilgelm and Richmond 2019).

Cancer immunotherapy has significantly advanced in recent years, offering a diverse range of strategies and approaches that hold great promise for the treatment of various types of cancer. The success of cancer immunotherapy lies in its ability to stimulate the body's innate or adaptive immune system to combat tumors, making it an effective strategy for cancer treatment. However, the clinical application of immunotherapy for cancer patients still faces challenges associated with safety and efficacy, including autoimmune reactions, off-targeting, tumor penetration, and cytokine release syndrome (Z. Zhao et al. 2019).

## 1.2 Chimeric antigen receptor (CAR) T cells

Chimeric antigen receptor (CAR) T-cell therapy has revolutionized cancer treatment, particularly in hematologic malignancies, by harnessing the power of the immune system to target and eliminate cancer cells. CAR T cells are genetically engineered to express synthetic receptors that specifically recognize antigens present on cancer cells, thereby initiating a targeted immune response. Among the various CAR T-cell therapies, anti-CD19 CAR T cells have demonstrated remarkable efficacy in treating B-cell malignancies.(Kochenderfer et al. 2015; Rosenberg and Restifo 2015; Yip and Webster 2018).

The structure of the CAR protein is a critical determinant of its functionality and therapeutic efficacy in CAR T-cell therapy. The CAR protein typically comprises distinct domains that facilitate targeted recognition and activation of T cells against cancer cells (**Figure 1.1** right). The extracellular domain of the CAR protein commonly includes a single-chain variable fragment (ScFV) derived from an antibody, enabling specific recognition of tumor antigens (Johnson et al. 2015). This recognition domain is essential for directing the CAR T cells towards the targeted cancer cells. Additionally, the intracellular domain of the CAR protein incorporates CD3ζ signaling motifs which contain immunoreceptor tyrosine-based activation motifs (ITAM) to transmit the primary signal during TCR engagement, and costimulatory domains like 4-1BB or CD28, which are crucial for T cell activation and proliferation upon antigen binding (Weinkove et al. 2019). The CD28 domain is used by the FDA-approved axicabtagene ciloleucel and brexucabtagene autoleucel, both targeting CD19. The 4-1BB signaling domain is used by the approved CD19-targeting lisocabtagene maraleucel and tisagenlecleucel, and by idecabtagene vicleucel which targets B cell maturation antigen (BCMA) (Pan et al. 2022). The structural design of the CAR protein is meticulously engineered to optimize its specificity, affinity, and signaling capacity, thereby enhancing the anti-tumor activity of CAR T cells (Srivastava and Riddell 2015).

Currently, all clinically approved CAR T cell therapies are based on ex-vivo engineering of CAR T cells. However, the costs and complex personalized procedures for producing targeted immune cells remain major obstacles for the widespread implementation of CAR T-cell therapy as a standard-of-care in cancer treatment. Clinical-scale manufacturing of CAR T lymphocytes is personalized and involves several protocols to isolate, genetically modify, and selectively expand the redirected cells before infusing them back into the patient (**Figure 1.1** left) (Levine et al. 2017).

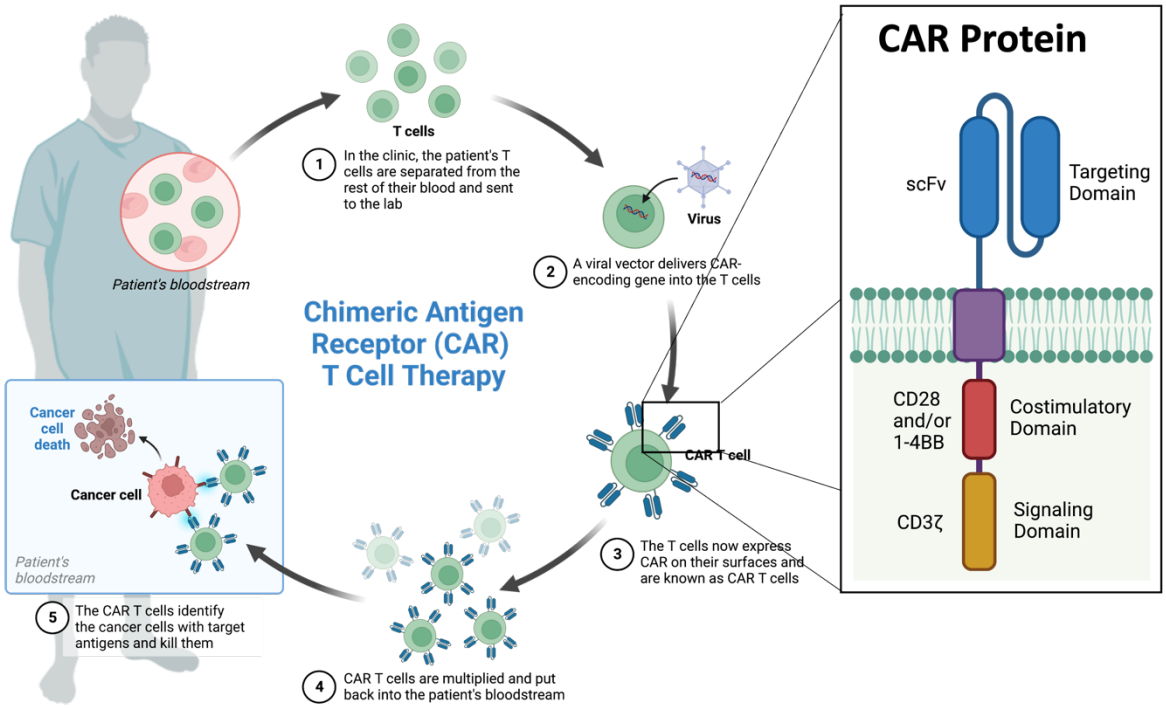


**Figure 1.1** Current CAR T cell therapy. Current T cell therapy includes several steps of collecting patient's T cells, transfecting them with CAR genes ex vivo, expanding and re-introducing CAR T cells into the patient's bloodstream to kill cancer.

For this reason, there has been a surge of groups eagerly trying to develop in situ solutions for CAR T cell generation. Many of these approaches center around the use of viral vectors for

gene delivery. Notably, companies such as EXUMA Biotech and Umoja Biopharma are actively engaged in the development of viral gene delivery systems for CAR T cell expression, exemplified by EXUMA Biotech's in vivo CAR/TCR therapy platform (GCAR) and Umoja Biopharma's VivoVec surface-engineered LV vector-based off-the-shelf viral-vector particles for the generation of CAR-T cells in vivo (Umoja Biopharma, n.d.; Challener 2023).

However, the use of viral delivery in vivo has raised significant concerns regarding inflammatory responses. Of particular concern is the potential for innate immune responses against viral vectors, especially in the context of repeated administration using mRNA. Additionally, a 10-year follow-up study in dogs revealed stable integration of vector genomes into the host genome, reigniting concerns about the potential for oncogenic integration of adeno-associated virus (AAV) (Bulcha et al. 2021). These findings underscore the need to explore non-viral delivery methods for mRNA, given the potential risks associated with viral vectors.

Despite the success of CAR T cell therapy, one of its major limitations is its restricted penetration into solid tumors. The immunosuppressive tumor microenvironment significantly impedes the function and persistence of CAR-T cells within the tumor site (Maalej et al. 2023). Furthermore, the extracellular matrix forms physical obstacles that preclude sufficient infiltration of CAR T cells into solid tumors, inhibiting their approach and recognition of tumor cells (H. J. Li et al. 2021; Pan et al. 2022). Moreover, the immunosuppressive tumor microenvironment and the lack of effective chemokines for inducing CAR-T tropism in the tumor tissues contribute to poor CAR-T infiltration into solid tumors (Hu et al. 2022).

## 1.3 Chimeric antigen receptor macrophage (CAR-M) therapy

CAR macrophages (CAR-M) have been developed as a novel cell therapy approach for the treatment of solid tumors. They have shown potent anti-tumor activity in pre-clinical solid tumor models (Blumenthal et al. 2021). CAR-Ms have the potential to overcome key challenges faced by cell therapies in the solid tumor setting, such as tumor infiltration, immunosuppression, lymphocyte exclusion, and target antigen heterogeneity (Ohtani et al. 2020). Macrophages are the most prominent type of phagocyte in the immune system and form several subpopulations with specialized roles. M1 macrophages are effector cells of pathogen and tumor defense. Macrophages are capable of killing target cells *via* phagocytosis (Velmurugan et al. 2016; Klichinsky et al. 2017; Morrissey et al. 2018) and MHC-II presentation of antigens, as well as the secretion of cytokine and effector molecules (Chanmee et al. 2014; Curren Smith 2015).

However, macrophages infiltrating tumors in large numbers are referred to as tumor-associated macrophages (TAMs), which can make up 50% of tumor mass (Murdoch, Giannoudis, and Lewis 2004). They lose their capability to migrate and to lyse tumor cells and the presence of high numbers of TAMs is associated with poor clinical prognosis (Bingle, Brown, and Lewis 2002). The high prevalence of macrophages in solid tumors makes them a promising vehicle for CAR therapy, provided that the suppressive tumor microenvironment, consisting of tumor-associated macrophages, myeloid-derived suppressor cells, and regulatory T cells, can be overcome (Klichinsky et al. 2017; Murad et al. 2021). The CAR enhances the secretion of cytokines of TAMs, polarizes TAMs to the inflammatory/anti-tumor M1 type, and enhances the phagocytic function of TAMs and the activity of anti-tumor cells in vivo (Zhang et al. 2020; M. Li et al. 2022). However, identifying robust non-viral methods of macrophage engineering is essential to reduce cost, manufacturing complexity, and potential inflammatory responses associated with viral vectors, (Pan et al. 2022) highlighting the need for innovative

delivery systems for effective macrophage-based immunotherapy.

### 1.4 Chemokine based treatments

Adoptive T cell therapy (ACT) and chimeric antigen receptor (CAR) T cell therapy have significantly advanced cancer treatment. However, their efficacy in addressing solid tumors is limited due to challenges in penetrating the tumor microenvironment (TME), inefficient trafficking, and poor local persistence in tumor tissue (Akbay et al. 2017). To improve the immune cell infiltration and cancer prognosis of solid tumors, strategies to enhance immune cell penetration into the TME are urgently needed. One emerging strategy involves modifying immune cells to overexpress chemokine receptors on their surface, which can improve their migration toward chemotactic gradients within the TME. (Kohli, Pillarisetty, and Kim 2022) ( **Figure 1.2**).

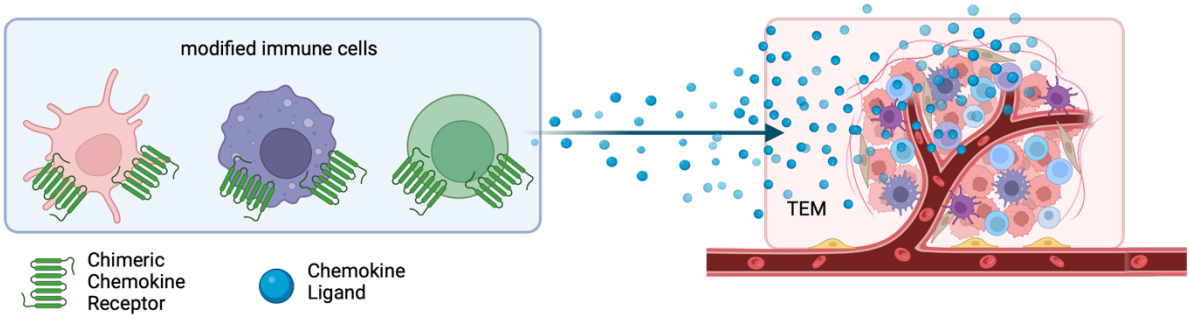


**Figure 1.2** Chemokine modified immune cells can guide effector immune cells to the tumor microenvironment by chemotaxis based on chemokine ligand concentration gradients.

Chemokines, a group of small proteins, play a crucial role in guiding the migration of immune cells within the TME. They are classified into four main classes based on the location of the first two cysteine (C) residues in their protein sequence: CC, CXC, C, and CX3C chemokines. Most chemokine receptors are transmembrane-spanning heterotrimeric G-protein-coupled receptors, and their binding to cognate chemokines induces G-protein coupling and subsequent activation of downstream signaling proteins involved in cell migration, such as

Rac, Rho, and Cdc42. (Schulz et al. 2016) The infiltration of immune cells in the TME is a key factor in cancer prognosis, and chemokines play an essential role in guiding the migration of both activating and suppressive immune cell types. (Barnes and Amir 2017; Burugu, Asleh-Aburaya, and Nielsen 2017; Ladányi 2015)

Of particular interest is the chemokine receptor CXCR4, which has been shown to guide immune cells to tumors. For instance, natural killer (NK) cells genetically engineered with a CAR to overexpress CXCR4 along with the target antigen receptor demonstrated enhanced mobilization towards CXCL12 (stromal cell-derived factor 1, SDF-1) (Müller et al. 2015). CXCL12 is a key chemokine present in the TME and has been implicated in attracting immune cells expressing its receptor, CXCR4. Moreover, high expression of CXCL12 has been associated with poor prognosis in cancer, as it directly activates various responses through the CXCL12/CXCR4 pathways, such as cell migration, survival, and proliferation (Lang et al. 2019). Additionally, CXCL12 has been linked to promoting tumor vascularization by recruiting endothelial cells to the TME (Kryczek et al. 2007)

Utilizing CXCL12 to guide immune cells, such as cytotoxic T cells or M1 type macrophages, to the tumor and increase immune cell penetration into solid tumors represents a promising strategy to address the current limitations of adoptive immune cell therapy. This approach holds potential for improving the efficacy of ACT and CAR T cell therapy in treating solid tumors. Further research and clinical studies are warranted to explore the full potential of this strategy in cancer treatment.

## 1.5 Nucleic acid delivery in immunotherapy

mRNA-based CAR T cell therapy has emerged as an encouraging approach to improve the safety profile of CAR T cell therapy and reduce the risk of side effects. Traditional CAR T cell therapy has been associated with severe systemic toxic effects, including cytokine release syndrome and neurotoxicity, particularly in patients with high disease burden (Brown et al. 2016). However, *in vitro* transcribed mRNA CAR T cells offer a safer alternative by transiently reprogramming T cells with mRNA that encodes chimeric membrane antigen receptor protein against tumor-specific antigens, thereby circumventing on-target off-tumor toxicity ((Rajan, Bramanti, and Mazzon 2020). Furthermore, mRNA-based CAR T cells have shown potential in reducing short-term disease burden as effectively as virally engineered CAR T cells, indicating their efficacy in cancer treatment (Billingsley et al. 2021).

The transient expression of CARs in mRNA CAR T cells serves as a platform to evaluate the safety of CAR T directed against tumor antigens in clinical trial settings, thereby avoiding potential unrelenting on-target off-tumor effects of stably transduced CAR T cells (Tchou et al. 2017; Y.-H. Chen, Jiang, and Lee 2023). Moreover, mRNA-based CAR T cells may mitigate potential off-target toxicity due to their transient expression (Foster et al. 2021). Additionally, mRNA-based CAR expression may offer a means to modulate side effects such as cytokine release syndrome associated with CAR T cell therapy, thus improving the safety profile of the treatment (Billingsley et al. 2020; Fitzgerald et al. 2017).

The current state of non-viral in-situ mRNA-based technologies for generating chimeric T cells is characterized by limited reports and ongoing research efforts to address existing challenges. Rurik, J.G. et al. recently demonstrated a promising outcome in treating cardiac injury in mice by delivering mRNA to T cells using lipid nanoparticle (LNP) technology (Rurik et al. 2022). However, it is important to note that LNPs have been associated with drawbacks such as toxicity (Ndeupen et al. 2021), inflammatory responses, and off-target effects (Di et al.

2022; Carrasco et al. 2021), which may limit their suitability for in-situ CAR T cell therapy (Bessis, GarciaCozar, and Boissier 2004; Zhou et al. 2017).

Polymeric nanocarriers have the potential to minimize toxicity and allow for precise manipulation of their chemical properties to facilitate targeted delivery (Yang, Mixich, et al. 2023; Cabral et al. 2018). Within this category, polyion complex (PIC) micelles, employing block copolymers comprising a hydrophilic neutral segment and a polycationic block, present adjustable physicochemical characteristics, surface modification capabilities, and biocompatibility, thereby enhancing delivery efficiency (Jarak et al. 2021).

## 1.6 Polyion complex (PIC) micelles

Polymeric micelles are a promising platform for the delivery of nucleic acid cargo, such as mRNA, due to their ability to provide charge shielding, improved colloidal stability, and efficient self-assembly. These micelles consist of block copolymers, typically containing a neutral hydrophilic block, such as poly(ethylene glycol) (PEG), for charge shielding and improved colloidal stability, in addition to a block that loads the cargo (Cabral et al. 2018). The block responsible for loading the nucleic acid cargo usually contains cationic charges, enabling self-assembly by simply mixing negatively charged nucleic acid with the partially charged block ionomer (Kataoka, Harada, and Nagasaki 2001). The resulting polyion complex (PIC) micelle exhibits a core-shell structure with the mRNA cargo loaded on the inside and shielded by a PEG shell (Uchida et al. 2013; Q. Chen et al. 2017).

To further enhance the stability and efficacy of polymeric micelles for nucleic acid delivery, the polymers can be modified with thiol groups for crosslinking or hydrophobic moieties to improve stability in biological environments, highlighting the flexibility of polymer-based nucleic acid delivery systems (Dirisala et al. 2019). Previous research has also emphasized the critical role of chain flexibility in polymeric carriers for stabilizing mRNA into nanosized micelles (Miyazaki et al. 2020). This suggests that using a block ionomer with a flexible backbone, such as PEG-poly(glycidyl), for self-assembly into PIC micelles may be a promising approach to ameliorate the delivery of mRNA, which is still hindered by challenges of safely and efficiently stabilizing the RNA cargo.(Yang, Miyazaki, et al. 2023)

Increasing the interactions between the PIC micelle and the mRNA, including design elements to promote π-π-stacking between mRNA and the carrier are another option to increase the micelle's stability. π-π-stacking interactions between proteins and nucleobases in RNA have been widely reported (Wilson, Holland, and Wetmore 2016; Wilson et al. 2021; Sivasakthi, Anbarasu, and Ramaiah 2013). The advanced stability and mRNA delivery due to π-π

interactions have been demonstrated with tyrosinated polymeric carriers (Yang, Miyazaki, et al. 2023). Among amino acids, phenylalanine (Phe) amino acid in proteins was found to be a major contributor to the interaction with RNA *via* π-π-stacking interactions. Indeed, the studies assigned nearly half (45 %) of the interactions between proteins and RNA to Phe, and found that more than 60% of Phe in proteins engage in π-π-stacking with RNA. For that reason, carriers with Phe have been discovered to engage in strong interactions with RNA, and were able to load large-sized self-replicating (RepRNA) in their cores (Mixich, Boonstra, et al. 2024).

In addition to stability and cargo loading, the escape of the carrier from the endosomal compartment after cellular uptake is a major challenge for non-viral delivery systems (Varkouhi et al. 2011; Kargaard, Sluijter, and Klumperman 2019; Rehman, Zuhorn, and Hoekstra 2013). Outstanding endosomal escape has been linked to improved cellular gene delivery efficacy, as evidenced by research on delivery systems utilizing block copolymer poly(ethyleneglycol)-b-poly(N-N-(2-aminoethyl)-2-aminoethyl-aspartamide) (PEG−PAsp(DET)). These systems have demonstrated the ability to induce membrane destabilization at pH 5.5 while showing minimal effects at pH 7.4. The pH-selective endosomal membrane destabilization has played a crucial role in the successful application of these systems for gene delivery, leading to enhanced transfection and minimal cytotoxicity (Yang, Mixich, et al. 2023).

Furthermore, the targeted delivery of mRNA to immune cells presents a major challenge due to the hard-to-transfect nature of immune cells. Overcoming these challenges is crucial for the successful in-situ delivery of mRNA to immune cells. In conclusion, polymeric micelles offer a versatile platform for nucleic acid delivery, with the potential to address challenges related to stability, cargo loading, and targeted delivery. Further research into the design and modification of block copolymers for self-assembly into PIC micelles, as well as strategies to enhance endosomal escape and immune cell targeting, will be essential for advancing the field of mRNA delivery for immunotherapy and other applications.

## 1.7 Targeting ligands

Ligand-installed nanocarriers are constructed based on the affinity between the ligands and receptors on target cells. The identity of unique receptors on target cells and the corresponding ligand provide the molecular basis of "recognition-binding" functions for targeting nanocarriers. Through ligand-receptor interactions, the system can deliver mRNA to certain types of cells or tissues (Deshayes et al. 2013), promote cellular uptake by receptor-mediated endocytosis (Oyewumi et al. 2004) and they can modulate signaling pathways (Allen 2002; Kanapathipillai, Brock, and Ingber 2014). Certain ligands can even improve intracellular delivery after cell uptake by facilitating endosomal escape, a critical step for the successful translation of mRNA after endocytosis (**Figure 1.3**) (Mi, Cabral, and Kataoka 2020a; Houseley and Tollervey 2009).

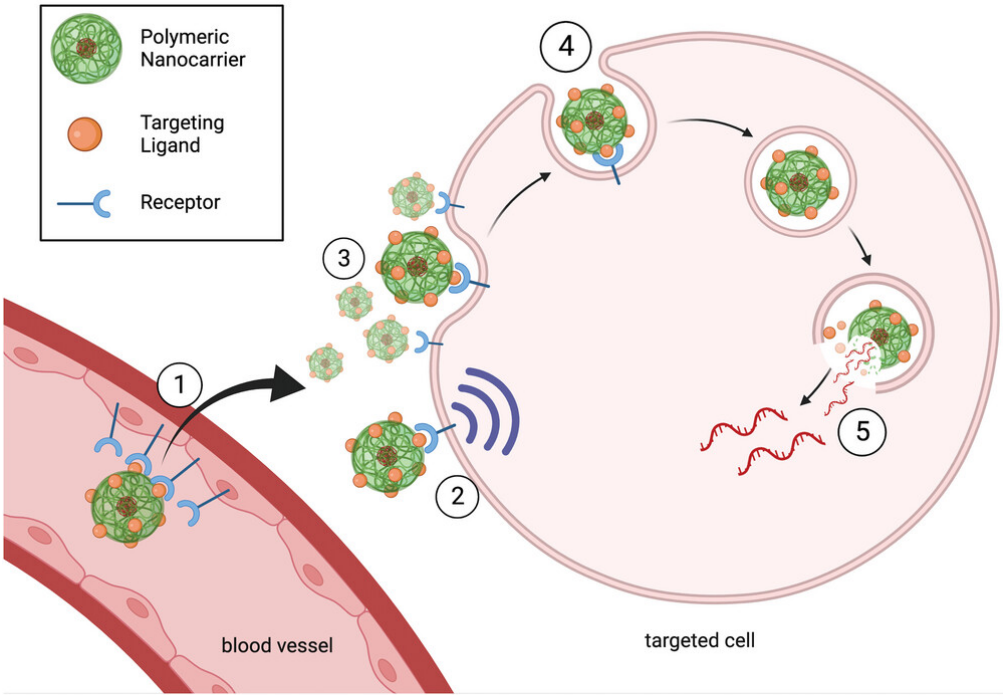


**Figure 1.3** Ligand mediated cell uptake. 1) Active ligand-mediated transport through blood vessels. 2) Ligand-mediated cell signaling 3) Ligand-mediated retention on cell surface. 4) Ligand-mediated endocytosis. 5) Endosome escape through ligand interactions.

T-cell therapy aims to reprogram cytotoxic T cells in our immune system to recognize

and kill diseased cells. But T cells are known to be hard to transfect and besides physical transfection methods, targeted delivery is usually necessary to accomplish meaningful transfection efficiencies. CD8 and CD3, which are expressed on the surface of T cells, are commonly targeted to direct and internalize nanoparticles into T cells (Moffett et al. 2017; N. N. Parayath et al. 2020). Moffett et al. demonstrated that programing T-cells ex vivo through a CD3-targeted PBAE-based mRNA polyplex can express genome-editing agent in anti-cancer T-cells. However, CD3 antibodies might also trigger cellular responses leading to T-cell anergy and immunosuppression (Wolf et al. 1994). Parayath et al. electrochemically adsorbed CD8 antibody fragments on PBAE polymer loading mRNA to initiate rapid receptor-induced endocytosis and deliver mRNA to T-cells (N. N. Parayath et al. 2020). However, the conjugation of full antibody may accelerate the clearance of antibody-installed nanocarriers from blood circulation, as the Fc region would facilitate their recognition by immune cells and the reticuloendothelial system (RES). To circumvent these issues, antibody fragments, i.e., the binding sites without the Fc fragment, were proposed as targeting moieties. The most frequently used anti-body fragments for nanocarriers are the Fab (≈50 kDa) (Mi, Cabral, and Kataoka 2020a).

Similarly, the uptake of other immune cells, such as macrophages can be improved by targeting ligands targeting moieties overexpressed on those immune cells. Targeting macrophages or dendritic cells with mannose targeting ligands has been the subject of extensive research due to the potential applications in antigen delivery and immune modulation. Mannose receptors, which are expressed on the surface of macrophages and dendritic cells, have been identified as key targets for ligand-mediated uptake of antigens (Lane et al. 1998; White et al. 2006; Ni, Singh, and Wang 2002; Thalla et al. 2020). The active targeting approach using mannosylated ligands has been explored to target the mannose receptor on the surface of macrophages, in addition to passive targeting (Fukuda, Mochizuki, and Sakurai 2015). The use

of mannose as a targeting moiety has been incorporated into various delivery systems, such as cationic albumin and solid lipid nanoparticles, to achieve macrophage targeting delivery of immunostimulatory agents (Shinchi et al. 2021). Overall, the extensive body of research supports the potential of targeting macrophages and dendritic cells with mannose targeting ligands for antigen delivery, immune modulation, and gene delivery applications.

## 1.8 Overview of this dissertation

The primary objective of this research was to develop a novel mRNA delivery platform for the in situ generation of chimeric immune cells for cancer therapy (**Figure 1.4**). The study aimed to capitalize on the unique advantages offered by RNA-based non-viral nanoparticles with targeting ligands while addressing challenges related to stability in physiological milieus and targeted delivery to hard-to-transfect immune cells. To achieve this, the research utilized anti-CD19 CAR and Chemokine mRNAs, along with a novel PEG-poly(glycidyl)-based polymeric carrier modified with phenylalanine to enhance stability and improve endosomal escape. Additionally, targeting ligands such as anti-CD8 Fab' and mannose were employed to facilitate enhanced and targeted delivery to $CD8^+$ cytotoxic T cells and macrophages for the *in situ* generation of chimeric receptors on immune cells.

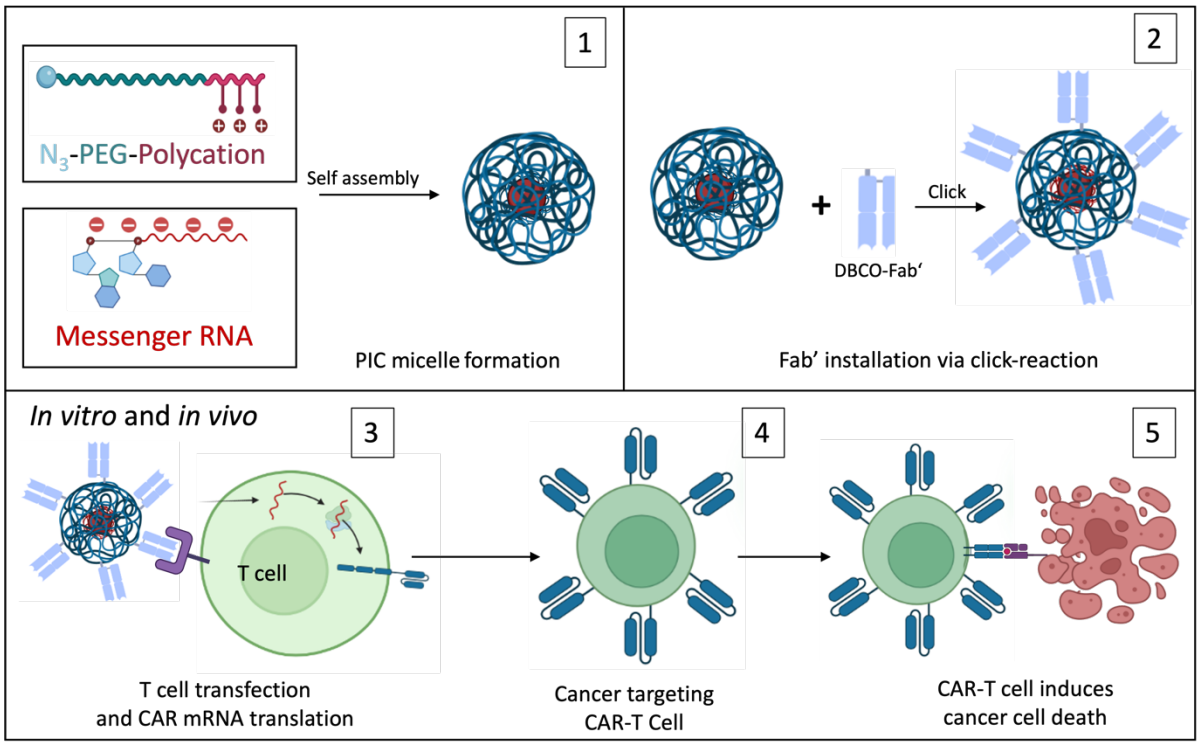


**Figure 1.4** Research layout. 1) Formation of PIC micelles by mixing block-copolymers with a polycationic block with mRNA encoding the protein for chimeric antigen receptors (CARs) against cancer. 2) Installing anti-CD8 Fab' targeting ligands on the surface of the micelles *via*

click reaction. 3) Targeted delivery of the mRNA to T cells and expression of CAR-protein and produce 4) cancer targeting CAR T cells *in situ*. 5) CAR T cells induce dell death of cancer cells.

Chapter 2 focuses on the in silico design of anti-CD19 CAR encoding plasmid at the DNA level, followed by the preparation and characterization of the plasmid DNA. Chapter 3 centered on the preparation and characterization of the polymer, the condensation of mRNA into nanosized micelles using this polymer, and the assessment of the system's efficacy in terms of uptake, endosome escape, and protein expression. Chapter 4 investigates targeting ligands for different immune cells, their installation on the surface of the nanoparticle, and evaluates their effectiveness in transfecting targeting cells *in vitro*. Chapter 5 analyzes the generation of functional anti-CD19 CAR T cells, the effective expression of CXCR4 on immune cells, and their impact *in vitro* and *in vivo* in cancer models. Finally, Chapter 6 provides a comprehensive conclusion and offers insights into potential future research directions to address remaining challenges and further enhance the current system.

# Chapter 2.

# Design and Synthesis of mRNAs

## 2.1 Introduction

mRNA for clinical applications is synthesized using *in vitro* transcription (IVT) with a DNA template containing the appropriate promoter sequence for RNA polymerases derived from bacteriophages such as SP6 or T7. The template DNA used generally consists of a linearized piece of plasmid DNA containing a polymerase promoter upstream of the desired sequence and is used to produce run-off transcripts with the compatible RNA polymerase. mRNA typically requires 5' cap and 3' poly(A) structures to be efficiently translated in the cytosol. The poly(A) can be added enzymatically or can be incorporated directly into the plasmid DNA. The 5'cap can be added co-transcriptionally or in a separate step using a capping enzyme derived from the vaccinia virus. Purification can be done in several ways, including precipitation, affinity-based columns, and chromatography methods (Pascolo 2004; Geall, Mandl, and Ulmer 2013; Weissman et al. 2013)

Chimeric antigen receptors (CARs) are designed to be expressed on immune cells and generally consist of intracellular and extracellular domains. Extracellular domains most commonly consist of single-chain variable fragments (scFvs) with high affinity and specificity to the target antigen. CD19 is an appealing target for immunotherapy because it is uniformly expressed by the vast majority of B-cell malignancies and has been successfully implemented in CAR T cell treatments. The 1D3 hybridoma from ATCC produces an IgG2aκ antibody that specifically recognizes murine CD19. The variable regions of this hybridoma can be used for CAR T cell therapy (Kochenderfer et al. 2010). Intracellular domains consist of signaling domains delivered through TCR/CD3ζ and co-stimulatory domains, such as CD28 or 4-1BB, essentially reproducing the checkpoints of T cell activation (Srivastava and Riddell 2015) on T cells, both of which are provided only by activated APCs.

In this chapter, a T7-anti-CD19 CAR plasmid is designed in silico and generated using a ligation reaction. The source plasmid containing a T7 promoter sequence encoding for Gluc is

digested with restriction enzymes and the desired coding sequence encoding anti-CD19 CAR protein that can specifically recognize murine CD19 is generated *via* PCR with necessary overlaps of restriction enzymes to generate complementary sticky ends (**Figure 2.1**). The identity of the resulting plasmid is checked using restriction digestion and Sanger sequencing and used as a template for *in vitro* transcription (IVT) to generate anti-CD19 CAR mRNA. Template DNA containing Gluc and chemokine receptor 4 with turbo-GFP (CXCR4-tGFP) were also synthesized by IVT. To confirm the successful synthesis, the resulting mRNAs are analyzed by capillary gel electrophoresis.

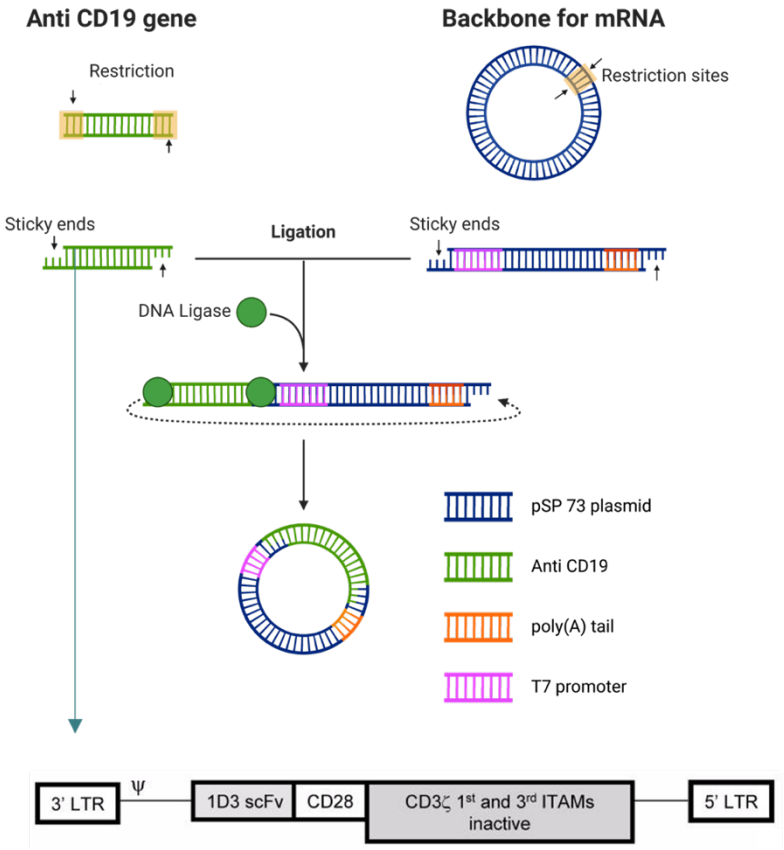


**Figure 2.1** The desired anti-CD19 CAR sequence is amplified using PCR with primers including restriction sites complementary to the backbone pSP73.pA-Gluc plasmid, and digested *via* restriction digestion. The backbone containing a T7 polymerase promoter, poly(A), and Gluc sequences is digested to remove the Gluc sequence and to create sticky ends. The two fragments are combined *via* T4 DNA ligation.

## 2.2 Materials and methods

### *2.2.1 Materials*

Sodium acetate buffer (pH 4.5), Dulbecco's Phosphate-Buffered Saline (D-PBS), and sodium hydroxide (NaOH), were purchased from Fujifilm Wako Pure Chemical, Co., Inc. (Osaka, Japan). 1 M HEPES buffer pH 7.4, was purchased from Cambridge Isotope Laboratories, Inc. (Massachusetts, USA). MSGV1-1D3-28Z.1-3 mut anti-CD19 CAR plasmid was purchased from Addgene (Watertown, MA, U.S.A.). All restriction enzymes, T4 DNA Ligation Kit, Stellar chemically competent E. coli cells and the CloneAmp HiFi PCR premix were obtained from Takara Bio (Shiga, Japan). The mMESSAGE mMACHINE T7 Ultra Kit and Luria-Bertani (LB) broth were purchased from Thermo Fisher Scientific (Waltham, MA, U.S.A). NucleoSpin Plasmid kit and the NucleoBond Xtra Maxi kit were purchased from Macherey Nagel (Düren, Germany). RNeasy Mini kit was obtained from Qiagen (Hilden, Germany), PCR primers were purchased from FASMAC Inc. (Kanagawa, Japan). The pSP73.pA-Gluc plasmid DNA was kindly gifted by Dr. Eger Boonstra.

### *2.2.2 Plasmid amplification with competent E coli. cells*

Stellar chemically competent E. coli cells (Takara Bio, Shiga, Japan) were thawed on ice. 50 µl cell suspension was transformed with 1 ng plasmid DNA solution by heat shocking at 42 °C for precisely 45 seconds. Cells were recovered in 500 µl SOC medium at 37 °C for 1 hour, plated at several densities on LB-Agar plates containing 50 µg/ml ampicillin, and incubated overnight at 37 °C. Single, isolated colonies were picked and transferred to culture tubes containing 3 ml LB broth containing 50 µg/ml ampicillin and incubated under shaking for 6 hours. These pre-cultures were used to inoculate larger overnight cultures for either miniprep (5 ml) or maxiprep (300 ml). Plasmid isolation from E. coli was performed using either a NucleoSpin Plasmid kit (Macherey Nagel, Düren, Germany) for minipreps or a NucleoBond Xtra Maxi kit (Macherey Nagel, Düren, Germany) for maxipreps following the included

instructions. Final DNA concentrations were measured using NanoDrop ND-1000 spectrophotometer (Thermo Fisher Scientific, MA, USA).

### *2.2.3 Restriction digestion of plasmid DNA*

Restriction digestion of plasmid DNA was performed following a standard reaction containing 1 µl restriction enzyme per µg DNA in a final volume of 20 µl appropriate buffer. The reaction was incubated at 37 °C in a thermocycler (Takara Bio, Shiga, Japan) for 1 hour for miniprep identification or 2 hours for other applications. If applicable, enzymes were heat-inactivated at 65 °C for 15 minutes after digestion was complete.

### *2.2.4 pSP73.pA backbone plasmid DNA isolation*

For T4-ligation assembly, pSP73.pA-Gluc plasmid DNA was digested as described above with XbaI and HindIII in M buffer to remove the Gluc coding sequence. After digestion, the DNA was purified *via* agarose gel electrophoresis as described above. The larger band was excised and the DNA was isolated using a QIAquick Gel Extraction kit (Qiagen, Hilden, Germany) following the included instructions. The final DNA concentration was measured using a NanoDrop ND-1000 spectrophotometer.

### *2.2.5 PCR of Anti CD-19 CAR plasmid DNA for T4 ligation*

MSGV1-1D3-28Z.1-3 mut plasmid DNA was used as a template for a PCR to generate an insert with ends homologous to the ends of the pSP73.pA backbone. The reaction mixture was assembled with CloneAmp HiFi PCR premix (Takara Bio, Shiga, Japan), 1 ng template DNA, and 0.2 µM forward and reverse primers (**Table 2.1**). A thermocycler was programmed for 35 cycles of denaturing at 98 °C for 10 seconds, annealing at 50 °C for 5 seconds, and extension at 72 °C for 5 seconds. The PCR product was subjected to agarose gel electrophoresis as described above. The resulting band was excised and isolated using a QIAquick Gel Extraction kit following the included instructions. The DNA concentration was measured using a NanoDrop ND-1000 spectrophotometer.

**Table 2.1** Primer sequences for generating PCR fragment of anti-CD19 CAR insert for T4 DNA ligation

| Primer name | Primer sequence |
|---|---|
| FWD primer | CGAGCAGCTGAAGCTTACCATCCTCTAGCCC |
| REV primer | CCGGGGATCCTCTAGATCGACTCATCTGGGG |

The resulting DNA fragment was then digested *via* restriction digestion using XbaI and HindIII in M buffer as described above, and the larger band was purified using a QIAquick Gel Extraction kit following the included instructions. The DNA concentration was measured using a NanoDrop ND-1000 spectrophotometer.

*2.2.6 Assembly of T7-anti-CD19-CAR plasmid DNA*

The T7-anti-CD19-CAR plasmid DNA was assembled using T4 ligation. 45 ng of linear pSP73.pA vector and 85 ng MSGV1-1D3-28Z.1-3 mut fragment were prepared in 19 µL T4 DNA ligase buffer. Then 1 µL T4 DNA ligase was added and the reaction and the reaction mixture incubated at 16 °C for 2 hours. The resulting plasmid was amplified using Stellar chemically competent E. coli cells as described above to collect 4 precultures. After confirming the plasmid assembly *via* gel electrophoresis, one of the pre-cultures was used to inoculate larger overnight cultures of Stellar chemically competent E. coli cells for maxiprep. Plasmid isolation from E. coli was performed using either a NucleoBond Xtra Maxi kit (Macherey Nagel, Düren, Germany) following the instructions. Final DNA concentration was measured using a NanoDrop ND-1000 spectrophotometer (Thermo Fisher Scientific, MA, USA).

*2.2.7 Sanger sequencing of T7-anti-CD19-CAR plasmid DNA*

The T7-anti-CD19-CAR plasmid DNA sequence was further confirmed using Sanger sequencing. Two primers were designed (**Table 2.2**) and mixed with The T7-anti-CD19-CAR plasmid DNA (35 ng/µl) at 0.45 µM primer concentration. Sanger sequencing was performed by FASMAC Inc. (Kanagawa, Japan) using a BigDye Terminator v3.1 Cycle Sequencing Kit and a 3130xl Genetic Analyzer (Thermo Fisher Scientific, Waltham, MA, USA).

**Table 2.2** Sanger sequencing primer sequences of T7-anti-CD19-CAR plasmid DNA

| Primer name | Primer sequence |
|---|---|
| Seq 1 | ATTACCGCCTTTGAGTGAGC |
| Seq 2 | AACAGCAGAAGAAACAGAGG |

*2.2.8 In vitro transcription of plasmid DNA*

The template for IVT was prepared by digesting the T7-anti-CD19-CAR plasmid with BglII restriction enzyme and the CXCR4-tGFP chemokine plasmid with PmeI restriction enzyme as described above. The DNAs were purified by ethanol precipitation, adding 1/10th volume 0.5 M EDTA, 1/20th volume 3 M sodium acetate, and 2 volumes of ethanol. The mixture was chilled at -20 °C for 30 minutes and centrifuged at maximum speed for 15 minutes. The pellet was dried and resuspended in nuclease-free water. The template DNA was used for an *in vitro* transcription (IVT) reaction using a MEGAscript T7 Transcription kit in accordance to the included instructions. The reaction was incubated at 37 °C in a thermocycler for 2 hours. Turbo DNase included in the kit was added and the reaction was further incubated for 15 minutes to remove the template DNA. The RNA was isolated using an RNeasy Mini kit (Qiagen, Hilden, Germany) following the included RNA cleanup protocol. The RNA was eluted in nuclease-free water in multiple steps to increase the yield.

*2.2.9 mRNA size analysis with capillary gel electrophoresis*

RNA size was estimated with capillary gel electrophoresis. The RNA was diluted to 100 ng/μL in nuclease-free water and then denatured at 70 °C for 2 minutes before analysis. Capillary gel electrophoresis was performed with a 2100 Bioanalyzer Instrument (Agilent Technologies, Santa Clara, CA, USA) using an RNA 6000 Nano kit (Agilent Technologies, Santa Clara, CA, USA) according to the manufacturer's instructions.

## 2.3 Results and discussion

A plasmid was designed in silico for use as a template to generate Anti-CD19 CAR mRNA. The plasmid contains the necessary T7 promoter sequence in a pSP73.pA backbone sequence and the anti-CD19 CAR gene derived from the MSGV1-1D3-28Z.1-3 mut (Plasmid #107227). This design was realized using a ligation strategy by combining a pSP73.pA backbone with the anti-CD from19 CAR sequence amplified by PCR (**Figure 2.1**). First, the source plasmid was digested with XbaI and HindIII to remove the Gluc sequence. The following agarose gel electrophoresis showed a band corresponding to the excised Gluc fragment of around 600 bp as well as a band corresponding to the size of the pSP73.pA backbone at around 2550 bp (**Figure 2.2a**). This, and the absence of any further bands indicates a successful exertion of Gluc from the backbone plasmid.

Next, the desired anti-CD19 CAR coding sequence was amplified from the MSGV1-1D3-28Z.1-3 mut plasmid using PCR. The primers were originally designed to contain terminal sequences that are homologous to the cut ends of the pSP73.pA backbone for Gibson assembly. In addition, the restriction sites for XbaI and HindIII were also incorporated. By performing PCR with these primers **(Table 2.1**) a fragment was obtained with terminal sequences homologous to the pSP73.pA backbone. Eventually, Gibson assembly was not used and the PCR fragment was further digested with XbaI and HindIII to create compatible sticky ends for T4 DNA ligation. The fragment was analyzed by agarose gel electrophoresis and the resulting band corresponded to the expected fragment size of around 1500 bp **(Figure 2.2b**). Both fragments were isolated from the agarose gel and combined using T4 DNA ligation. The assembly reaction was used to transform E. coli to amplify the final T7-anti-CD19 CAR plasmid.

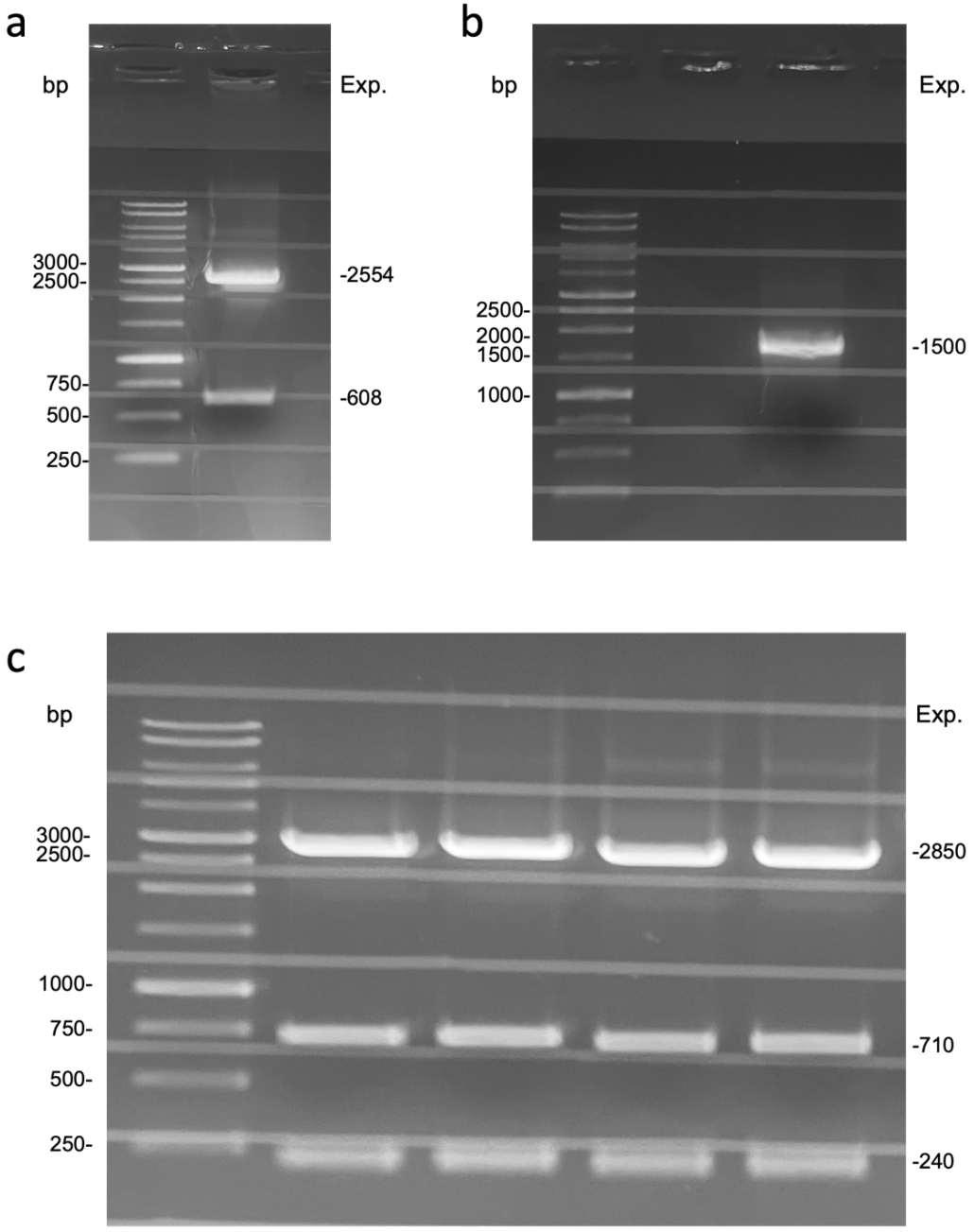


**Figure 2.2** Agarose gel (1% w/v) electrophoresis of DNA fragments generated by (a) restriction digestion of pSP73.pA-Gluc plasmid (b) PCR of MSGV1-1D3-28Z.1-3 mut plasmid followed by restriction digestion (c) restriction digestion of minipreps prepared from assembly *via* T4 DNA ligation using the fragments from (a) and (b).

Four colonies were selected and cultured by miniprep. The minipreps were digested using PvuII to assess plasmid identity. The restriction digestion with PvuII yielded band patterns matching the expected bands from the in silico digestion **(Figure 2.2c**). Sanger sequencing was done to further confirm the correct insertion of the anti-CD19 CAR coding sequence into the pSP73.pA backbone (**Figure 2.3**). Primers were chosen slightly upstream of the assembly joints. The results confirm the in silico sequence and the correct insertion of the anti-CD19 CAR coding sequence (**Figure 2.3**). These results confirm the correct assembly of T7-anti-CD19 CAR plasmid DNA, which can be used as a DNA template for IVT to generate anti-CD19 CAR mRNA

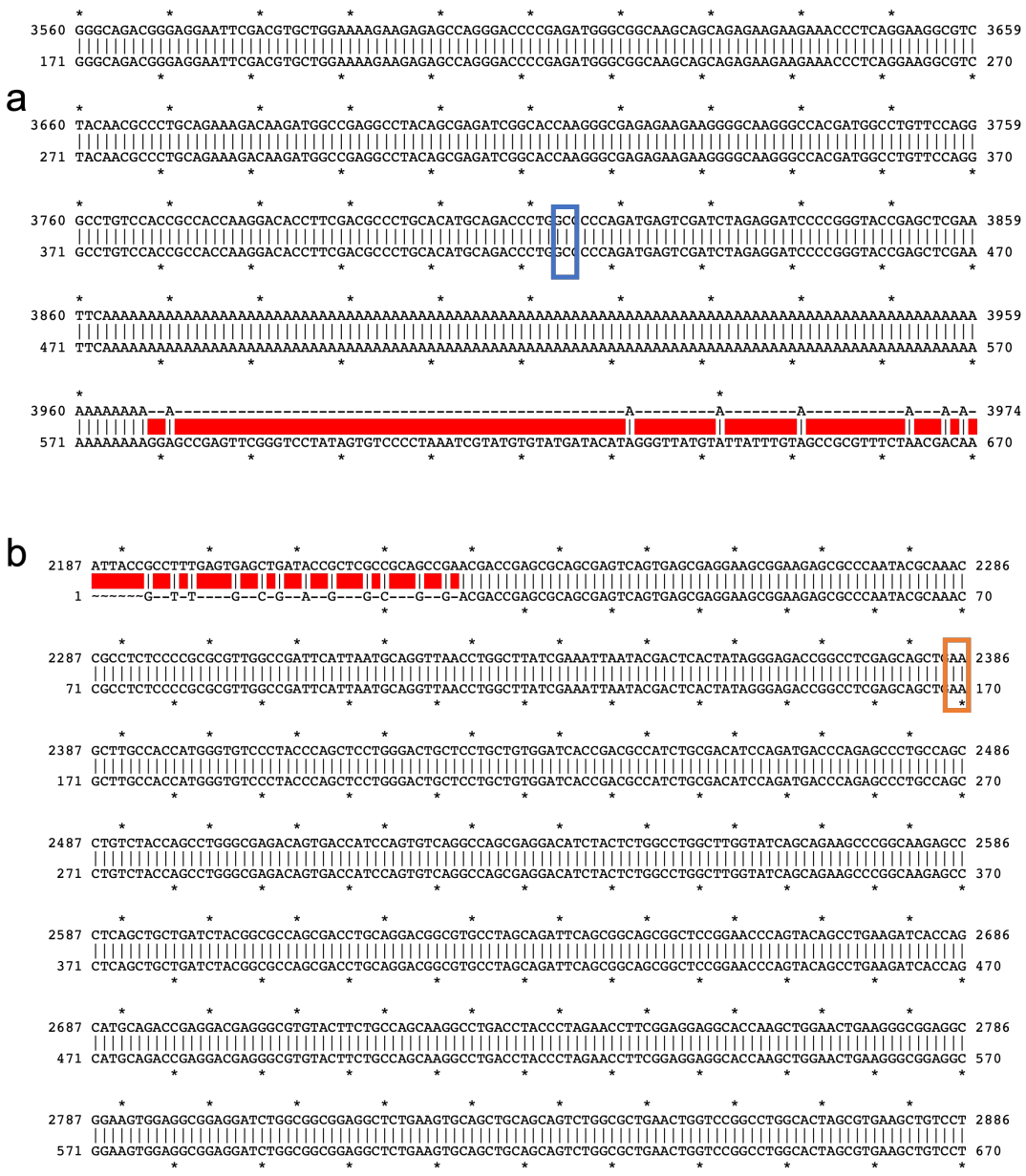


**Figure 2.3** Sanger sequence of T7-Anti-CD19-CAR plasmid DNA and alignment with *in silico* sequence using a) Primer Seq. 1 and b) Primer Seq. 2. The blue and orange squares mark the assembly points of the backbone and the anti-CD19 CAR sequence.

The T7-Anti-CD19-CAR plasmid was used along with a T7-CXCR4-tGFP plasmid and a plasmid encoding the reporter protein gaussian luciferase（Gluc) as a template for IVT. The templates contain a promoter for the T7 bacteriophage RNA polymerase which is widely used for IVT. Additionally, the T7-Anti-CD19-CAR and the T7-CXCR4-tGFP plasmids contain a 120-nucleotide long poly(A) sequence downstream of the coding sequence, eliminating the need to add a poly(A) tail after mRNA synthesis for these sequences. On the contrary, the T7-CXCR4-tGFP did not include a poly(A) sequence in the template, which required an *in vitro* poly(A) tailing reaction using E. coli Poly(A) Polymerase (E-PAP) and ATP after IVT to result in enhanced translation over untailed mRNAs maybe due to increased mRNA stability and translation efficiency (Bernstein, Peltz, and Ross 1989; Gallie 1991; Khaleghpour et al. 2001).

All of the mRNA were capped using an Anti-Reverse Cap Analog or ARCA (Jemielity et al. 2003; Peng et al. 2002). In ARCA, one of the 3' OH groups (closer to $^{7}$MG) is eliminated from the cap analog and is substituted with $–OCH_3$. This modification allows T7 RNA polymerase to initiate transcription only with the remaining –OH group and thus synthesize RNAs capped exclusively in the correct orientation. Substitution of traditional Cap Analog with ARCA allows for the synthesis of capped RNAs that are 100% functional, in contrast to transcription reactions using traditional cap analog where only half of the cap analog is incorporated in the correct orientation.

After cleanup by spin column, the resulting mRNAs were analyzed by capillary gel electrophoresis to assess the mRNA sizes. Gluc mRNA showed a peak of around 877 nt, which matches the *in silico* calculation of around 810 nt (**Figure 2.4a**). anti-CD19 CAR mRNA showed a peak of around 1553 nt, which matches the *in silico* calculation of around 1640 nt (**Figure 2.4b**). Finally, CXCR4-tGFP mRNA showed a peak of around 1950 nt, which matches the *in silico* calculation of around 1880 nt before poly(A) tailing (**Figure 2.4c**).

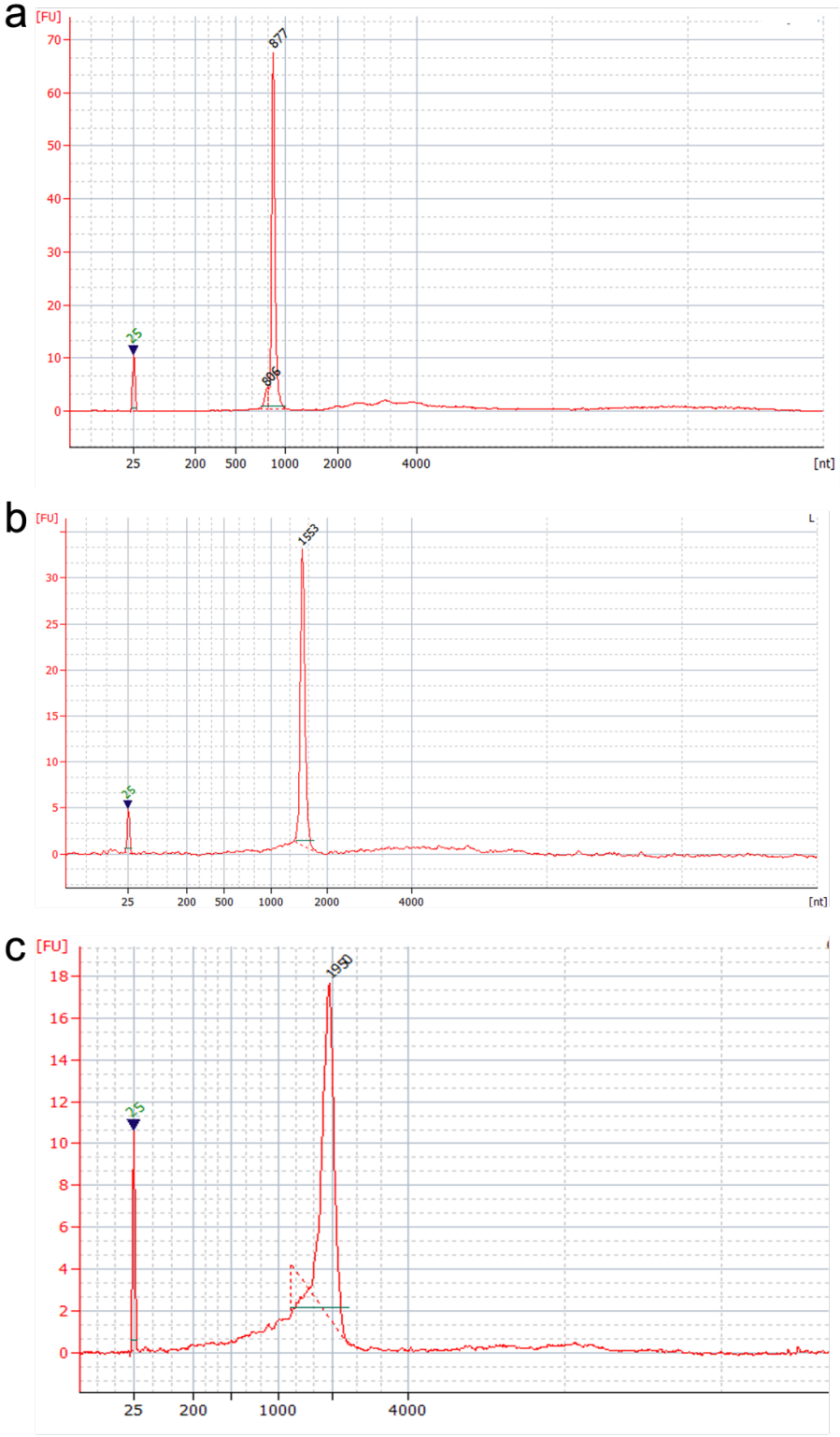


**Figure 2.4** Electropherograms using Bioanalyzer of mRNAs encoding various proteins. a) Electropherograms of mRNA encoding Gluc. b) Electropherograms of mRNA encoding anti-CD19 CAR. c) Electropherograms of mRNA encoding CXCR4-tGFP

The poly(A) length of CXCR4-tGFP mRNA was estimated to be around 70 nt. The length of the poly(A) tail can have a great impact on the expression efficiency of mRNA. However, a wide variety of naturally occurring poly(A) lengths, combined with conflicting reports of naturally occurring poly(A) make it hard to predict the optimal length in IVT mRNA (Weill et al. 2012; Jalkanen, Coleman, and Wilusz 2014; Lima et al. 2017). Commerical mMESSAGE mMACHINE® T7 Ultra Kit, which was used to synthesize this mRNA, typically adds 50-100 A to their transcripts according to their instruction manual, which matches the poly(A) length of the CXCR4-tGFP mRNA.

This mRNA is generally suitable for *in vivo* application, but to further improve the translation efficiency of mRNA, pseudouridine (Ψ) could be incorporated into the mRNA in the future. It has been found in tRNA, rRNA, snRNA, mRNA, and other types of RNA (Carlile et al. 2014; Lovejoy, Riordan, and Brown 2014; Schwartz et al. 2014). Ψ is derived from uridine *via* a base-specific isomerization reaction called pseudouridylation. It allows the nucleobase to rotate more freely (Adachi et al. 2021) and generally stabilizes the RNA. Further, it seems that Ψ increases the protection of the RNA against nucleases. N1-methyl-Ψ is a further derivative. Indeed, it has been reported that N1-methyl-Ψ diminished the activity of innate immune sensors and that N1-methyl-Ψ performed even better than Ψ in improving the translational capacity and reducing cytotoxicity of modified mRNA when tested in several human cell lines, primary human cells, and in animals (intradermal and intramuscular injection in mice) (Andries et al. 2015). It has been used for Covid-19 vaccines like Pfizer-BioNTech added N1-methyl-Ψ to their COVID-19 mRNA vaccine candidate (comirnaty® or BNT162b2) (Morais, Adachi, and Yu 2021b).

Alternative purification techniques, like poly(A) binding columns or size-specific methods such as chromatography, may also offer improved efficacy in obtaining a pure product. Chromatography-based approaches have been associated with an impact on RNA immune

responses due to the presence of dsRNA contaminants arising from the IVT process (Karikó et al. 2011). Consequently, pharmaceutical companies commonly employ chromatography-based methods for purifying IVT RNA, whereas such methods are less practical on a laboratory scale.

## 2.4 Conclusion

A DNA template encoding anti-CD19 CAR in a backbone with T7 was designed in silico and constructed using T4 DNA ligation. Transformation into E. coli resulted in accurate and efficient cloning with correct plasmid identity in all selected clones. mRNAs encoding the reporter protein Gluc, anti-CD19 CAR, and CXCR4-tGFP including ARCA caps and poly(A) tails were prepared from template DNA using IVT. Size analysis using capillary gel electrophoresis revealed a product with a clear, single peak, indicating sufficient purity for subsequent experiments.

# Chapter 3.

# Preparation and Characterization of mRNA-Loaded PIC Micelles

## 3.1 Introduction

In this chapter, we explore the properties of a block ionomer composed of a poly(glycidyl) flexible backbone, modified with phenylalanine. The design of this polymer aims to enhance interactions with mRNA through the flexible backbone (Miyazaki et al. 2020) and the stabilizing influence of π-π interactions between phenylalanine and RNA (Yang, Miyazaki, et al. 2023). Additionally, the block ionomer incorporates a terminal -$N_3$ group to facilitate surface modifications, enabling the attachment of targeting ligands such as antibodies, antibody fragments, or mannose groups to target immune cells. The presence of a poly(ethylene glycol) (PEG) block is crucial for maintaining micelle stability under physiological conditions and acts as a shield against surface charge. Furthermore, phenylalanine is conjugated to the polymer *via* hydrolyzable ester bonds through Steglich esterification, leaving the primary amine as an ionizable group.

This polymer was used to condense various mRNAs into micelles. These micelles were characterized in terms of morphology, surface charge, and stability, to study their properties. Further, their ability to transfect cells and express mRNA *in vitro* was confirmed. It is noteworthy that block catiomers with moieties that ionize at endosomal pH can result in micelles with the ability to disrupt endosomal membranes, thereby promoting the release of payloads from endosomes into the cytosol. (Smith et al. 2019; Shima, Akagi, and Akashi 2014). To confirm pH-dependent action, the apparent pKa of the carrier is determined, and the endosomal escape quantified.

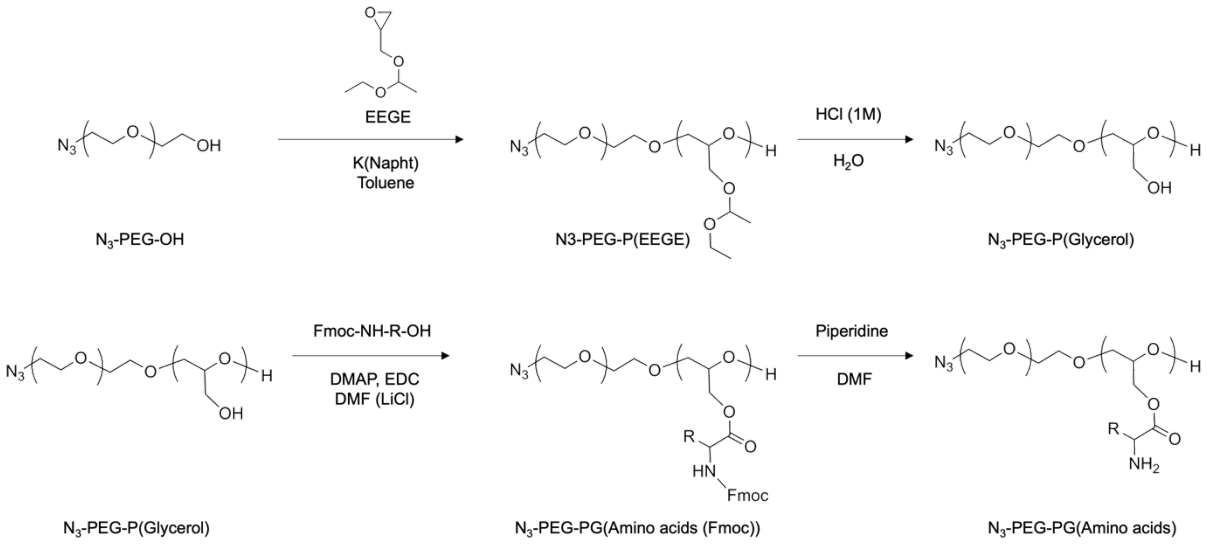


**Figure 3.1** Synthesis of α-azide-poly(ethylene glycol)-block-poly(glycerol) ($N_3$-PEG-PG) copolymers by ring-opening polymerization, followed by the conjugation of amino acids *via* Steglich esterification, and subsequent deprotection of amine to obtain $N_3$-PEG-poly(glycidyl(amino acids)) ($N_3$-PEG-PG(AA))

## 3.2 Materials and methods

### *3.2.1 Materials*

α-azide-poly(ethylene glycol) (PEG-OH) was purchased from Nanosoft Polymers (Winston-Salem, NC, USA). N-(9H-fluoren-9-ylmethoxy)carbonyl-L-phenylalanine (Fmoc-Phe-OH) (purity > 98.0%), potassium (K) (purity > 99.5%), Triton X-100, N-(9H-fluoren-9-ylmethoxy)carbonylglycine (Fmoc-Gly-OH) and (purity > 98.0%), hydrochloric acid (HCl) were purchased from Sigma-Aldrich (St. Louis, MO, U.S.A). N-(4-Pyridyl)dimethylamine (DMAP) (purity > 99.0%), N,N-dimethylformamide (DMF) (purity > 99.5%), and 1-Ethyl-3-(3-dimethylaminopropyl)carbodiimide (EDC) (purity > 98.0%) were purchased from Tokyo Chemical Industry Co., Ltd. (Tokyo, Japan). PTFE filters (0.22 μm) were purchased from Merck KGaA (Darmstadt, Germany). Diethyl ether, piperidine (purity > 98.0%), ethanol, sodium acetate buffer pH 4.5, naphthalene (purity > 98.0%), sodium hydroxide (NaOH), Fluorescamine, LDH-Cytotoxicity Tests, and Dulbecco's Phosphate-Buffered Saline (D-PBS), were obtained from Fujifilm Wako Pure Chemical, Co., Inc. (Osaka, Japan). Cy5 Label IT Nucleic acid labeling kit was purchased from Mirus Bio (Madison, WI, USA). Tetrahydrofuran (THF) (super dehydrated, purity > 99.5%) was purchased from Kanto Chemical, Co., Inc. (Tokyo, Japan). *In vivo* JetPEI and JetMESSENGER were obtained from Polyplus-transfection (Illkirch-Graffenstaden, France). Renilla Luciferase Assay was purchased from Promega (Madison, WI, USA). Dimethylsulfoxide-d6 + 0.05% TMS (DMSO-d6) was purchased from Cambridge Isotope Laboratories, Inc. (Massachusetts, USA). 8-well chambered borosilicate cover glasses, Penicillin-Streptomycin, LysoTracker Green, Dulbecco’s Modified Eagle’s Medium (DMEM), MEGAscript T7 Transcription kit, T-PER lysis buffer, and 1 M HEPES buffer (pH 7.4) were purchased from Thermo Fisher Scientific (Waltham, MA, U.S.A). ReverTra Ace qPCR RT Master Mix kit was obtained from Toyobo (Osaka, Japan). (1-Ethoxyethyl)glycidyl ether (EEGE) was purchased from Syphonix, Inc. (Wake Forest, NC,

USA). Lipofectamine MessengerMAX was purchased from Invitrogen (Waltham, MA, USA). Fetal bovine serum (FBS) was purchased from Cytiva (Marlborough, MA, USA). 96-well plates were purchased from Corning Inc. (Corning, NY, USA). RC Dialysis tubes MWCO: 3,500 Da were obtained from Repligen (Waltham, MA, USA). Cell-counting kit-8 (CCK-8) and Hoechst 33342 solution (Hoechst) were purchased from Dojindo Molecular Technologies Inc., (Tokyo, Japan). N,N-Dimethylformamide (DMF) (purity > 99.7%) was purchased from Junsei Chemical Co.Ltd. (Tokyo, Japan).

### *3.2.2 Cell culture*

Human Pancreas adenocarcinoma (BxPC-3) cells were obtained from DS Pharma Biomedical Japan (Osaka, Japan), HEK-293 and HeLa cells from RIKEN Cell Bank (Tsukuba, Japan). HEK293, HeLa and BxPC-3 cells were cultured in Dulbecco's modified Eagle's medium (DMEM; Sigma-Aldrich, St. Louis, MO, USA) with 4500 mg/l glucose, L-glutamine, sodium pyruvate, and sodium bicarbonate supplemented with 10% fetal bovine serum (FBS; Cytiva, Marlborough, MA, USA) in a humidified incubator at 37 °C and 5% CO2.

### *3.2.3 Synthesis of flexible $N_3$-PEG-PG(Phe)*

First, 145 mg (5.6 μmol) of $N_3$-PEG-PEEGE was dissolved in 1 M HCl and stirred at room temperature for 16 hours to obtain $N_3$-PEG-PG. The resulting product was then purified by dialysis using a membrane with a molecular weight cutoff (MWCO) of 3,500 Da. Subsequently, 82 mg (4.9 μmol, yield 89%) of the purified product weas collected after freeze-drying the solution. Next, Fmoc-Phe-OH was conjugated to the backbone *via* Steglich Esterification using 75 mg (4.5 μmol) of $N_3$-PEG-PG dissolved in 7 mL of dimethylformamide (DMF) containing 10 mM LiCl under an argon atmosphere. Then, 740 mg (1.9 mmol, 5 eq. of OH) of Fmoc-Phe-OH was added to the solution. The solution was cooled on ice and sparged with argon for 5 minutes under stirring. Subsequently, 53 mg of 4-dimethylaminopyridine (DMAP) (0.43 mmol, 1.1 eq. of OH) was added. The solution was stirred and sparged with

argon for another five minutes before 0.270 mL (1.6 mmol, 4 eq. of OH) of 1-ethyl-3-(3-dimethylaminopropyl)carbodiimide (EDC) was added dropwise. The ice bath was removed after 35 minutes, and the solution was stirred at room temperature under argon and exclusion of light overnight to obtain $N_3$-PEG-PG(Phe-Fmoc). The solution was filtered, and the filtrate was dialyzed against DMF. The Fmoc protection groups were removed by adding 25% (v/v) of piperidine for 1 hour. The product was then dialyzed against DMF, followed by dialysis against deionized water at 4 °C, and dried *via* freeze-drying. The final product, $N_3$-PEG-PG(Phe), was characterized using an ECS-400 1H-NMR spectrometer (400 MHz; JEOL, Tokyo, Japan) at 80 °C in DMSO-d6 at a concentration of 10 mg/mL.

### *3.2.4 Cytotoxicity of $N_3$-PEG-PG(Phe)*

HEK293 cells were seeded in 96-well plates at $1x10^4$ cells/well. After incubation overnight, the cell culture media were replaced by cell culture media containing 0.00, 0.025, 0.05, 0.1, 0.02, and 0.04 mg/mL $N_3$-PEG-PG(Phe). After 24-h incubation, the cell viability was determined by CCK-8 assay following the manufacturer's protocol. Absorption at 450 nm was measured using an Infinite M200 microplate reader (Tecan, Männendorf, Switzerland).

### *3.2.5 Hydrolysis of $N_3$-PEG-PG(Phe)*

The detachment of Phe from the polymer over time was determined *via* UV-VIS spectrometry. $N_3$-PEG-PG(Phe) was dissolved in water and dialyzed using a Mini Dialysis Kit with a 8 kDa cut off (Cytiva; Malborough, MA, USA) against water at r.t. for 28 h. The Phe concentration inside the dialysis tube was determined at several time points *via* NanoDrop at an absorbance of 260 nm to calculate the conjugation. A concentration curve was measured using aqueous solutions of $N_3$-PEG-PG(Phe) at several concentrations.

### *3.2.6 Preparation of mRNA loading Phe(m) micelles*

Micelles containing mRNA were produced through self-assembly by mixing diluted polymer solution with mRNA solution. A 1 mg/ml stock solution of polymer was prepared by

dissolving $N_3$-PEG-PG(Phe) in 10 mM sodium acetate (pH 4.5) buffer and filtering the solution through a 0.22 μm filter to remove debris. The polymer solution was then diluted with sodium acetate (pH 4.5) buffer to the desired concentration. mRNA solutions were prepared by diluting mRNA in 10 mM HEPES (pH 7.4) buffer to appropriate concentrations for the required amine/phosphate (N/P) ratios and mixed with the polymer solutions in a 1.5 ml hypertube by placing the mRNA solution in the bottom of the tube and the polymer solution on the wall of the tube and vortexing briefly. The resulting Phe(m) micelles were allowed to equilibrate on ice for 30 minutes before use.

*3.2.7 Particle characterization via dynamic light scattering*

The micelle's particle size distributions were characterized by dynamic light scattering (DLS) using a Zetasizer Nano ZS (Malvern Panalytical, Malvern, UK). Phe(m) micelle solutions were diluted to 20 ng/μL RNA concentration in 10 mM HEPES (pH 7.4) buffer and transferred to a low-volume quartz cuvette. Measurements were performed at 25 °C with a 50 mW frequency doubled DPSS Nd:YAG laser (λ=532 nm) at a detection angle of 173°. Hydrodynamic diameters and polydispersity indices (PDI) were calculated according to the cumulant method.

*3.2.8 Particle characterization via zeta potential measurement*

The zeta potential of the particles was measured by electrophoretic light scattering (ELS) using a Zetasizer Nano ZS equipped with a 50 mW frequency doubled DPSS Nd:YAG laser (λ=532 nm). The sample was diluted to 1.25 ng/μl RNA in 10 mM HEPES (pH 7.4) buffer, loaded in a folded capillary cell, and equilibrated to 25 °C before measurement. The zeta potential was obtained using Smoluchowski's equation.

*3.2.9 Fluorescent labeling of nucleic acids*

mRNA were fluorescently labeled with a Label IT Nucleic acid labeling kit following the manufacturer's instructions. Cy5-labeled mRNAs were purified using EtOH precipitation. The

final concentration of the labeled mRNA was determined by using a NanoDrop ND-1000 spectrophotometer (Thermo Fisher Scientific, Waltham, MA, USA)

*3.2.10 Determination of mRNA number per Phe(m)*

mRNA was labeled with Cy5 using Label IT kit as described above. To determine the amount of Cy5 per mRNA, FCS was performed to obtain the counts per mRNA. Then Phe(m) with various N/P ratios were made using the Cy5-labled mRNA, and free mRNA was removed by ultrafiltration with a molecular weight cutoff (MWCO) of 100 kDa. To determine the number of mRNA per micelle, fluorescence correlation spectroscopy (FCS) was measured using an LSM780 confocal microscope equipped with ConfoCor3 and a 40X water objective at room temperature. Cy5-labeled free mRNA and micelles were detected using a HeNe laser at 633 nm to obtain the counts per micelle. The counts were divided by the number of counts per mRNA to obtain the number of mRNA per micelle.

*3.2.11 Determination of the association number of polymer per Phe(m)*

Phe(m) with varying N/P ratios were prepared as described previously, diluted 10 times, and free polymer was separated *via* ultrafiltration with MWCO of 100 kDa. The amount of free polymer was determined from the filtrate. Fluorescamine was added, and after 1 hour, the fluorescence intensity was measured using an Infinite M200 microplate reader (Tecan, Männendorf, Switzerland), with a concentration curve of free polymer with fluorescamine as a reference. The number of polymers associated with the micelles was determined by subtracting the number of free polymers from the total number of polymers added and dividing it by the number of micelles determined by the number of mRNA per micelle.

*3.2.12 Particle Characterization via TEM*

To prepare the Phe(m) micelles for observation using transmission electron microscopy (TEM), a dilution was made in 10 mM HEPES buffer with a pH of 7.4, resulting in a final RNA concentration of 0.25 ng/μL. Subsequently, the micelles were stained on a carbon film support

grid by adding an equal volume of a 2% w/v uranyl acetate solution and incubating the sulution for 5 minutes. The imaging of the micelles was performed using a JEM-1400 electron microscope (JEOL, Tokyo, Japan) operating at an acceleration voltage of 120 kV.

*3.2.13 Anion stability assay*

Stability against anion exchange reaction was assessed using fluorescence correlation spectroscopy (FCS). Gluc RNA was fluorescently labeled with Cy5 using a Label IT Nucleic Acid Labeling kit, Cy5 (Mirus Bio, Madison, WI, USA). Phe(m) micelles were prepared with fluorescently labeled mRNA and phenylalanine-conjugated polymer at N/P = 6 and Gly(m) micelles were prepared with fluorescently labeled mRNA and glycine-conjugated polymer, which was provided by Dr. Boonstra Eger at N/P = 3 and diluted in 10 mM HEPES buffer (150 mM NaCl) with different concentrations of dextran sulfate. The samples were incubated at room temperature for 30 minutes and FCS measurements were made using an LSM 780 confocal laser scanning microscope (Zeiss, Oberkochen, Germany) equipped with a ConfoCor 3 module and a 40X water objective. The HeNe laser (633 nm) was used for the excitation of Cy5-labeled mRNA. The measurement was performed at room temperature and a normalized autocorrelation curve was obtained from 10 repeats of 10 s each per sample. Alexa Fluor 647 was used as a reference, stock solutions of Alexa Fluor 647 in water were diluted to the desired concentration to obtain structural parameters.

*3.2.14 In vitro expression in HEK-293 cells*

mRNA expression was assessed by transfecting HEK-293 cells with mRNA encoding Gluc and measuring supernatant luminescence. Cells were seeded overnight in 96-well plates at a density of $1x10^4$ viable cells per well. Cells were transfected with 200 ng mRNA encoding Gluc by adding Phe(m) micelles prepared as described earlier, or with Lipofectamine MessengerMAX reagent (Invitrogen, Waltham, MA, USA) at a 3:1 Lipofectamine:RNA ratio (v/w) following the manufacturer's instructions. Supernatant was collected after 48 hours and

luminescence was measured using a GloMax 96 automated microplate luminometer (Promega, Madison, WI, USA) as described above.

*3.2.15 Cellular uptake and endosomal escape*

BxPC-3 cells were seeded at a density of $3x10^4$ viable cells/well in 8-well chambers and incubated overnight in DMEM supplemented with 10% FBS and 1% PS under 5% CO2 at 37°C. Phe(m) micelles were prepared using $N_3$-PEG-PG(Phe) and Cy5-labeled Fluc mRNA at a ratio of N/P = 6. Subsequently, naked Cy5-labeled mRNA and Cy5-labeled mRNA-loaded micelles were administered to each well at a concentration of 700 ng mRNA per well, with a relative fluorescence intensity of 400 RFU. At various time intervals, cells from a well were washed, stained with DAPI solution (1:100 in D-PBS) to visualize the nucleus, and stained with LysoTracker Green (1:200 in culture medium) to visualize the endosomes. The cellular uptake of the micelles was assessed using an LSM-780 confocal microscope equipped with a 40 × objective (C-Apochromat, Carl Zeiss, Germany). To evaluate the intracellular fate of mRNA, the degree of colocalization endosomes and the mRNA was quantified.

*3.2.16 pKa analysis of $N_3$-PEG-PG(Phe)*

Potentiometric titration was performed to determine the pKa of the inonizable amine in the phenylalanine sidechain of $N_3$-PEG-PG(Phe). 2 mg $N_3$-PEG-PG(Phe) was dissolved in water acidified to pH 2.4 with HCl. The acidic solution was then titrated by a 916 Ti-Touch automatic titrator (Metrohm, Herisau, Switzerland) using a 1 mM NaOH solution. The degree of protonation (α) was determined by finding the equivalence points (EP) from the derivative of the titration curve (ΔpH) and setting the lower EP as 100% and the higher EP as 0% protonation. The pKa is determined as the pH at an α of 0.5.

*3.2.17 LDH leakage assay of $N_3$-PEG-PG(Phe)*

To investigate the impact of $N_3$-PEG-PG(Phe) polymers on cellular membranes, HeLa cells were seeded in a 96-well plate at a density of 1 x $10^4$ viable cells per well. The cells were

allowed to attach to the bottom of the well by incubating them overnight at 37 °C and 5% $CO^2$ in an incubator. The cells were exposed to polymer solutions with varying concentrations in PBS (pH 5.5) or PBS (pH 7.4) buffers at 37 °C for 15 minutes. Following the exposure, the supernatant was transferred to a separate well plate and the dissolved lactate dehydrogenase (LDH) amount was quantified using an LDH-Cytotoxic Test in accordance to the included manual. UV absorbances (A560) were measured with an Infinite M200 microplate reader (Tecan, Männendorf, Switzerland). The relative LDH leakage was calculated as (A560 - A560,n.c.)/(A560,p.c. - A560,n.c).

## 3.3 Results and discussion

$N_3$-PEG-PG(Phe) was successfully synthesized following the scheme in **Figure 3.1**. At first, the synthesis of $N_3$-PEG-PEEGE was conducted by ring opening polymerization (ROP) using $N_3$-PEG-OH and EEGE in the presence of catalytic K-naph. The number of attached EEGE units in the resulting $N_3$-PEG-PEEGE was determined by $^1$H-NMR and was found to be around 89 (**Figure 3.2a**). The deprotection of the polymer was achieved by dissolving it in a 1 M HCl solution and stirring it for 1 hour. The complete deprotection of the resulting $N_3$-PEG-PG was confirmed by 1H-NMR (**Figure 3.2b**). Then, The conjugation of Fmoc-Phe-OH was conducted *via* Steglich esterification using EDC and DMAP. The removal of the Fmoc protection group was accomplished by adding 25% (v/v) piperidine and letting the reaction stir for 1 hour. Following dialysis and freeze-drying, the composition of the final product $N_3$-PEG-PG(Phe) was determined by $^1$H-NMR (**Figure 3.2c**). The Phe introduction rate was calculated to be 89%. The $N_3$-PEG-PG(Phe) polymers were used for subsequent micelle formations with mRNA.

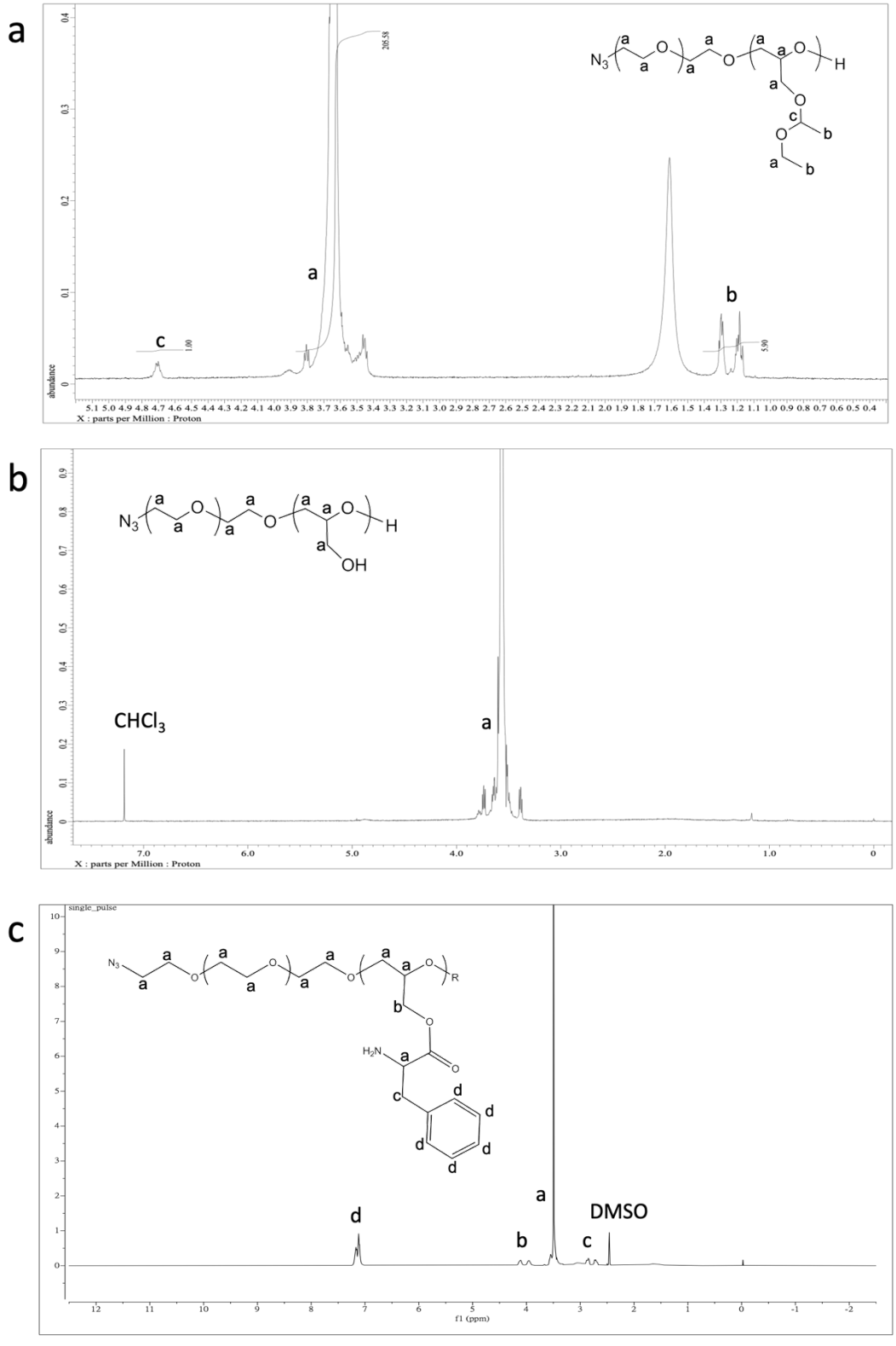


**Figure 3.2** $^{1}$H-NMR spectra of polymers. a) $^{1}$H-NMR spectrum of PEG-PEEGE. 89 units of EEGE were added. b) $^{1}$H-NMR spectrum of PEG-PG. Deprotection was confirmed c) $^{1}$H-NMR spectrum of PEG-PG(Phe). The conjugation rate of Phe was calculated to be around 89%.

To assess the toxicity of the polymer, CCK-8 cytotoxicity measurements were conducted. After 24 hours of incubation at several concentrations of polymer, the cytotoxicity remained low, even at very high concentrations of 0.4 mg/mL (**Figure 3.3a**). The polymer concentration in micelles among injections is intended to be around 0.23 mg/mL, and will be diluted once it enters the body, suggesting that the risk of cytotoxity of $N_3$-PEG-PG(Phe) will be low.

Furthermore, the detachment of Phe (**Figure 3.3b**) was inspected, highlighting the biodegradable nature of the ester bonds in the $N_3$-PEG-PG(Phe) polymer. Concentrated, cationic charges disperse with Phe detachment, further supporting the low toxicity of the system. Besides the essential amino acid Phe, the other degradation product, PEG-PG, is also highly biocompatible (Gosecki et al. 2016; Thomas, Müller, and Frey 2014; Kainthan et al. 2006), highlighting the safety of our polymeric nanocarrier. A similar conclusion was drawn in a recent study comparing degradable block copolymers conjugated with tyrosine, leucine, and glycine with PEG-poly(L-lysine) (PLL). In this study, PLL without the hydrolyzable ester bonds displayed low cell viability, while the viability of cells incubated with ester-conjugated polymers remained high (Yang, Miyazaki, et al. 2023).

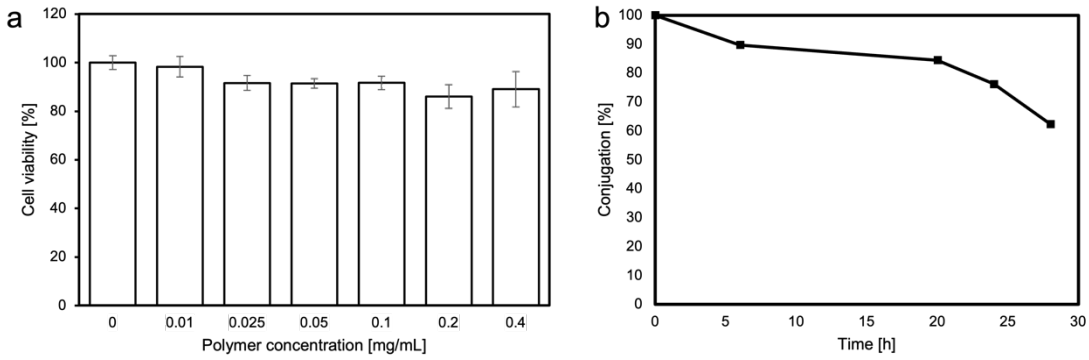


**Figure 3.3** *In vitro* assessment of a) cell viability of HEK-293 cells after 24 h incubation with $N_3$-PEG-PG(Phe) at various concentrations and b) biodegradability of $N_3$-PEG-PG(Phe). The polymer was dialyzed against water and the detachment of Phe from the polymer was measured *via* UV-VIS at several time points. Data are presented as the mean ± S.D. (n = 3)

The ability of $N_3$-PEG-PG(Phe) to condense various mRNA generated in the previous chapter into micelles was assessed by mixing the polymer with RNA at different amine/phosphate (N/P) ratios. **Figure 3.4a** shows the DLS measurement of Phe(m) encapsulating commercial Fluc-mRNA at various N/P mixing ratios. The polymer was able to form micelles at various mixing ratios. As seen in **Figure 3.4a,b**, the micelle size decreased with increasing N/P ratio. This suggests a more condense particle, likely due to increased Phe-conjugated polymers forming a core with mRNA. At N/P = 6, the micelles had a diameter of around 55 nm and polydispersity index (PDI) of around 0.18, suggesting compact and monodisperse particle formation. The zeta potential at this mixing ratio was neutral, which is desirable to prevent off-targeting and protein corona formation in biological environments. This is one of the reasons why many systems employ a shielding moiety such as PEG in their mRNA delivery systems.

Anti-CD19 CAR mRNA, which was synthesized according to the previous chapter, was used to form Phe(m) at different N/P ratios and characterized by DLS to demonstrate the ability of $N_3$-PEG-PG(Phe) to encapsulate a variety of mRNAs **Figure 3.4c**. The spectrum revealed that N/P ratio of 4 makes micelles with a size of 66 nm and a PDI of 0.238, N/P ratio of 6 makes micelles with a size of 60 nm and a PDI of 0.178, and N/P ratio of 8 makes micelles with a size of 59 nm and a PDI of 0.206. This indicates that highly monodisperse micelles are formed with anti-CD19 CAR mRNA at N/P ratio of 6.

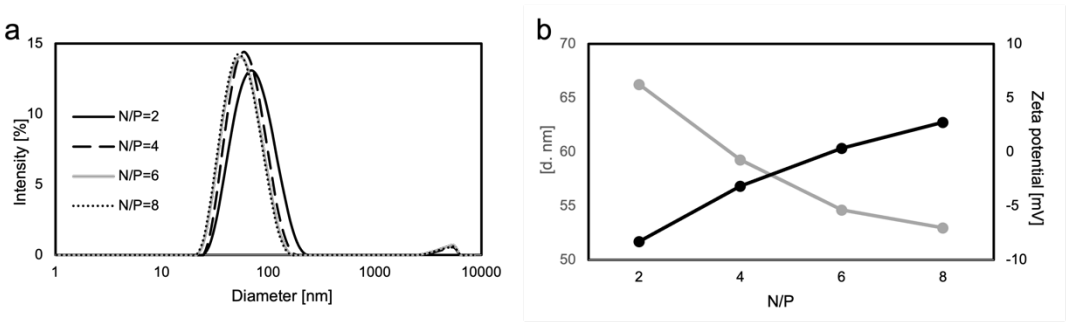


| N/P ratio | Size [nm] | PDI | Derived Countrate |
|---|---|---|---|
| 4 | 66 | 0.238 | 9022 |
| 6 | 60 | 0.178 | 9942 |
| 8 | 59 | 0.206 | 11092 |

| N/P ratio | Size [nm] | PDI | Derived Countrate |
|---|---|---|---|
| 4 | 66 | 0.332 | 6558 |
| 6 | 46 | 0.167 | 6427 |
| 8 | 50 | 0.178 | 8928 |

**Figure 3.4** DLS and zeta potential measurements of Phe(m) with various mRNAs. a) DLS measurements of Phe(m) encapsulating Fluc mRNA at various N/P ratios. b) The size and zeta potential of Phe(m) encapsulating Fluc mRNA. c) Phe(m) encapsulating anti-CD19 mRNA at several N/P ratios. d) Phe(m) encapsulating CXCR4-tGFP mRNA at several N/P ratios

CXCR4-tGFP mRNA, which was synthesized according to the previous chapter, and also used to form Phe(m) at different N/P ratios and characterized by DLS **Figure 3.4d**. The spectrum revealed that the formation of micelles at an N/P ratio of 4 is poor with an average size of 66 nm and a PDI of 0.332. This might be caused by incomplete encapsulation of mRNA by the polymer, or micelle aggregation leading to bigger structures and polydispersity at this N/P ratio. N/P ratio of 6 makes micelles with a size of 46 nm and a PDI of 0.167, and N/P ratio of 8 makes micelles with a size of 50 nm and a PDI of 0.178. This indicates that highly monodisperse micelles are formed with anti-CD19 CAR mRNA at N/P ratio of 6. Interestingly at an N/P ratio of 8, the micelle formation was poor compared to the other N/P ratios, which has not been observed with the other mRNAs At this mRNA size, the amount of polymer might

exceed the amount capable to fully encapsulate the mRNA leading to aggregations and polydispersity due to interactions of free polymer.

Overall N/P ratio of 6 has been optimal for the formation of condense and monodisperse micelles for various mRNAs including mRNAs encoding reporter proteins, as well as therapeutic mRNAs such as antiCD19 CAR mRNA and CXCR4-tGFP mRNA.

The number of mRNA molecules per micelles has been determined by FCS measurements. Phe(m) with varying N/P ratios were produced using Cy5-labeled mRNA. The counts per free mRNA and micelles are shown in **Table 3.1**. By dividing the counts per micelle through the counts per free mRNA, the number of mRNA per micelle was determined.

**Table 3.1** FCS results of micelles encapsulating Cy5-labeled mRNA.

| Sample | Counts per molecule [kHz] | mRNA/Phe(m) | Phe(m)/1 µg mRNA |
|---|---|---|---|
| Free mRNA | 11.608 | | |
| N/P = 2 | 23.563 | 2.03 | $4.74 \times 10^{11}$ |
| N/P = 4 | 16.198 | 1.40 | $6.89 \times 10^{11}$ |
| N/P = 6 | 13.165 | 1.13 | $8.54 \times 10^{11}$ |
| N/P = 8 | 11.168 | 0.96 | $1.00 \times 10^{12}$ |

At an N/P ratio of 2, approximately 2 mRNA molecules are encapsulated within the micelles. With increasing N/P ratio, the amount of encapsulated mRNA decreases, until it reaches 1 at N/P = 8. This correlates with the decreasing size of the micelles observed in **Figure 3.4**, where higher N/P ratios correlated to more condensed micelles.

The association number of polymers per micelle was determined by calculating the number of polymers associated with micelles and dividing it by the total number of micelles. The total number of micelles in a micelle solution containing 1 µg Fluc mRNA is shown in **Table 3.2**. It was calculated by dividing the number of mRNA in 1 µg Fluc mRNA by the

number of mRNA molecules per micelle (**Table 3.1**). To determine the number of associated polymers in the micelle solutions, micelles with Fluc mRNA at a concentration of 3.3 µg/mL mRNA were made and the free polymer was collected from the filtrate after ultrafiltration. The concentration of free polymer was determined by measuring the fluorescence intensity with a picroplate reader after it was labeled with fluorescamine for 1 hour. A concentration curve of $N_3$-PEG-PG(Phe) labeled with fluorescamine was prepared and the concentration of each micelle solution was determined to be around 0.037 mg/mL (**Figure 3.5**).

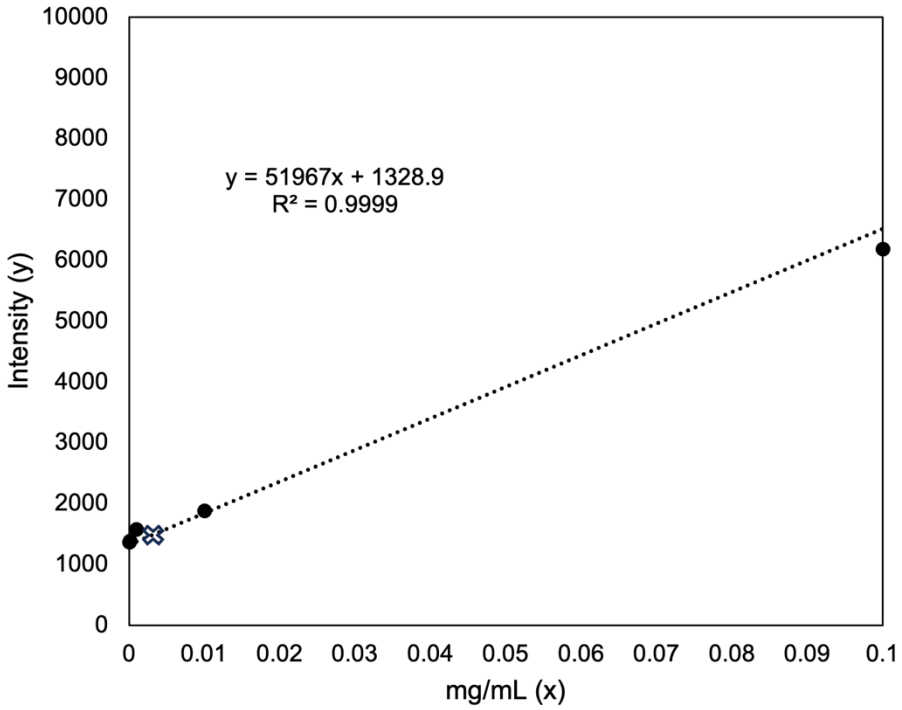


**Figure 3.5** concentration curve of $N_3$-PEG-PG(Phe) labeled with fluorescamine measured with a microplate reader. The fluorescence intensity of the free polymer after ultrafiltration was 1521 which correlates to 0.0037 mg/mL.

By subtracting the concentration of free polymer from the concentration of polymer added to each N/P ratio, the number of polymers associated with mRNA micelles per µg was calculated (**Table 3.2**). Also, by dividing the number of polymers associated by the number of micelles, the number of polymers per micelle was determined.

**Table 3.2** The number of micelles per 1 μg mRNA determined by FCS. The number of $N_3$-PEG-PG(Phe) polymers per 1 μg mRNA calculated by the total amount minus the free polymer determined by a microplate reader. The number of $N_3$-PEG-PG(Phe) polymer per Phe(m)

| Sample | Phe(m)/1 μg mRNA | Polymer/1 μg mRNA | Polymer/micelle |
|---|---|---|---|
| N/P = 2 | $4.74x10^{11}$ | $2.47x10^{13}$ | 52.0 |
| N/P = 4 | $6.89x10^{11}$ | $7.22x10^{13}$ | 104.9 |
| N/P = 6 | $8.54x10^{11}$ | $1.20x10^{14}$ | 140.3 |
| N/P = 8 | $1.00x10^{12}$ | $1.67x10^{14}$ | 166.5 |

The number of polymers per micelle increases steadily up to N/P ratio of 6, where approximately 140 polymers form one micelle. Considering there is approximately one mRNA in each micelle (**Table 3.1**) this correlates to 1929 phosphates per micelle. With approximately 140 polymers associated, and each polymer bearing 79 units of Phe, the total number of amines per micelle would be around 11,060 which is a N/P ratio of around 5.7, which is close to the estimated ratio. At the mixing ratio of N/P 8, the number of polymers associated correlated to an N/P ratio of 6.8 instead of 8. This suggests, that the number of associated polymers per micelle doesn't increase linearly and a saturation of polymers is most likely accomplished around the N/P ratio of 6. Beyond this N/P ratio, most of the additional polymer will likely not be associated with the mRNA.

Next, Phe(m) were characterized by TEM at two different N/P ratios to characterize the particles. As expected, Particles mixed at a lower N/P ratio have a less uniform and larger morphology than particles mixed at a N/P ratio of 6 (**Figure 3.6**), which also displayed condense, homogeneous particles during DLS measurements. The histogram confirms the average size of nanoparticles formed at N/P = 6 is smaller and more homogeneous than at N/P = 2. It is likely, that the mixing ratio of N/P = 2 does not adequately encapsulate mRNA

condense in its core. This further manifests N/P ratio of 6 to form suitable micelles and this formulation will be used for further experiments.

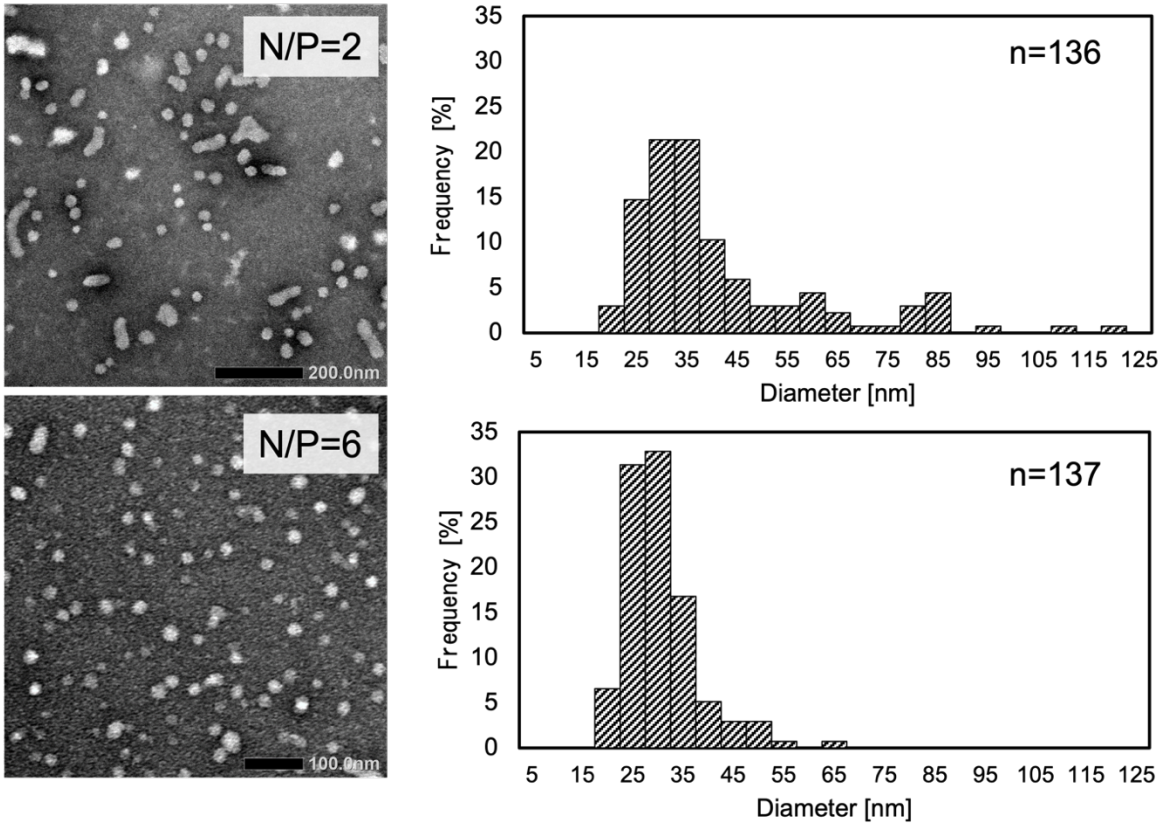


**Figure 3.6** TEM images and histogram of Phe(m) at N/P ratio = 2 and N/P ratio = 6.

Micelle stability plays a crucial role in the successful *in vivo* application. The ability of the polymer to protect the mRNA from attack by anion exchange reactions was investigated. FCS analysis revealed that anion exchange started from a sulfate/phosphate (S/P) ratio of 2, but remained intact even at a very high S/P ratio of 4, which indicates a high stability of Phe(m) against anion exchange in biological environments (**Figure 3.7**). Compared to Phe(m) micelles formed from glycine-conjugated polymer, Phe(m) were able to protect mRNA more effectively. This enhanced stability of micelles incorporating polymers bearing side chains of amino acids engaging in π-π interactions has been recently reported and is in alignment with the results (Mixich et al. 2024; Yang, Miyazaki, et al. 2023).

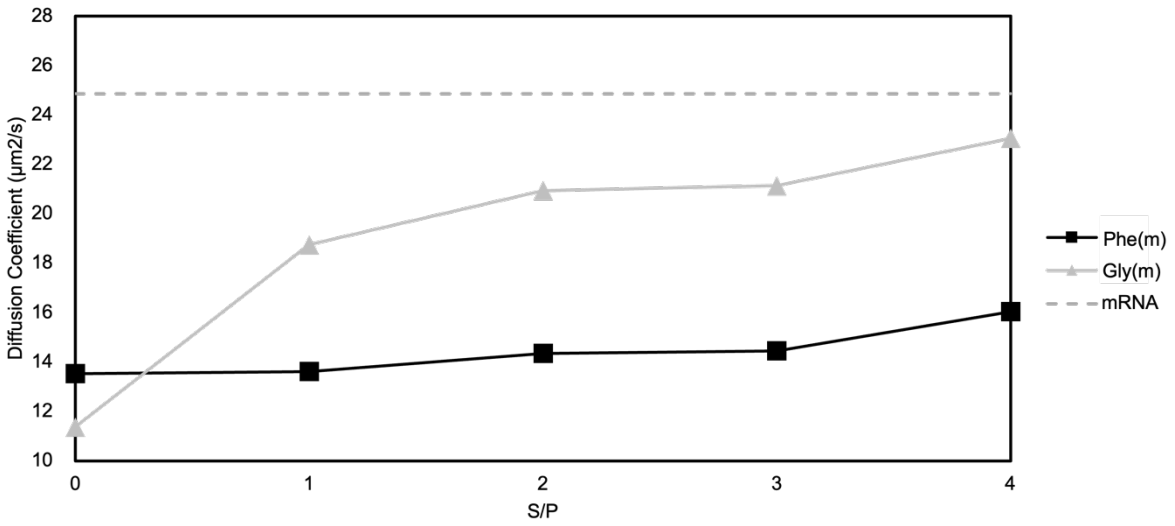


**Figure 3.7** Stability against anion exchange of Phe(m) at N/P ratio 6 and Gly(m) at N/P ratio 3 determined by FCS. The diffusion coefficient of free mRNA is marked as dotted line.

The pKa of the polymer was investigated, as ionizable polymers have demonstrated the ability to destabilize endosomal membranes, promoting endosome escape (Smith et al. 2019; Schmaljohann 2006; Kongkatigumjorn et al. 2018). The escape of the endosome and release to the cytoplasm is necessary for mRNA to be translated, therefore it is in important aspect of mRNA delivery systems. **Figure 3.8a** shows $N_3$-PEG-PG(Phe)'s degree of protonation against pH, determined by titration. The pKa of $N_3$-PEG-PG(Phe) was further found to be around 5.95 (**Figure 3.8b**), which indicated less than 10% of the primary amines in the polymer are in a protonated state at pH 7.4. However, at the endosomal pH of 5.5 the charge of primary amines greatly increases to more than 85% of protonation. Overall, the pKa value of $N_3$-PEG-PG(Phe) indicates its potential to induce pH-dependent membrane disruption at endosomal pH.

To confirm this hypothesis an endosome escape experiment was performed. The ability of Phe(m) to deliver mRNA inside cells and escape the endosome was assessed by CLSM. BxPC-3 cells were incubated with Phe(m) loading Cy5-labeled mRNA and measured at different time points. Before each measurement, the nucleus was stained with DAPI and the

endo/lysosomes stained with LysoTracker-Green. Yellow pixels represent co-localization.

After a 4-hour incubation period, the internalized mRNA was predominantly located within the endosomes of the cells, as indicated by an average colocalization coefficient of 0.75 (**Figure 3.8c**). Subsequently, at 8 hours and 24 hours, there was a gradual reduction in the colocalization of mRNA with the endosomes, reaching a colocalization coefficient of approximately 0.24 after 24 hours. These results provide evidence for the capacity of Phe(m) to facilitate the delivery of mRNA into the cytosol of cells, implying the existence of an endosomal escape mechanism.

The ability of the ionizable $N_3$-PEG-PG(Phe) to disrupt endosomal membranes at endosomal pH was further investigated by an LDH assay, simulating endosome membranes at neutral pH and endosomal pH. Indeed, $N_3$-PEG-PG(Phe) caused high LDH leakage at endosomal pH after 15 minutes in cells (**Figure 3.8d**). At pH 7.4 on the other hand, hardly any LDH leakage was detectable suggesting that there was little membrane disruption. This correlates with the low cytotoxicity observed at pH 7.4 in **Figure 3.3a**. Overall, these observations indicate that $N_3$-PEG-PG(Phe) induces a strong pH-dependent membrane disruption at endosomal pH. This further highlights the great potential of $N_3$-PEG-PG(Phe) for enhancing the endosomal escape or mRNA.

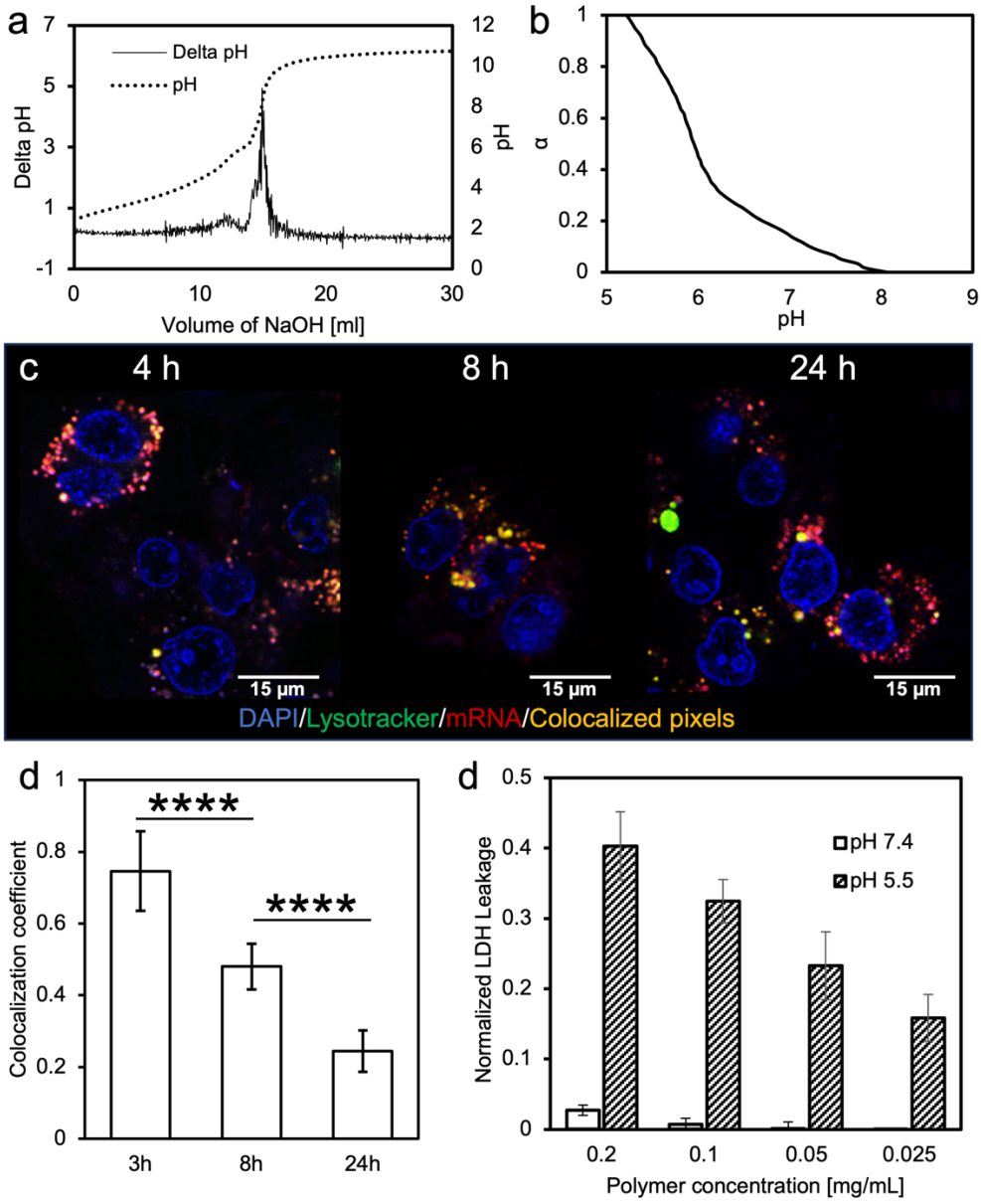


**Figure 3.8** a) Titration curve of $N_3$-PEG-PG(Phe) and the derivative titration curve (delta pH) of $N_3$-PEG-PG(Phe). b) Degree of protonation (α) plotted against the pH determined by titration. pKa at α = 0.5 is 5.95. c) Fluorescent confocal LSM images of HeLa cells transfected by Phe(m) loading Cy5-mRNA after 4 hours, 8 hours and 24 hours. Blue: DAPI; Green: Lysotracker, Red: mRNA; Yellow: colocalization of Lysotracker and mRNA. d) Colocalization coefficients of mRNA and endosomes at several time points. Data are presented as the mean ± S.D. (n = 20 cells). Statistical analysis *via* two-sided unpaired t-test (* $p < 0.05$, ** $p < 0.01$, *** $p < 0.001$, **** $p < 0.0001$). e) LDH leakage in response to the incubation with $N_3$-PEG-PG(Phe) in HeLa cells in at pH 7.4 and the endosomal pH 5.5. Data are presented as the mean ± S.D. (n = 3).

Finally, the ability of Phe(m) to effectively transfect cells and express reporter proteins *in vitro* was confirmed by transfecting HEK-293 and RAW 264.7 cells with mRNA encapsulating Gluc mRNA. Phe(m) resulted in robust protein expression several magnitudes above the naked mRNA group (**Figure 3.9a,b**). Furthermore, the transfections were performed in cell culture media containing RNase-rich fetal bovine serum (FBS). Reports of π interactions of the aromatic residues of RNase (Duh et al. 2015) raised the concern of RNase being associated with the Phe-containing micelle cores. However, Phe(m) are formed in RNase-free conditions, which prohibits RNase from being associated in the micelle's core with the mRNA. After the formation was complete, this data suggests that mRNA can be protected in the core to a degree that allows for strong protein expression in cells. This is in agreement with previous reports from our group, which showed increased protection from enzymatic attacks and anion exchange. (Yang, Miyazaki, et al. 2023; Mixich et al. 2024) This suggests that the increase of protection of the compactly condensed cores of Phe(m) effectively hinders RNase from associating with mRNA compared to cores without aromatic side chains. This is promising for implementing this system for the transfection of immune cells and for *in vivo* applications.

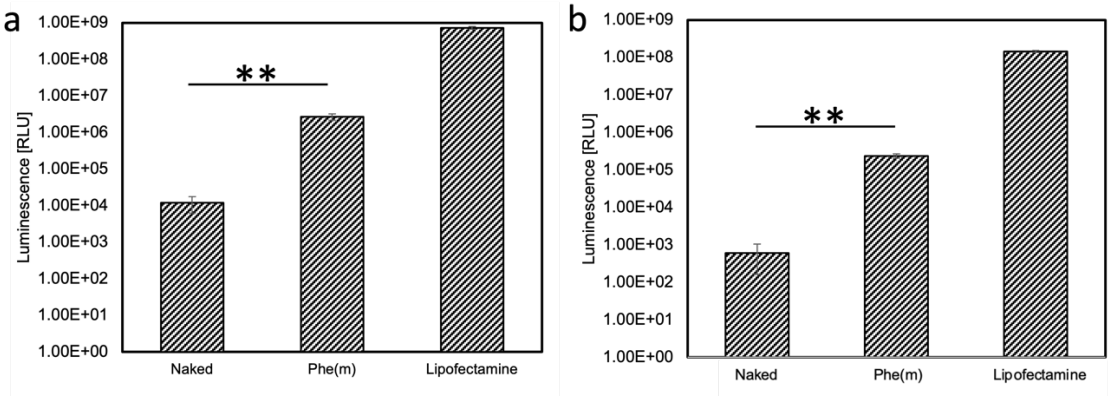


**Figure 3.9** Expression of Gluc in supernatant measured by luminometer in a) HEK-293 cells after 48 hours and b) RAW 264.7 cells after 24 hours. Cells were seeded in 96-well plates and transfected with 200 ng Gluc mRNA . Data are presented as the mean ± S.D. (n = 3). Statistical analysis *via* two-sided unpaired t-test (* $p < 0.05$, ** $p < 0.01$, *** $p < 0.001$)

## 3.4 Conclusion

The synthesis and characterization of a novel flexible block ionomer based on a poly(glycidyl) backbone modified with phenylalanine amino acid for the delivery of various mRNAs was performed. The polymer was designed with specific features including a terminal azide group for surface modifications, a PEG block for improved stability and shielding, and phenylalanine amino acids in the side chain for increased complexation with RNA cargo and enhanced endosomal escape

The polymer was then used to condense various mRNAs into Phe(m) micelles using the designed with $N_3$-PEG-PG(Phe) polymer. The resulting micelles exhibited small diameters of approximately 50 nm and narrow size distributions with low polydispersity index (PDI) at the optimal N/P ratio of 6. Furthermore, the micelles displayed a neutral surface charge and uniform, condensed cores with approximately 1 mRNA molecule associated with 140 polymers. Stability analysis against anion exchange demonstrated successful protection of mRNA by condensation with $N_3$-PEG-PG(Phe).

The pH-responsive properties of the polymer were investigated. The pKa of the polymer was determined to be 5.95, falling within the effective range for increased endosomal escape. Additionally, the phenylalanine amino acid in the polymer induced a pH-responsive membrane disruption and Phe(m) achieved robust endosomal escape of mRNA *in vitro*. This membrane disruptive effect was shown to be specific at endosomal pH, as evidenced by LDH leakage and CCK-8 cytotoxicity studies, which revealed high membrane damage at pH 5.5 but minimal disruption at pH 7.4.Finally, Phe(m)'s capabilities to successfully deliver and translate mRNA *in vitro*, leading to enhanced reporter protein expression, was demonstrated. This highlights the potential of Phe(m) to be used for the transfection of immune cells and for further *in vivo* applications.

# Chapter 4.

# Ligand Installation and Characterization of PIC Micelles

## 4.1 Introduction

Ligand-installed nanocarriers leverage the affinity between ligands and receptors for targeted drug delivery. These interactions can facilitate the delivery of mRNA to specific cells or tissues, and enhance cellular uptake through receptor-mediated endocytosis (Yang, Mixich, et al. 2023). The mRNA delivery to T cells is challenging, highlighting the importance of targeted delivery *via* ligands. CD8 is a protein expressed on cytotoxic T cell surfaces and is an attractive target for directing nanoparticles to T cells. Anti-CD8 Fab' antibody fragments are especially promising targeting ligands, due to their small size and missing Fc region, which helps to avoid size-dependent clearance and immune response to the ligand (Mi, Cabral, and Kataoka 2020b).

mRNA uptake in macrophages can be enhanced by targeting ligands targeting mannose receptors on their surface (Lane et al. 1998; White et al. 2006; Ni, Singh, and Wang 2002; Thalla et al. 2020). Previous research underscores the potential of mannose targeting ligands for the targeted delivery of therapeutic agents to macrophages and dendritic cells (Fukuda, Mochizuki, and Sakurai 2015). This makes mannose an attractive targeting ligand.

In this chapter, we explore the properties of polymeric PIC micelles formed with the phenylalanine-modified block ionomer and mRNA with various targeting ligands attached to their surfaces. Anti-CD8-Fab' ligands were chosen to deliver mRNA to T cells. Mannose was chosen as a ligand to deliver mRNA to macrophages. First, the anti-CD8 Fab' fragment was synthesized from the full antibody and attached to the surface of Phe(m) micelles to form Phe(m)-Fab'. They were characterized by DLS and the integrity of the micelle after the addition of Fab' was confirmed. The number of Fab' on the surface was determined by fluorescence correlation spectroscopy (FCS) measurements at different Fab' concentrations to determine the optimal feeding ratio and to confirm the installation of Fab'.

Next, the targeted delivery of mRNA by Phe(m)-Fab' to $CD8^+$ T cells was studied and the ability to induce robust protein expression in T cells using reporter proteins was investigated. Finally, macrophages were targeted by replacing the Fab' targeting ligand on the micelles with mannose creating Phe(m)-Man. The micelles were characterized, the mRNA delivery to macrophages assessed, and the protein expression between micelles bearing different concentrations of targeting ligand compared.

## 4.2 Materials and methods

### *4.2.1 Materials*

Dulbecco's Modified Eagle's Medium (DMEM), Dynabeads™ FlowComp™, Dynabeads™ Mouse T-Activator CD3/CD28, 1 M HEPES buffer pH 7.4, 8-well chambered borosilicate cover glasses, Gibco Sodium Pyruvate - 100 mM, Gibco MEM Non-Essential Amino Acids, DAPI (4',6-diamidino-2-phenylindole), Penicillin-Streptomycin, and RBC lysis buffer were purchased from Thermo Fisher Scientific (Waltham, MA, U.S.A). Maleimide-PEG4-DBCO was purchased from BroadPharm (San Diego, CA, U.S.A.). Ethylenediaminetetraacetic acid (EDTA) Buffer pH 8.0 was purchased from Takara Bio (Shiga, Japan). Interleukin (IL)-2, IL-7 and IL-15 were purchased from ProSpec-Tany TechnoGene Ltd. (Rehovot, Israel). Alexa Fluor488-NHS was purchased from Sigma-Aldrich (St. Louis, MO, U.S.A.). RPMI 1640 was purchased from Nacalai tesque, Inc. (Kyoto, Japan). Trans-Blot® TurboTM Transfer Pack, Lammli sample buffer, Tris/Glycine/SDS buffer, and Mini-PROTEAN TGX Gels (4-20 %, 15-well comb, 15 μL were purchased from Bio-Rad (Hercules, CA, U.S.A.). Recombinant Mouse CD8 alpha protein(Fc Chimera), anti-human IgG1(HRP), and Prism Ultra Protein Ladder were purchased from Abcam Inc. (Cambridge, United Kingdom). 2-Mercaptoethanol, DTT: DL-Dithiothreito, and CBB R-250: Coomassie Brilliant Blue R-250 were purchased from Tokyo Chemical Industry Co., Ltd. (Tokyo, Japan). Cy5 Label IT Nucleic acid labeling kit was obtained from Mirus Bio (Madison, WI, U.S.A.). Sulfo-Cy5-NHS was purchased from Funakoshi Co., Ltd. (Tokyo, Japan). PTFE filters (0.22 μm) were purchased from Merck KGaA (Darmstadt, Germany). RC Dialysis tubes MWCO: 3,500 Da were obtained from Repligen (Waltham, MA, U.S.A.). Renilla Luciferase Assay and Luciferase Assay was purchased from Promega (Madison, WI, USA). Hoechst 33342 and DAPI solutions were purchased from Dojindo Laboratories (Kumamoto, Japan). 96-well plates were purchased from Corning Inc. (Corning, NY, USA). SephadexTM 200 increase and the

ECL Western Blotting detection reagents were purchased from Cytiva (Marlborough, MA, U.S.A.). Lipofectamine MessengerMAX was obtained from Invitrogen (Waltham, MA, U.S.A.). Ammonium bicarbonate, V8 Protease, 10x Tris-buffered saline (TBS), and methanol were purchased from Fujifilm Wako (Osaka, Japan). Dimethylsulfoxide-d6 + 0.05% TMS (DMSO-d6) was purchased from Cambridge Isotope Laboratories, Inc. (Massachusetts, USA). MojoSort™ was purchased from BioLegend (San Diego, CA, U.S.A.). JetMESSENGER was purchased from Polyplus-transfection (Illkirch-Graffenstaden, France).

*4.2.2 Cell culture*

HEK-293 cells were obtained from RIKEN Cell Bank (Tsukuba, Japan). RAW 264.7 cells were obtained from DS Pharma Biomedical Japan (Osaka, Japan). HEK293 and RAW.264.7 cells were cultured in Dulbecco's modified Eagle's medium (DMEM; Sigma-Aldrich, St. Louis, MO, USA) with 4500 mg/l glucose, L-glutamine, sodium pyruvate, and sodium bicarbonate supplemented with 10% FBS and 1% PS in a humidified incubator at 37 °C and 5% CO2. T cells were cultured in complete RPMI 1640 supplemented with 1% heat inactivated FBS, 0.1% PS, sodium pyruvate, NEAA, HEPES 15 mM, and 2-mercaptoethanol, IL-2 (50 U/mL), IL-7, (20 U/mL) and IL-15 (20 U/mL).

*4.2.3 Mouse $CD8^+$ T cell extraction and activation*

The spleen of 10-week-old Balb/c or C57BL/6 mice were harvested and homogenized to single cell suspensions in 10 mL complete RPMI using the back of a 1 mL syringe and a 70 µm cell strainer. The suspension was centrifuged at 300xg for 5 minutes at 4 °C. Then the supernatant was carefully removed and the pellet was resuspended in 5 mL 1x RBC lysis buffer per spleen. After 4 minutes 25 mL isolation buffer was added and the solution was centrifuged at 300xg for 5 minutes at 4 °C. The supernatant was carefully removed and the pellet was resuspended in isolation buffer at $1x10^7$ cells per 100 µL. Then, $CD8^+$ mouse t cells were extracted using MojoSort™ Mouse CD8 T Cell Isolation Kit following the kit's instructions.

The resulting t cells were cultured in 24 well plates at $5x10^5$ cells per mL in 2 mL complete RPMI supplemented with 50 U/mL IL-2 and 25 U/mL IL7 and IL-15. After extraction, washed Dynabeads™ Mouse T-Activator CD3/CD28 for T-Cell Expansion and Activation were added to the wells in a ratio of 1:1 (cells:beads) according to the manufacturer's instructions and the T cells were incubated in a humidified incubator at 37 °C and 5% $CO_2$.

*4.2.4 Synthesis of DBCO-anti-CD8 Fab'*

Anti-CD8 Fab' was prepared according to **Figure 4.1**.

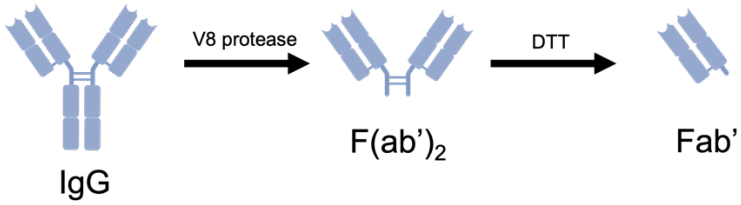


**Figure 4.1** Preparation scheme of of Fab' from IgG

Anti-CD8 antibody was dialyzed against ammonium bicarbonate (100 mM) for 24 hours at 4 °C, concentrated *via* ultrafiltration (MWCO = 10 kDa), and diluted to 10 mg/mL. Next, V8 protease (0.333 mg/mL) in ammonium bicarbonate (100 mM) was mixed with the antibody solution 1:1 and incubated for 18 hours using a thermo shaker (35 °C, 650 rpm). After the digestion was complete, an excess of cold water was added to stop the reaction and SSD-PAGE using an Amersham Imager (Cytiva, Marlborough, USA) to capture the images was conducted to confirm the digestion to F(ab')2. After preparing F(ab')2, the sample was purified by GPC using AKTApurifier (column: SephadexTM 200 increase).

To reduce the antibody and generate Fab', DL-Dithiothreitol (DTT) was added to ammonium bicarbonate (10 mM) in a concentration of 0.5 mmol/L. Subsequently, 100 µL of a 0.5 mg/mL F(ab')2 sample was mixed with an equal volume of DTT solution and allowed to react at 37 °C for 30 minutes. Following the reaction, the solution was transferred to a dialysis

membrane (MWCO = 3500) to remove unreacted DTT. Dialysis was performed against ammonium bicarbonate (10 mM)overnight. Fab' was characterized by SDS-PAGE. Finally, the Fab' was concentrated using ultrafiltration (MWCO = 10000), and the concentration was determined using a NanoDrop ND-1000 spectrophotometer (Thermo Fisher Scientific)

Finally, 5 equivalents of maleimide-$PEG_4$-DBCO (100 μg/mLin DMF) were added to a Fab' solution (0.5 mg/mL) and reacted at room temperature for 2 hours under shaking to synthesize Fab'-DBCO. The product was dialyzed against 10 mM HEPES (pH 7.4) (MWCO = 3500) to remove unreacted maleimide-$PEG_4$-DBCO. The concentration of the obtained solution was measured using a NanoDrop ND-1000 spectrophotometer (Thermo Fisher Scientific, Waltham, MA, USA).

*4.2.5 Preparation of Phe(m)-Fab'*

Micelles containing mRNA were produced through self-assembly by mixing diluted polymer solution with mRNA solution. A 1 mg/ml stock solution of polymer was prepared by dissolving N3-PEG-PG(Phe) in 10 mM sodium acetate (pH 4.5) buffer and filtering the solution through a 0.22 μm filter to remove debris. The polymer solution was then diluted with sodium acetate (pH 4.5) buffer to the desired concentration. mRNA solutions were prepared by diluting mRNA in 10 mM HEPES (pH 7.4) buffer to appropriate concentrations for the required amine/phosphate (N/P) ratios and mixed with the polymer solutions in a 1.5 ml hypertube by placing the mRNA solution in the bottom of the tube and the polymer solution on the wall of the tube and vortexing briefly. The resulting Phe(m) micelles were allowed to equilibrate on ice for 30 minutes. Then 10 (n/n)% anti-CD8-Fab'-$PEG_4$-DBCO was added to the solution and gently mixed. The solution was wrapped in Al-foil, and frozen overnight at -30 °C. It was then slowly thawed over several hours the next day at 4 °C, to allow anti-CD8-Fab'-$PEG_4$-DBCO to react with the polymer's azide end groups to form Phe(m)-Fab'.

*4.2.6 Characterization via dynamic light scattering*

Particle size distribution was characterized by dynamic light scattering (DLS) using a Zetasizer Nano ZS (Malvern Panalytical, Malvern, UK). Micelle solution was diluted to 20 ng/μL RNA concentration in 10 mM HEPES (pH 7.4) buffer and transferred to a low-volume quartz cuvette. Measurements were performed at 25 °C with a 50 mW frequency doubled DPSS Nd:YAG laser (λ=532 nm) at a detection angle of 173°. Hydrodynamic diameters and polydispersity indices were calculated according to the cumulant method.

*4.2.7 Fluorescent labeling of nucleic acids*

mRNA were fluorescently labeled with a Label IT Nucleic acid labeling kit following the manufacturer's instructions. Cy5-labeled mRNAs were purified using EtOH precipitation. The final concentration of the labeled mRNA was determined by using a NanoDrop ND-1000 spectrophotometer (Thermo Fisher Scientific, Waltham, MA, USA)

*4.2.8 Characterization via fluorescence correlation spectroscopy*

Anti-CD8-Fab'-$PEG_4$-DBCO was labeled with sulfo-Cy5-NHS according to the manufacturer's instructions. Free sulfo-Cy5-NHS was removed by dialysis using a dialysis membrane with a molecular weight cutoff (MWCO) of 100 kDa. Micelles with varying Cy5-labeled Fab' loading ratios of 0%, 1%, 5%, 10%, and 20% were prepared as described previously. The resulting micelles, along with Cy5-labeled Fab' as a control, were measured *via* fluorescence correlation spectroscopy (FCS) using an LSM780 confocal microscope equipped with ConfoCor3 and a 40X water objective at room temperature. Cy5-labeled free mRNA and micelles were detected using a HeNe laser at 633 nm. By analyzing the Cy5-labeled Fab' and micelle counts per molecule, the number of Fab' molecules bound per micelle was calculated.

*4.2.9 Cellular uptake in mouse $CD8^+$ T cells*

Mouse $CD8^+$ T cells were extracted, activated, and cultured as described above. After activation overnight, the activation beads were removed with a magnet, and the activated T

cells were transferred to 24 well plates at $5x10^5$ cells per well in 1 mL complete RPMI supplemented with 50 U/mL IL-2 and 25 U/mL IL7 and IL-15. Anti-CD8 antibody was added to one well in a concentration of 0.01 mg/mL and incubated for 30 minutes to block free CD8 on the T cells. Then, the cells were transfected using 3 µg Cy5-labled mRNA by adding naked mRNA, Phe(m), or Phe(m)-Fab' prepared as described earlier, and with Lipofectamine MessengerMAX prepared according to the manufacturer's instructions. T cells incubated with anti-CD8 antibody were also transfected using Phe(m)-Fab' to investigate the inhibition of the Fab' targeting ligand. After 6 h, 5 µL DAPI were added to each well and the cells were incubated for 30 min to stain the nucleus. Then, the T cells were collected and centrifuged at 400xg for 10 minutes at 4 °C. The T cells were washed with PBS to remove free Phe(m)-Fab', Cy5-labled mRNA, and DAPI. The cells were centrifuged again, the D-PBS was removed, and the cells were resuspended in 50 µL mounting solution. The solution was transferred to glass slides for CLSM measurements using an LSM 780 CLSM (Karl Zeiss, Oberkochen, Germany) (Cy5 Ex/Em: 633/697 nm, DAPI Ex/Em: 405/452 nm). The cellular uptake was quantified using Zen software (Karl Zeiss).

*4.2.10 Cellular uptake in mouse splenocytes*

The spleen of 10 weeks old C57BL/6 mice were harvested and homogenized to single cell suspensions in 10 mL complete RPMI using the back of a 1 mL syringe and a 70 µm cell strainer. The suspension was centrifuged at 300xg for 5 minutes at 4 °C. Then the supernatant was carefully removed and the pellet was resuspended in 5 mL 1x RBC lysis buffer per spleen. After 4 minutes 25 mL isolation buffer was added and the solution was centrifuged at 300xg for 5 minutes at 4 °C. The supernatant was carefully removed and the pellet of splenocytes was resuspended in complete RPMI supplemented with 50 U/mL IL-2 at a concentration of $2.7x10^6$ cells/mL. Then, 3 mL containing $8x10^6$ splenocyted were transferred to a 6 well plate and incubated in a humidified incubator at 37 °C and 5% CO2. Cy5-labeled mRNA containing

Phe(m) and Phe(m)-Fab' with 10% Fab' (n/n)% (Fab'/$N_3$) were prepared as described earlier, frozen overnight at -30 °C, and thawed at 4 °C to be used for the transfection experiment. Micelles containing 3 µg Cy5-labeled mRNA were added to the wells. 3 µg naked Cy5-labeled mRNA was added as a negative control, and 3 µg Cy5-labeled mRNA formulated with jetMESSENGER (Polyplus) following the manufacturer's instructions was added as a positive control. After 2.5 hours and 5 hours of incubation, splenocytes were separated into two groups. $CD8^+$ T cells were extracted from one group using MojoSort™ Mouse CD8 T Cell Isolation Kit following the kit's instructions. CD8- cells were extracted from the other group using a Dynabeads™ FlowComp™ Mouse CD8 Kit following the kit's instructions by collecting the supernatant from the final extraction step. The nuclei of the cells were stained with DAPI for 30 minutes, then the cells were centrifuged at 400xg for 10 minutes and washed with D-PBS to remove the remaining micelles, free Cy5-labled mRNA, and DAPI. The cells were centrifuged again, the D-PBS was removed, and the cells were resuspended in 50 µL mounting solution. The solution was transferred to glass slides for CLSM measurements using an LSM 780 CLSM (Karl Zeiss, Oberkochen, Germany) (Cy5 Ex/Em: 633/697 nm, DAPI Ex/Em: 405/452 nm). The cellular uptake was quantified using Zen software (Karl Zeiss).

*4.2.11 In vitro transfection of mouse $CD8^+$ T cells*

Mouse $CD8^+$ T cells were extracted, activated, and cultured as described previously. After 24 hours of activation, the activation beads were removed, and $5x10^5$ T cells were seeded in white 96-well plates in 100 µL complete RPMI supplemented with 50 U/mL IL-2 and 25 U/mL IL7 and IL-15. mRNA containing Phe(m) and Phe(m)-Fab' with 10% Fab' (n/n)% (Fab'/$N_3$) were prepared as described earlier, frozen overnight at -30 °C, and thawed at 4 °C to be used for the transfection experiment. Anti-CD8 antibody was added to five wells containing T cells in a concentration of 0.01 mg/mL and incubated for 30 minutes to block free CD8 on the T cells. The 96 well plate was centrifuged at 400xg for 10 minutes, and the T cell medium

was carefully removed and replaced by 50 µL Opti-MEM. Then Phe(m) and Phe(m)-Fab' micelles containing 300 ng Fluc encoding mRNA were added. 300 ng naked mRNA was added as a negative control and 300 ng Fluc mRNA with jetMESSENGER was added as a positive control. Phe(m)-Fab' micelles containing 300 ng mRNA were added to the wells that were treated with anti-CD8 antibody to assess the transfection inhibition of blocked CD8. After 30 minutes of incubation, the T cell medium that was removed was added back to the wells they were removed from, and the cells were incubated in a humidified incubator at 37 °C and 5% CO2 for 24 h

In a separate plate, Phe(m)-Fab' encapsulating Gluc mRNA were added to wells containing activated $CD8^+$ T cells at various concentrations. Gluc mRNA encapsulated by Lipofectamine Messenger MAX or jetMESSENGER were added at the same concentrations to different wells. After 24 hours, 50 µL of the supernatant of Gluc transfected T cells was transferred to a white 96 well well plate. The luminescence was measured using a GloMax 96 automated microplate luminometer (Promega, Madison, WI, USA) injecting 100 µL Renilla Luciferase assay reagent and integrating for 10 seconds. Measurements were corrected for background luminescence by measuring before the injection of the assay reagent

The 96 well plate containing Fluc transfected T cells was centrifuged at 400xg for 10 minutes and the medium was replaced with 50 µL 1x cell lysis buffer and the cells were incubated for 30 minutes to ensure complete cell lysis. The luminescence was measured using a GloMax 96 automated microplate luminometer (Promega, Madison, WI, USA) injecting 100 µL Luciferase assay reagent and integrating for 10 seconds. Measurements were corrected for background luminescence by measuring before the injection of the assay reagent.

*4.2.12 Synthesis of Man-PEG-PG(Phe)*

Mannose was added to $N_3$-PEG-PG(Phe) *via* click-reaction using mannose-alkyne. 80 mg (0.003 mmol) $N_3$-PEG-PG(Phe) was dissolved in 2 mL $CH_2Cl_2$. 7.7 mg (0.03 mmol)

Propargyl α-D-mannopyranoside was added and the solution was stirred at room temperature. 2 mL solution containing 1.1 mg CuI (0.2 equ. to alkyl), 1.6 mg DIPEA (0.4 equ. to alkyl) and 0.7 mg HOAc (0.4 equ. to alkyl) in $CH_2Cl_2$ was prepared and 200 µL were added to the polymer solution. The mixture was stirred at room temperature for 2 hours and then transferred into a dialysis tube (MWCO = 10 kDA). The product was dialyzed against $CH_2Cl_2$ 3 times and the solvent was removed using a rotary evaporator. Man-PEG-PG(Phe) was collected in water, dried by freeze-drying, and analyzed by an ECS-400 $^1$H-NMR spectrometer (400 MHz; JEOL, Tokyo, Japan) at 80 °C in DMSO-d6 (10 mg/mL).

*4.2.13 Preparation of Phe(m)-Man*

To form Phe(m)-Man micelles, Man-PEG-PG(Phe) and $N_3$-PEG-PG(Phe) were dissolved in RNase free acetate buffer pH 4.5 (10 mmol) at a concentration of 1 mg/mL. Then, the solutions were filtered using a 0.22 µm filter, and a 1:1 mixture ( Man-PEG-PG(Phe) 50%) was prepared resulting in 3 polymer solutions with various Man-concentrations (0%, 50%, 100%). Polymer solutions were diluted in 10 mM sodium acetate (pH 4.5) buffer to appropriate concentrations for the amine/phosphate (N/P) ratio 6, and mixed in a 1.5 ml microcentrifuge tube by placing mRNA solution in 10 mM HEPES (pH 7.4) to the bottom of the tube and the polymer solution on the wall of the tube and vortexing briefly. The micelles were allowed to equilibrate on ice for 30 minutes and then characterized *via* dynamic light scattering using a Zetasizer Nano ZS (Malvern Panalytical, Malvern, UK) as described above.

*4.2.14 Cellular uptake of in RAW 264.7 cells*

To assess the cellular uptake of mRNA in RAW 264.7 cells, Phe(m)-Man with various mannose concentrations containing Cy5-labled mRNA were incubated with RAW 264.7 cells. $3x10^4$ RAW 264.7 cells were seeded in 8 well chambers and incubated overnight in a humidified incubator at 37 °C and 5% CO2. Phe(m)-Man with various mannose concentrations (0%, 50%, 100%) containing Cy5-labled mRNA were prepared as described above. Then,

micelles containing 600 ng Cy5-labeled mRNA were added to the cells. 600 ng naked Cy5-labeled mRNA was added to one chamber as a negative control. After 8 h incubation in the incubator, the cells were washed and stained for 10 minutes with a Hoechst 33342 solution (1:100 in D-PBS; Dojindo Laboratories, Kumamoto, Japan). Finally, cells were washed with D- PBS and fixed with 4% paraformaldehyde (Fujifilm Wako, Osaka, Japan) for 10 minutes. Fluorescence imaging was performed using an LSM 780 CLSM (Karl Zeiss, Oberkochen, Germany) (Cy5 Ex/Em: 633/697 nm, Hoechst Ex/Em: 405/452 nm). Cellular uptake was quantified using Zen software (Karl Zeiss).

*4.2.15 In vitro transfection of macrophages*

mRNA expression in macrophages was assessed by transfecting 264.7 cells with mRNA encoding Fluc and measuring the luminescence. RAW 264.7 cells were seeded overnight in white 96-well plates at a density of $1x10^4$ cells per well. Cells were transfected with 300 ng mRNA encoding Fluc by adding Phe(m)-Man micelles with mannose ligand concentrations of 0%, 50% and 100%. Additionally, 300 ng naked mRNA was added as a negative control. After 24 hours, the cells were washed with D-PBS and 40 µL 1x cell lysis buffer was added to each well. After 30 minutes of incubation time, the luminescence was measured using a GloMax 96 automated microplate luminometer (Promega, Madison, WI, USA) injecting 100 µl luciferase assay reagent (Promega) and integrating for 10 seconds. Measurements were corrected for background luminescence by measuring before the injection of the assay reagent.

## 4.3 Results and discussion

The anti-CD8 Fab' antibody fragment was prepared as described above (**Figure 4.1**). After the reduction of $F(ab')_2$ to Fab' by DTT, SDS-PAGE was performed to confirm the success of the reaction (**Figure 4.2a**). The single band around the size of 48 kDa on the right side indicates the successful reduction to Fab' without any remaining $F(ab')_2$. To confirm the ability of the Fab' to bind to CD8, a Western blot was performed. Both, the full anti-CD8 IgG, as well as the anti-CD8 Fab' was successfully binding to CD8 (**Figure 4.2b**). The line of Fab' was fainter than that of its IgG, suggesting a slightly decreased binding affinity. These results confirm the successful synthesis of anti-CD8 Fab', which will further be used as a targeting ligand on micelles after DBCO conjugation.

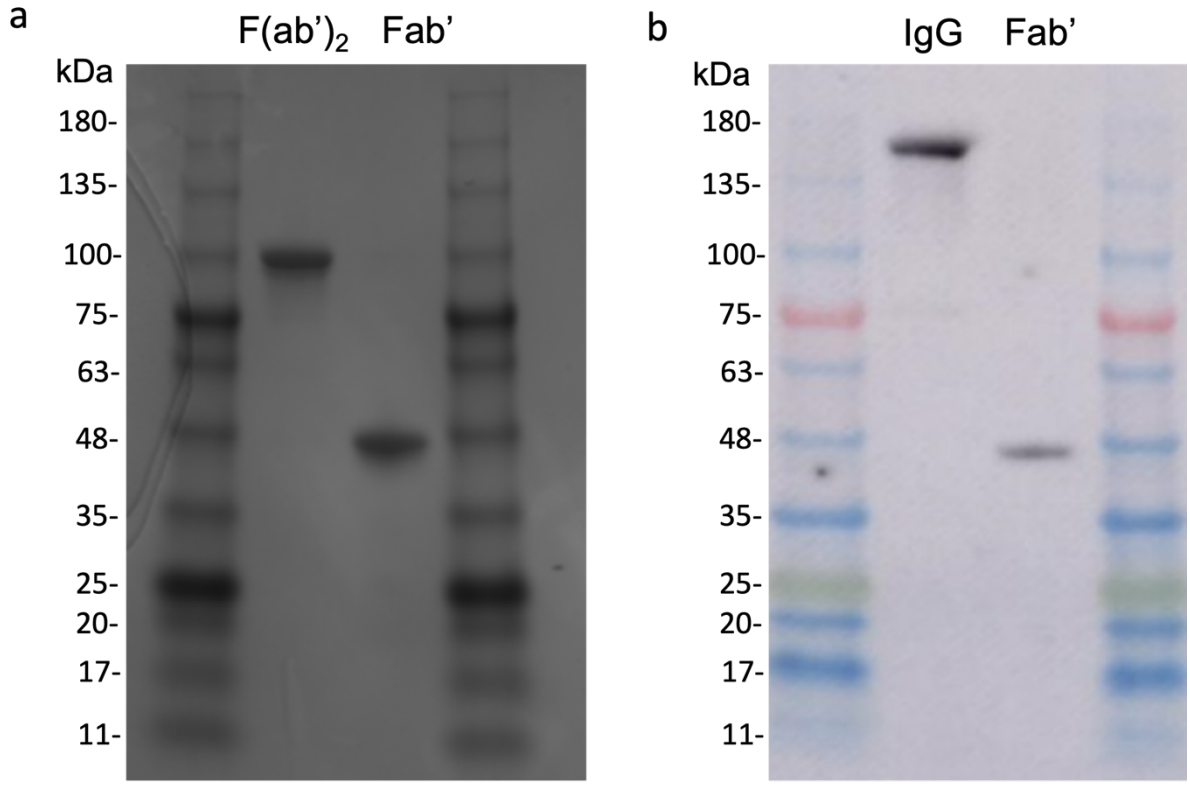


**Figure 4.2** Characterization of Fab'. a) SDS-PAGE of anti-CD8 $F(ab')_2$ and anti-CD8 Fab'. b) Western blot analysis of full anti-CD8 IgG and Fab' fragment.

Phe(m)-Fab' micelles loading mRNA were prepared as described above using

different %(n/n) of DBCO-Fab'. 0%-20% of Fab' were used and attached *via* click reaction and characterized by DLS (**Figure 4.3a,b**). The size and the zeta potential stay mostly unchanged, despite the addition of Fab' on the micelle's surface. This suggests that the micelle morphology or surface interactions of Phe(m)-Fab' can be expected to be similar to that of Phe(m). Also, the micelle did not break during the freeze-thawing process, but remained intact, which supports the high stability of the micelle.

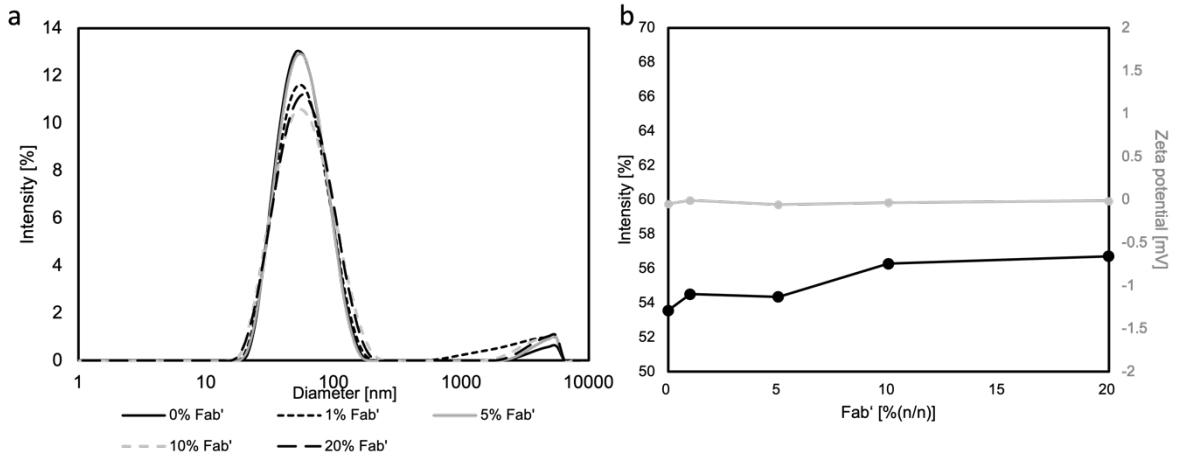


**Figure 4.3** Phe(m)-Fab' characterization of micelles with different Fab' %(n/n). a) shows the DLS and b) shows the zeta potential of the micelles with the corresponding particle sized determined by DLS.

The confirmation of Fab' addition to the surface of micelles was investigated through FCS measurements using labeled Fab' and labeled mRNA. The results of the FCS measurements are presented in **Table 4.1**. The data indicates that the number of Fab' modifications to micelles increased as the loading ratio increased until 10 %(n/n). When comparing the attachment after addition of 10% (n/n) and 20% (n/n), there was no additional Fab' detected, with the maximum number of Fab' around 2.2 per micelle (**Figure 4.4).** This suggests that the optimal amount of Fab' attachment to the micelles is achieved at a loading ratio of around 10% using these conditions.

**Table 4.1** FCS measurement results of Phe(m)-Fab'

| Sample | Fab' [%] | Counts [kHz] | Diffusion time [ms] | Fab' attachment |
|---|---|---|---|---|
| Fab' | | 1.82 | 304 | |
| Phe(m)-Fab' | 0 | 0.00 | 0 | 0.0 |
| | 1 | 2.38 | 2310 | 1.3 |
| | 5 | 3.20 | 2246 | 1.8 |
| | 10 | 3.95 | 2217 | 2.2 |
| | 20 | 4.05 | 2185 | 2.2 |

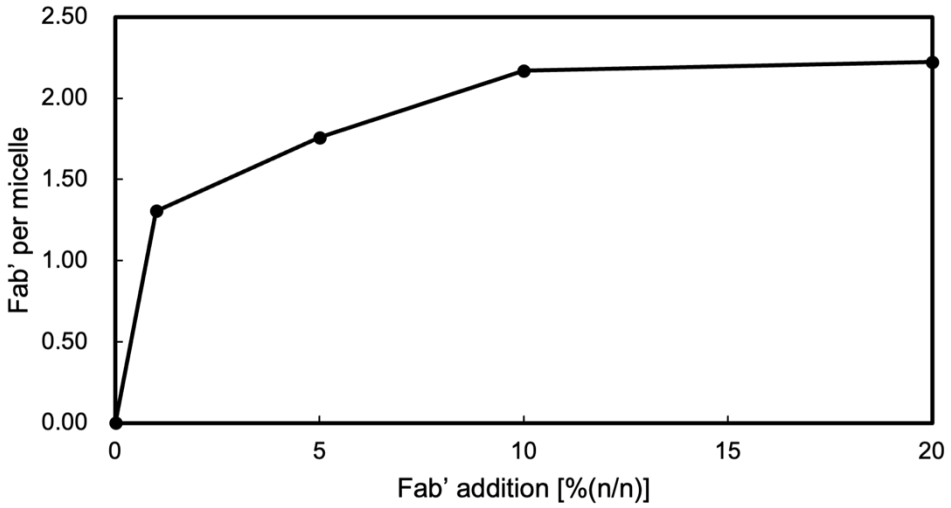


**Figure 4.4** The number of attached Fab' per micelle at various Fab' %(n/n) additions. The number of Fab' on the surface increases up to 2.2 Fab'/micelle by the addition of 10 %(n/n) after which no additional Fab' was attached.

Considering that the number of polymers per micelle was calculated to be around 140, that means 14 Fab' per micelle were added to the solution and most of the Fab' remains free and is not installed at the micelle's surface. Strategies to increase the Fab' attachment might be worth exploring as ligand density is a crucial factor in targeted delivery systems (Mi, Cabral, and Kataoka 2020b). Further exploring DBCO linkers with different PEG spacers, or optimizing reaction conditions, might affect the total number of Fab' attached to the micelle's

surface (S. Chen et al. 2017). Another possible influence of the number of Fab' is that the cleanup of the micelle solution *via* dialysis prior to FCS measurement might affect the micelle. This cleanup procedure is usually not implemented in the Phe(m)-Fab' preparation to reduce the steps of the formation protocol and to keep external influences on the micelle at a minimum.

The effect of Fab' on Phe(m)-Fab was evaluated by measuring the cellular uptake of Cy5-labeled mRNA in $CD8^+$ primary mouse T cells transfected in various conditions. The results of the CLSM measurements are shown in **Figure 4.5a,b**. Compared to naked mRNA or Phe(m), Phe(m)-Fab' had high cellular uptake, similar to that of T cells transfected with Lipofectamine. This suggests that targeted delivery to T cells is supported by the addition of anti-CD8 Fab' on the micelle's surface. This is further supported by the inhibition of cellular uptake after CD8 on the surface of the T cells was blocked by anti-CD8 antibodies.

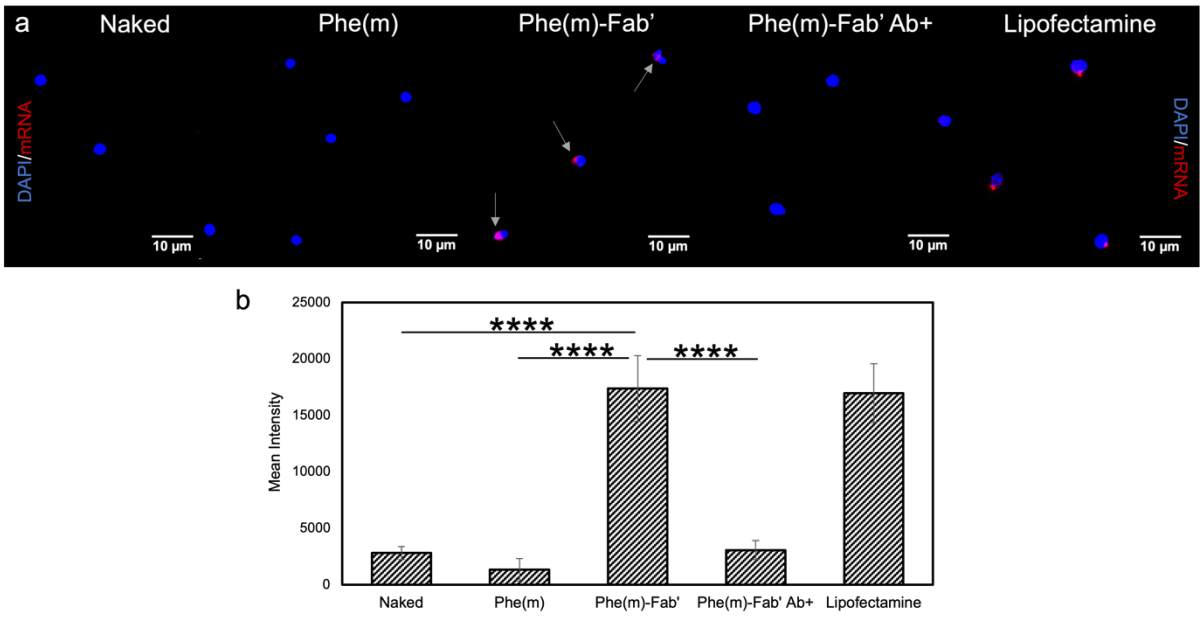


**Figure 4.5** *In vitro* assessment of targeted mRNA delivery of Phe(m)-Fab' to primary $CD8^+$ T cells. A) CLSM images of T cells after treatment with naked Cy5-labeled mRNA, Cy5-labeled mRNA in Phe(m), Phe(m)', Phe(m)-Fab' with T cells after blocking free CD8 on the T cell surface, or lipofectamine. B) mean intensities of Cy5 in T cells based on CLSM images. Data is presented as the mean ± S.D. (n = 20). Statistical analysis *via* two-sided unpaired t-test (* $p < 0.05$, ** $p < 0.01$, *** $p < 0.001$, ****$p < 0.0001$)

To demonstrate the targeted delivery of mRNA in the presence of other cells, splenocytes were transfected with micelles with or without targeting ligand, and the cellular uptake of Cy5-labeled mRNA in $CD8^+$ T cells and $CD8^-$ splenocytes was analyzed *via* confocal laser scanning microscopy (CLSM). The results revealed differential cellular uptake patterns in the two cell types based on the delivery system used (**Figure 4.6a,b**).

In $CD8^-$ splenocytes, Phe(m) and jetMESSENGER exhibited the highest cellular uptake of Cy5-labeled mRNA, indicating efficient non-targeted delivery. Conversely, in $CD8^+$ T cells, Phe(m)-Fab' and jetMESSENGER outperformed the other groups in terms of mRNA delivery. These findings suggest the non-specific nature of jetMESSENGER, as it demonstrated high uptake in both $CD8^+$ T cells and CD8- splenocytes. The targeted delivery of mRNA is crucial for the *in situ* generation of modified immune cells. Off-target transfection may lead to the accumulation of cancer cells in transfected regions, potentially resulting from the local expression of cancer antigen receptors or cancer-attracting chemokine receptors. Therefore, the selective transfection of T cells by Phe(m)-Fab', even in the presence of other $CD8^-$ cells, holds promise for its potential implementation in immunotherapy.

Furthermore, it was observed that Phe(m)-Fab' performed similarly in delivering mRNA to $CD8^+$ T cells; however, in contrast to jetMESSENGER, it resulted in minimal transfection of $CD8^-$ cells. This indicates a targeted delivery approach by Phe(m)-Fab' specifically to $CD8^+$ T cells. The results also demonstrate that there was no significant difference between the uptake at 2.5 hours and 5 hours, which suggests rapid uptake of the system occurs within the initial 2.5 hours. Rapid uptake is crucial to allow for sufficient mRNA delivery before particle degradation *in vivo*. This, together with the targeted delivery Phe(m)-Fab' demonstrated, highlights the potential of the system for *in situ* applications targeting T cells.

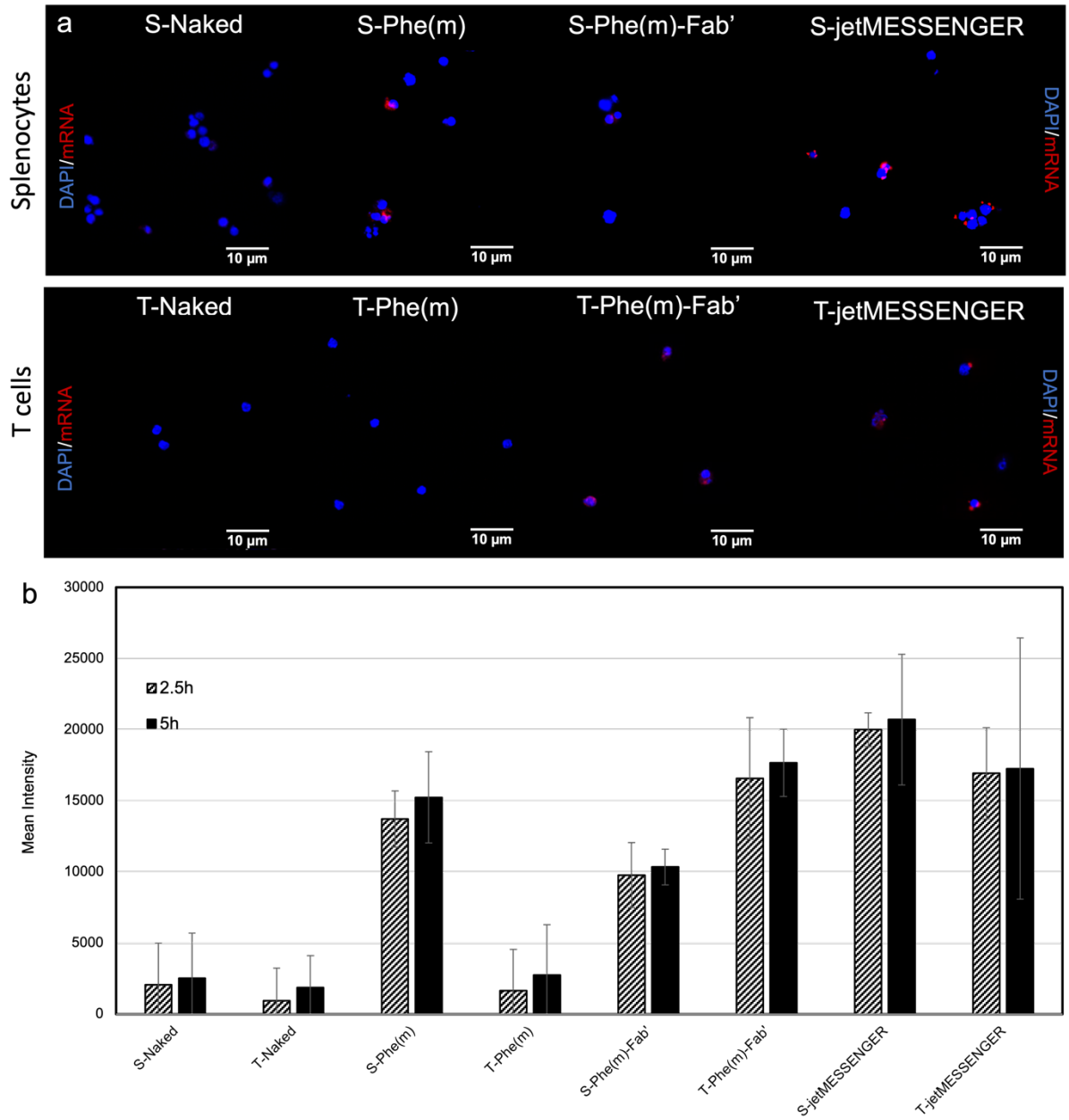


**Figure 4.6** *In vitro* assessment of targeted mRNA delivery of Phe(m)-Fab' to $CD8^-$ splenocytes and $CD8^+$ T cells. a) CLSM images of cells after treatment with naked Cy5-labeled mRNA, Cy5-labeled mRNA in Phe(m), Phe(m)', Phe(m)-Fab' or jetMESSENGER after 2.5 hours incubation. b) Mean intensities of Cy5 in $CD8^+$ T cells and $CD8^-$ splenocytes after 2.5 and 5 hours incubation time based on CLSM images. Data is presented as the mean ± S.D. (n = 20).

Primary $CD8^+$ T cells were transfected with 300 ng Fluc mRNA to confirm the translation of proteins in T cells using naked mRNA and micelles. The results indicated that Phe(m)'

generated enhanced protein expression in T cells compared to the other groups (**Figure 4.7a**) However, when antibodies blocked the CD8 on T cells before transfection, the transfection was inhibited. Similarly, Phe(m) micelles without any targeting ligand were unable to produce robust protein expression. This suggests that the targeting ligand on the surface of the micelles successfully facilitated cellular uptake and expression of mRNA in T cells *in vitro*.

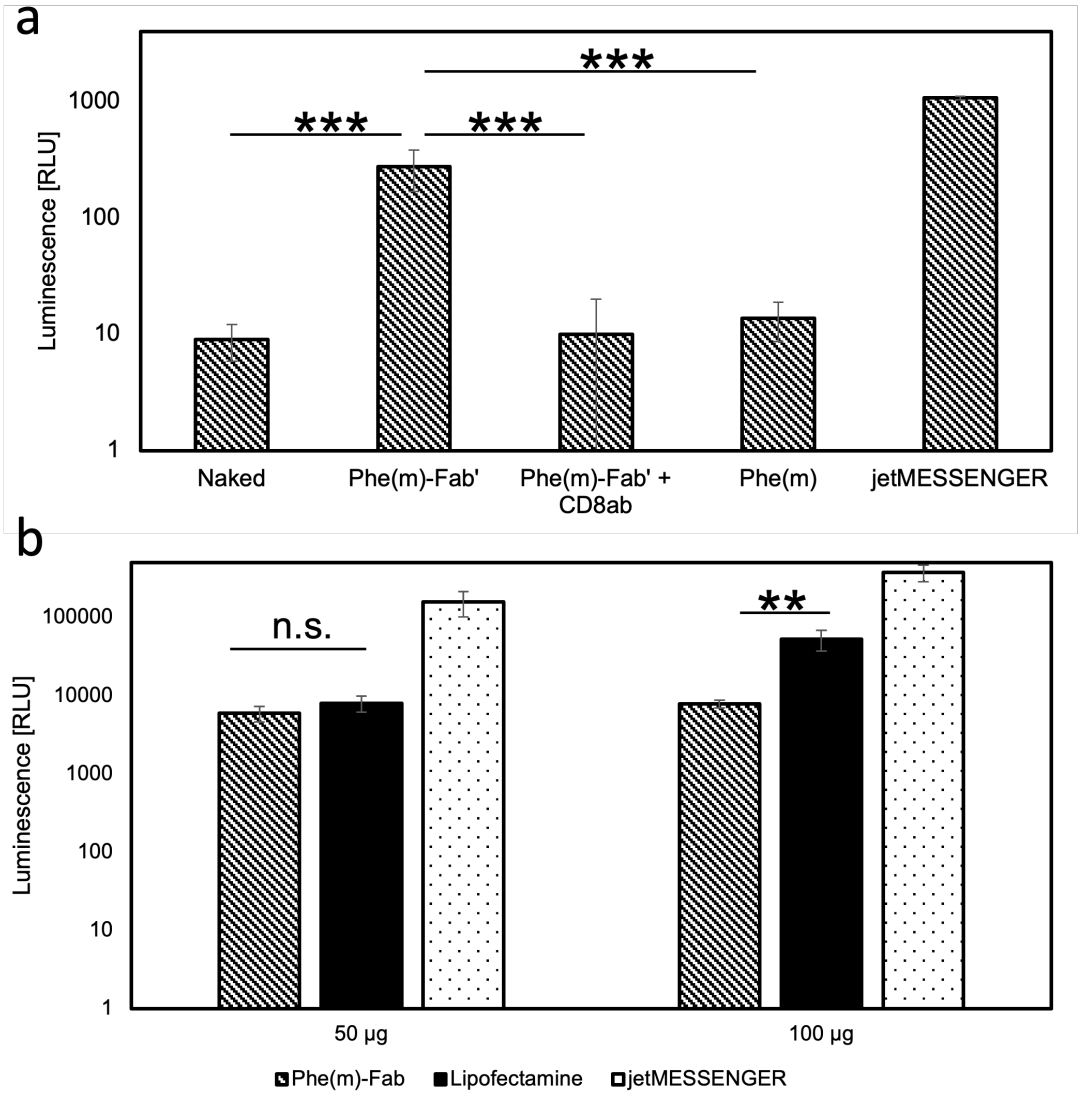


**Figure 4.7** Expression of reporter proteins in primary $CD8^+$ cells. a) Expression of Fluc measured by luminometer after 24 hours in primary $CD8^+$ T cells. Cells were transfected with 300 ng Fluc encoding mRNA and data are presented as the mean ± S.D. (n = 4). Statistical analysis *via* two-sided unpaired t-test (* $p < 0.05$, ** $p < 0.01$, *** $p < 0.001$). b) Expression

of Gluc in primary $CD8^+$ T cells measured by luminometer after 24 hours incubation with different mRNA amounts. Data are presented as the mean ± S.D. (n = 4). Statistical analysis *via* two-sided unpaired t-test (* $p < 0.05$, ** $p < 0.01$, *** $p < 0.001$)

In another transfection experiment Phe(m)Fab' was compared to Lipofectamine MessengerMAX and jetMESSENGER at different mRNA concentrations using Gluc mRNA as a reporter protein (**Figure 4.7b**). In this experiment, jetMESSENGER outperformed Phe(m)-Fab' in both concentrations. However, no significant difference in expression levels between Lipofectamine and Phe(m)-Fab' was observed at a low mRNA dose of 50 µg.

Lipofectamine MessengerMAX is a commercial transfecting reagent and is very effective in transfecting cells *in vitro*. It is based on a phospholipid and forms liposomes with mRNA, and is designed for *in vitro* transfections. Phe(m)-Fab' was able to generate comparable protein expression to the commercial transfecting reagent at low doses, which is impressive, as Lipofectamine generally acts as a positive control in transfection studies, and lipid-based nanoparticles are commonly used for mRNA delivery systems.

jetMESSENGER is another commercial transfecting reagent based on a polymeric linear polyethylenimine (PEI) derivative. It is interesting to note that the polymeric transfection reagent outperformed the ionizable lipid formulation in transfecting T cells. In a comparison with Phe(m)-Fab', jetMESSENGER did result in higher protein expression *in vitro* with $CD8^+$ T cells in all mRNA concentrations. However, these experiments do not reflect realistic conditions during *in vivo* administration, and conclusions about the effectiveness of *in situ* treatments based on these comparisons are not sufficient. For example, our system was able to outperform jetMESSENGER in other important aspects, such as the specificity to deliver mRNA to T cells (**Figure 4.6a,b**). Also, Lipofectamine and jetPEI based reagents are associated with cytotoxicity (T. Wang et al. 2018), whereas our system did not show toxicity (**Figure 3.3a**).

Overall these *in vitro* assessments demonstrated great potential for targeted mRNA delivery to T cells by Phe(m)-Fab'. The micelles specifically delivered mRNA and enhanced the expression of reporter protein in T cells, highlighting the potential of anti-CD8 Fab' as a targeting ligand on Phe(m) to modify T cells *in vivo*.

Macrophages hold great potential for cancer immunotherapy. They exist in large numbers, and compared to T cells, can infiltrate solid tumors more effectively. Also, while tumor-associated M2 macrophages suppress the activity of other immune cells, they themselves do not lose their phagocytic capacity and are less affected by the immunosuppressive environment in the TME (Pan et al. 2022). As a proof of concept, and to demonstrate the versatility of this delivery system, the targeting ligand was changed from anti-CD8 Fab' to mannose to target immune cells like macrophages with this system.

The targeting ligand was attached to the polymer before micelle assembly *via* click reaction. The reaction was successful and the conjugation of mannose to the polymer was determined to be close to 100 % by $^{1}$H-NMR (**Figure 4.8)**

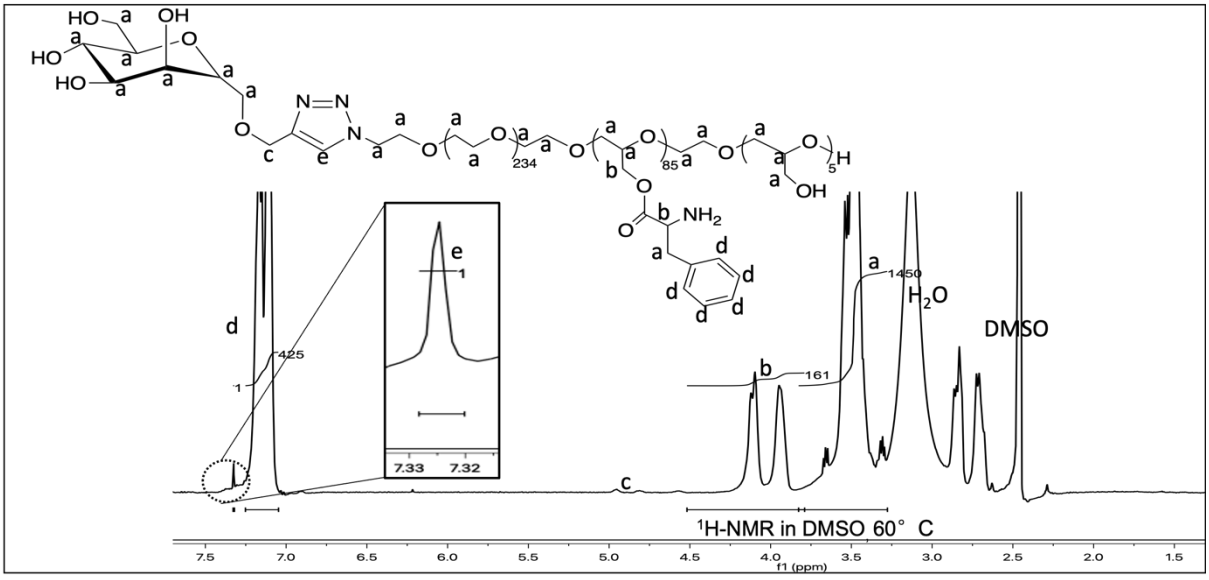


**Figure 4.8** $^{1}$H-NMR spectrum of Man-PEG-PG(Phe). The conjugation rate of mannose to the polymer was close to 100 %.

This polymer was used in conjunction with unconjugated $N_3$-PEG-PG(Phe) to form Phe(m)-Man micelles with mRNA at various % of mannose on the micelle's surface. Phe(m)-Man was characterized by DLS (**Figure 4.9**). The DLS analysis revealed that nanosized micelles with compact size and monodisperse distribution were formed at N/P ratio 6 for all measured Phe(m)-Man. Phe(m)-Man 0% resulted in 55 nm micelles with a PDI of 0.11, Phe(m)-Man 50% resulted in 53 nm micelles with a PDI of 0.10, and Phe(m)-Man 100% resulted in 51 nm micelles with a PDI of 0.08. These are in alignment with Phe(m) and Phe(m)-Fab' suggesting successful micelle formation even when different ligands are attached.

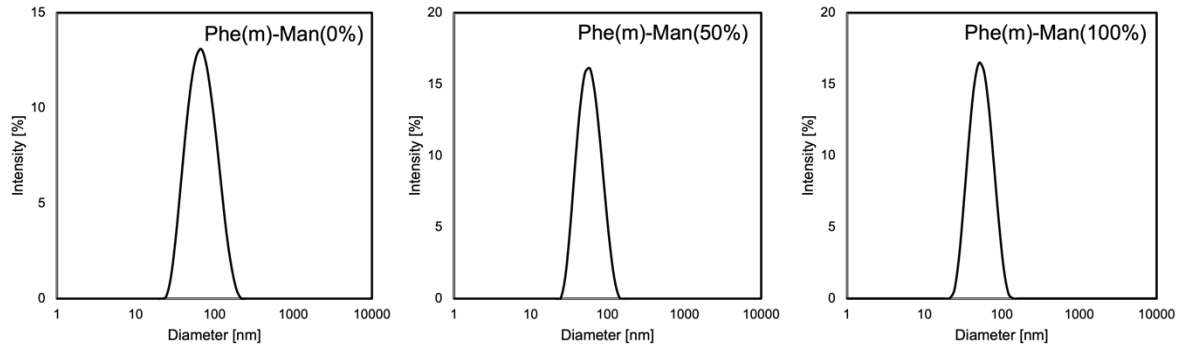


**Figure 4.9** DLS measurements of Phe(m)-Man at different mannose targeting ligand concentrations.

The ability to deliver mRNA to macrophages, and the impact of mannose' on Phe(m)-Man was evaluated by measuring the cellular uptake of Cy5-labeled mRNA in RAW 264.7 macrophage cells transfected with micelles bearing various mannose concentrations. **Figure 4.10a** shows CLSM images after RAW 264.7 cells were incubated with Phe(m)-Man containing Cy5-labeled mRNA for 8 hours. The results indicated a concentration-dependent increase in mRNA uptake with the highest uptake observed in cells incubated with Phe(m)-Man 100%. The uptake is quantified in **Figure 4.10b** and suggests that the addition of mannose on the nanoparticle increases the delivery of mRNA to macrophages.

To further prove this hypothesis, RAW 264.7 cells were transfected with Phe(m)-Man of

various mannose concentrations, and the reporter protein expression was measured. The protein expression in RAW 264.7 cells was found to increase with increasing mannose modification of the micelle, with the highest expression observed in the micelle with 100% mannose, several times higher than Phe(m) without any targeting ligand.

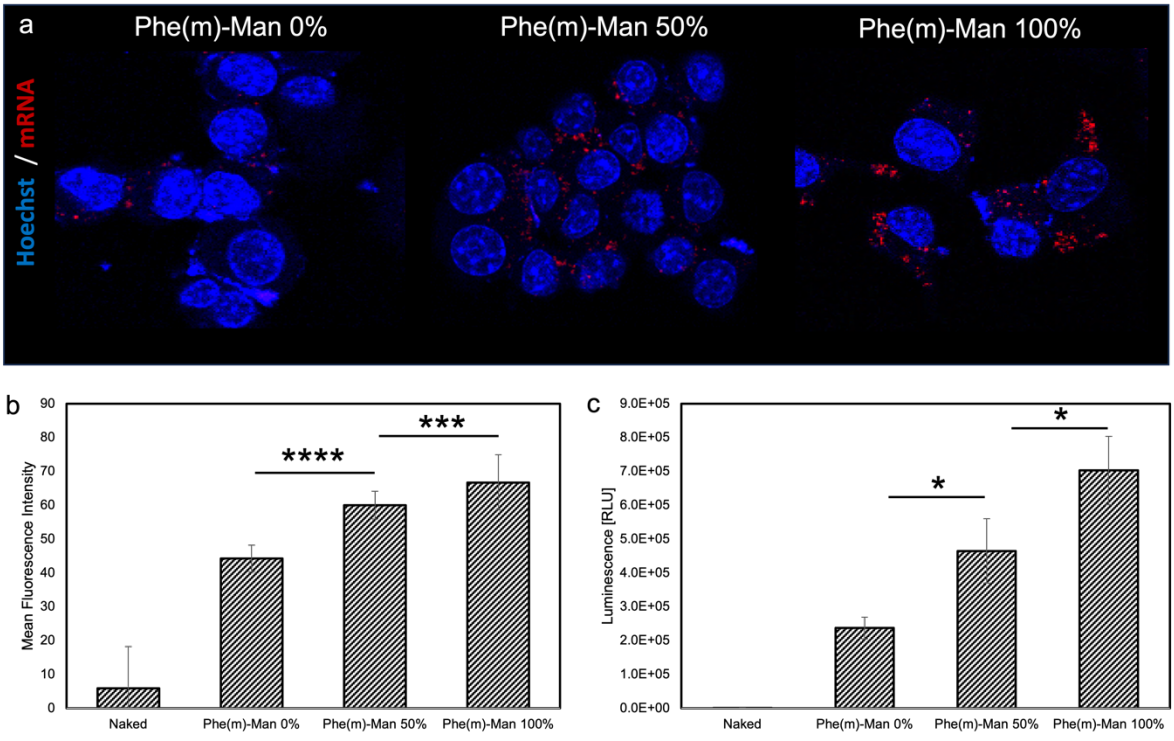


**Figure 4.10** *In vitro* assessment of targeted mRNA delivery of Phe(m)-Man RAW 264.7 macrophage cells. a) CLSM images of RAW 264.7 cells after 8 hours of treatment with Cy5-labeled mRNA in Phe(m)-Man 0%, Phe(m)-Man 50% or Phe(m)-Man 100% with RAW 264.7 cells. b) mean intensities of Cy5 in T cells based on CLSM images. Data is presented as the mean ± S.D. (n = 20). Statistical analysis *via* two-sided unpaired t-test (* $p < 0.05$, ** $p < 0.01$, *** $p < 0.001$, ****$p < 0.0001$). c) Expression of Fluc measured by luminometer after 24 hours in RAW 264.7 cells treated with different micelles or naked mRNA. Cells were transfected with 300 ng Fluc encoding mRNA and data are presented as the mean ± S.D. (n = 5) Statistical analysis *via* two-sided unpaired t-test (* $p < 0.05$, ** $p < 0.01$, *** $p < 0.001$, ****$p < 0.0001$)

Furthermore, the ability to customize the targeting ligand for different immune cell types underscores the versatility and potential clinical utility of the delivery system. This aligns with the principles of personalized medicine and targeted therapeutics, where the ability to tailor the delivery system to specific immune cell populations can significantly enhance its effectiveness in diverse therapeutic applications.

## 4.4 Conclusion

Anti-CD8 Fab' targeting ligands were successfully digested from full antibodies and attached successfully *via* click reaction to the surface of Phe(m)-Fab'. DLS measurements of Phe(m)-Fab' at N/P ratio of 6 using various Fab' %(n/n) revealed minimal impact on the micelle's size or surface charge after Fab' installation. The optimal feeding ratio of Fab' was determined to be 10 %(n/n) with an attachment of 2 Fab' per micelle

The attachment of anti-CD8 Fab' targeting ligands significantly improved the uptake of Cy5-mRNA in cytotoxic T cells mediated by the interactions with CD8 on the T cells surface. This was demonstrated by the reduced uptake of mRNA when CD8 on the T cell's surface was blocked by anti-CD8 antibodies before incubation with Phe(m)-Fab'. This effect was reproduced in transfection experiments, where Phe(m)-Fab' specifically enhanced the expression of reporter protein in T cells. Impressively, targeted uptake in T cells by the Fab' targeting ligand was also observed when whole splenocytes were transfected with Phe(m)-Fab' suggesting specific delivery of mRNA to T cells, even in the presence of other splenocytes.

To demonstrate the versatility of this system micelles with mannose instead of Fab' as a targeting ligand were successfully prepared and Phe(m)-Man at N/P = 6 with varying mannose conjugations were characterized by DLS. It was revealed that Phe(m)-Man forms condense, monodisperse micelles at mannose concentrations of 0 %, 50 % and 100 %. Phe(m)-Man demonstrated targeted delivery and enhanced uptake in the macrophage cell line RAW 264.7. Mannose ligand attachment on the micelle further resulted in enhanced protein expression of reporter protein *in vitro* in RAW 264.7 cells.

This highlights the ability of Fab' to induce targeted delivery of mRNA to T cells and is promising for the implementation of Phe(m)-Fab' to generate T cells with chimeric receptors for enhanced cancer therapy. The versatility of this system is underscored by the enhanced transfection of macrophages by replacing Fab' with mannose targeting ligands.

# Chapter 5.

# Biological Evaluation

## 5.1 Introduction

The success of *in situ* cell therapy depends on the generation of functional cancer-targeting T cells. This chapter investigates the potential of Phe(m)-Fab' to engineer T cells by delivering functional mRNA resulting in the transient expression of cancer-targeting proteins on T cells. Experiments will be conducted with the goal in mind to develop an off-the-shelf treatment for the transient generation of modified T cells *in vivo*.

First, the expression of anti-CD19 CAR protein and CXCR4-tGFP protein from their respective IVT synthesized mRNA will be investigated and the generation of modified T cells using Phe(m)-Fab' will be confirmed. The expression of mRNA over time will also be investigated to confirm the transient expression of the protein on T cells engineered by mRNA. Next, the efficacy of the engineered T cells to target and fight cancer cells will be assessed. Anti-CD19 CAR T cells will be generated using Phe(m)-Fab' and the ability to kill cancer cells expressing CD19 will be assessed. To generate T cells with enhanced penetration into solid tumors, the migration of CXCR4 T cells transfected by Phe(m)-Fab' towards 4T1 cancer cells will also be investigated in an invasion assay. Finally, the expression of protein *in vivo* will be investigated. First, the *in vivo* expression of the reporter protein Fluc and the functional CXCR4-tGFP mRNA in 4T1 tumor-bearing mice.

## 5.2 Materials and methods

### *5.2.1 Materials*

Sodium acetate buffer pH 4.5, 4% paraformaldehyde, and Dulbecco's Phosphate-Buffered Saline (D-PBS) were purchased from Fujifilm Wako Pure Chemical, Co., Inc. (Osaka, Japan). Dynabeads™ FlowComp™, Dynabeads™ Mouse T-Activator CD3/CD28, Dulbecco's Modified Eagle's Medium (DMEM), Penicillin-Streptomycin, 1 M HEPES buffer pH 7.4, 8-well chambered borosilicate cover glasses, Gibco Sodium Pyruvate - 100 mM, Gibco MEM Non-Essential Amino Acids, DAPI (4',6-diamidino-2-phenylindole), and RBC lysis buffer were purchased from Thermo Fisher Scientific (Waltham, MA, U.S.A). BD Tumor Dissociation Reagent was purchased from Beckton, Dickson and Company BD Biosciences (San Jose, CA, U.S.A.) Ethylenediaminetetraacetic acid (EDTA) Buffer pH 8.0 was purchased from Takara Bio (Shiga, Japan). Interleukin (IL)-2, IL-7 and IL-15 were purchased from ProSpec-Tany TechnoGene Ltd. (Rehovot, Israel). Alexa Fluor488-NHS was purchased from Sigma-Aldrich (St. Louis, MO, U.S.A.). RPMI 1640 was purchased from Nacalai tesque, Inc. (Kyoto, Japan). 2-Mercaptoethanol was purchased from Tokyo Chemical Industry Co., Ltd. (Tokyo, Japan). Cy5 Label IT Nucleic acid labeling kit was purchased from Mirus Bio (Madison, WI, U.S.A.). PTFE filters (0.22 μm) were purchased from Merck KGaA (Darmstadt, Germany). RC Dialysis tubes MWCO: 3,500 Da were obtained from Repligen (Waltham, MA, U.S.A). Corning® BioCoat™ Matrigel® Invasion Chamber, 8.0 μm PET Membrane for 24-well plates, and well plates were purchased from Corning Inc. (Corning, NY, USA). Fetal bovine serum (FBS) was purchased from Cytiva (Marlborough, MA, U.S.A.). Hoechst 33342 solution was purchased from Dojindo Laboratories (Kumamoto, Japan). MojoSort™ and all labeled antibodies were purchased from BioLegend (San Diego, CA, U.S.A.). JetMESSENGER was purchased from Polyplus-transfection (Illkirch-Graffenstaden, France). Lipofectamine MessengerMAX was purchased from Invitrogen (Waltham, MA, U.S.A.).

*5.2.2 Cell culture*

A20, 4T1, and RAW 264.7, T cells were obtained from DS Pharma Biomedical Japan (Osaka, Japan), 4T1-HA cells were kindly gifted from Mr. Pengwen Chen and Human embryonic kidney 293 (HEK-293) cells from RIKEN Cell Bank (Tsukuba, Japan). HEK293 cells were cultured in Dulbecco's modified Eagle's medium (DMEM; Sigma-Aldrich, St. Louis, MO, USA) with 4500 mg/l glucose, L-glutamine, sodium pyruvate, and sodium bicarbonate supplemented with 10% FBS and 1% PS. A20 were cultured in RPMI 1640 medium supplemented with 10% FBS and 1% PS. Suspended and attached cells were used for passages. 4T1 and 4T1-HA were cultured in RPMI 1640 medium supplemented with 10% FBS and 1% PS. T cells were cultured in complete RPMI 1640 supplemented with 1% heat inactivated FBS, 0.1% PS, sodium pyruvate, NEAA, HEPES 15 mM, and 2-mercaptoethanol, IL-2 (50 U/mL), IL-7, (20 U/mL) and IL-15 (20 U/mL).All cells were cultured in a humidified incubator at 37 °C and 5% CO2.

*5.2.3 Animal experiments*

All animal experiments were conducted according to the Guidelines for the Care and Use of Laboratory Animals and with the approval of the Animal Experiment Committee of the University of Tokyo. 7-week-old or 12 weeks old female BALB/c or C57BL/6 mice were purchased from Jackson Laboratory Japan (Yokohama, Japan) and kept in a climate-controlled animal facility with a 12-hour light cycle and provided food and water ad libitum.

*5.2.4 Expression of CAR and CXCR4 mRNA in RAW 264.7 cells*

To confirm the functionality of CXCR4 and CAR mRNA, RAW 264.7 cells were transfected with CXCR4-GFP encoding mRNA using Lipofectamine MessengerMAX and characterized by CLSM measurements. 8-well chambers were seeded with $3x10^4$ RAW 264.7 cells and incubated in a humidified incubator at 37 °C and 5% CO2 overnight. The cells were transfected using 300 ng CXCR4-tGFP or anti-CD19 CAR mRNA formulated with

Lipofectamine MessengerMAX. After incubation overnight, the cells were washed and stained for 10 minutes with a DAPI solution (1:100 in D-PBS). Then, the medium of T cells transfected with CAR mRNA was replaced with 100 µL of D-PBS containing FITC-conjugated CD19-protein to attach to anti-CD19 CAR T cells. After 40 minutes of incubation time, the cells were washed with D-PBS two times and finally resuspended in 50 µL mounting solution and transferred to glass slides. The slides were measured using an LSM 780 CLSM (Karl Zeiss, Oberkochen, Germany) (DAPI Ex/Em: 405/452 nm, FITC/tGFP Ex/Em: 488/561 nm)

### *5.2.5 Expression of anti-CD19 CAR mRNA in mouse CD8$^+$ T cells*

To assess the generation of anti-CD19 CAR T cells, mouse CD8$^+$ T cells were transfected with anti-CD19 CAR mRNA and characterized by CLSM. Mouse CD8$^+$ T cells were extracted, activated, and cultured as described earlier. After 24 h, the activation beads were removed, and the T cells were seeded in a 24-well plate at a density of $3.5x10^5$ cells/well in 1 mL complete RPMI supplemented with 50 U/mL IL-2 and 25 U/mL IL7 and IL-15. Anti-CD19 CAR encoding mRNA containing Phe(m) and Phe(m)-Fab' with 10% Fab' (n/n)% (Fab'/$N_3$) were prepared as described earlier, frozen overnight at -30 °C, and thawed at 4 °C to be used for the transfection experiment. Phe(m) and Phe(m)-Fab' micelles containing 3 µg mRNA were added to the cells respectively. 3 µg naked mRNA was added as a negative control and the plate was incubated in a humidified incubator at 37 °C and 5% CO2 for 24 hours. The cells were collected in 1.5 mL tubes, and centrifuged at 400xg for 10 minutes. Then, the medium was replaced with 100 µL of D-PBS containing FITC-conjugated CD19-protein to attach to anti-CD19 CAR T cells and DAPI to stain the nucleus. After 40 minutes of incubation time, the cells were washed with D-PBS two times to remove any free FITC-conjugated CD19-protein and DAPI, and finally resuspended in 50 µL mounting solution and transferred to glass slides. The slides were measured using an LSM 780 CLSM (Karl Zeiss, Oberkochen, Germany) (DAPI Ex/Em: 405/452 nm, FITC Ex/Em: 488/561 nm). The amount of FITC-conjugated CD19-protein on

the cell surface was quantified using Zen software (Karl Zeiss).

*5.2.6 Expression profile of anti-CD19 CAR mRNA*

The expression time of anti-CD19 CAR on T cells was observed. Mouse $CD8^+$ T cells were extracted, activated, cultured, and transfected with jetMESSENGER encapsulating anti-CD19 CAR mRNA as described above. The expression of CAR was measured after staining the nucleus and the CAR by using an LSM 780 CLSM (Karl Zeiss, Oberkochen, Germany) (DAPI Ex/Em: 405/452 nm, tGFP Ex/Em: 488/561 nm) as described above at several time points over 6 days.

*5.2.7 Killing assay of anti-CD19 CAR T cells*

$5x10^3$ adherent A20 cells were seeded in 50 µL medium in transparent 96-well plates and incubated overnight. Mouse $CD8^+$ T cells were extracted, activated and cutured for 24 hours as described above. Then, they were transfected with anti-CD19 CAR mRNA using Phe(m), Phe(m)-Fab', naked mRNA, or jetMESSENGER as described above and incubated for another 24 hours. $2x10^4$ transfected T cells in 100 mL complete RPMI supplemented with 50 U/mL IL-2, and 25 U/mL IL-7 and IL-15 were added to the wells with A20 cells. After 30 hours of incubation time, the supernatant was removed and the remaining A20 cells were characterized by CCK-8 assay following the manufacturer's protocol. Absorption at 450 nm was measured using an Infinite M200 microplate reader (Tecan, Männendorf, Switzerland).

*5.2.8 Expression of CXCR4-tGFP mRNA in mouse $CD8^+$ T cells*

To assess the generation of CXCR4-tGFP T cells, mouse $CD8^+$ T cells were transfected with CXCR4-tGFP mRNA and characterized by CLSM. Mouse $CD8^+$ T cells were extracted, activated, and cultured as described earlier. After 24 h, the activation beads were removed, and the T cells were seeded in a 24-well plate at a density of $3.5x10^5$ cells/well in 1 mL complete RPMI supplemented with 50 U/mL IL-2 and 25 U/mL IL7 and IL-15. CXCR4-tGFP encoding mRNA containing Phe(m)-Fab' with 10% Fab' (n/n)% (Fab'/$N_3$) were prepared as described

earlier, frozen overnight at -30 °C, and thawed at 4 °C to be used for the transfection experiment. Phe(m)-Fab' micelles containing 3 µg mRNA were added to the cells respectively. 3 µg naked mRNA was added as a negative control, and 3 µg mRNA in jetMESSENGER were added as a positive control, and the plate was incubated in a humidified incubator at 37 °C and 5% CO2 for 24 hours. The cells were collected in 1.5 mL tubes, and centrifuged at 400xg for 10 minutes. Then, DAPI solution was added to stain the nucleus. After 15 minutes of incubation time, the cells were washed with D-PBS and finally resuspended in 50 µL mounting solution and transferred to glass slides. The slides were measured using an LSM 780 CLSM (Karl Zeiss, Oberkochen, Germany) (DAPI Ex/Em: 405/452 nm, tGFP Ex/Em: 488/561 nm). The mean intensity of tGFP on the cell surface was quantified using Zen software (Karl Zeiss).

*5.2.9 Expression profile of CXCR4-tGFP mRNA*

The expression time of CXCR4-tGFP on T cells was observed. Mouse $CD8^+$ T cells were extracted, activated, cultured, and transfected with jetMESSENGER encapsulating CXCR4-tGFP mRNA as described above. The expression of CXCR4-tGFP was measured after staining the nucleus using an LSM 780 CLSM (Karl Zeiss, Oberkochen, Germany) (DAPI Ex/Em: 405/452 nm, tGFP Ex/Em: 488/561 nm) as described above at several time points over 6 days.

*5.2.10 Invasion assay of CXCR4 T cells*

The migration and invasion of CXCR4 T cells towards CXCL12 expressing 4T1 cancer cells was assessed by invasion assay. $3x10^4$ viable 4T1 cells were seeded on the bottom of a 24-well plate and incubated overnight. On the next day, the medium was replaced to complete RPMI supplemented with 50 U/mL IL-2 and 25 U/mL IL7 and IL-15. Then, Corning® BioCoat™ Matrigel® Invasion Chambers, 8.0 µm containing 1 mL complete RPMI supplemented with 50 U/mL IL-2 and 25 U/mL IL7 and IL-15 with $2.5x10^4$ mouse $CD8^+$ T cells was added to the wells. The T cells were extracted, activated, cultured, and transfected with CXCR4-tGFP mRNA as described before. To transfect the T cells, naked mRNA, Phe(m),

Phe(m)-Fab' or Lipofectamine MessengerMAX was used. The chambers were incubated for 24 hours to allow the T cells to migrate through the Matrigel. Then, the number of T cells in the supernatant of the bottom well was counted using a hemocytometer.

*5.2.11 In vivo luciferase expression*

*In vivo* reporter protein expression was assessed by subcutaneous injection of Fluc-mRNA-loaded micelles in mice bearing 4T1-HA tumors. Phe(m) or Phe(m)-Fab' encapsulating mRNA encoding for Fluc were prepared at N/P = 6 and injected intratumoral at the 4T1-HA tumor site at a dose of 5 µg mRNA per mouse. As a negative control, the same amount of naked mRNA was administered in the same way. Luciferase expression was measured by injecting 200 µL VivoGlo Luciferin solution (15 mg/ml in D-PBS; Promega, Madison, WI, USA) intravenously, and imaging luminescence in an IVIS imaging system (PerkinElmer, Waltham, MA, USA) for 10 seconds under anesthesia with isoflurane.

*5.2.12 IVIS of in situ generated CXCR4-tGFP$^+$ cells*

The expression of CXCR4 *in vivo* was investigated by IVIS measurements. 13 weeks old BALB/c mice were inoculated subcutaneously with $0.5x10^5$ viable 4T1 cells close to the breast. When tumors were established, mice were randomized, and Phe(m)-Fab' or Phe(m) containing 5 µg of CXCR4-tGFP mRNA was injected subcutaneously. Naked mRNA was injected in the same way as a negative control. After 30 hours, the tGFP expression was measured using an IVIS imaging system (PerkinElmer, Waltham, MA, USA) for 10 seconds under anesthesia with isoflurane.

*5.2.13 Flow cytometry of in situ generated CXCR4-tGFP$^+$ cells in organs*

The expression of CXCR4 *in vivo* was investigated. BALB/c mice were inoculated subcutaneously with $0.5x10^5$ viable 4T1 cells close to the breast. When subcutaneous tumors were established, mice were randomized, and Phe(m), Phe(m)-Fab' containing 5 µg of CXCR4-tGFP mRNA was injected subcutaneously. Naked mRNA was injected in the same

way as a negative control. mRNA formulated with *in-vivo* jetPEI according to the manufacturer's instructions was injected in the same way as a positive control. After 24 hours, the mice were sacrificed and spleen, lymph nodes, and tumor were collected. Tumors were digested with a BD Tumor Dissociation Reagent (Beckton, Dickson and Company BD Biosciences San Jose, CA, U.S.A.) and homogenized to a single-cell suspension. Red blood cells were lysed using RBC lysis buffer according to the manufacturer's instructions. Spleen and lymph nodes were homogenized to a single cell suspension and the red blood cells of spleen were lysed using RBC lysis buffer. Then, $1x10^6$ of each cell type was resuspended, in 100 µL isolation buffer and the Fc receptors on the cell's surface were blocked for 40 minutes at 4 °C. After washing the cells with isolation buffer two times, a cocktail containing anti-CD45-APC antibody and anti-CD8-PE antibody in isolation buffer was added and the cells were incubated for 40 minutes. Finally, the cells were washed with isolation buffer two times and transferred to a FACS tube through the cell strainer. The cells were analyzed by flow cytometry using a BD FACSAria™ III Cell Sorter (BD Bioscience, Franklin Lakes, NJ, USA).

## 5.3 Results and discussion

The generation of chimeric immune cells using synthesized anti-CD19 CAR mRNA and CXCR4-tGFP mRNA was confirmed through a series of transfection experiments. RAW 264.7 cells were transfected with Lipofectamine MessengerMAX to introduce the synthesized mRNA into the cells. The expression of the proteins was subsequently confirmed using CLSM. Following the transfection of anti-CD19 CAR mRNA, the cells were stained with CD19 protein conjugated with FITC to visualize the expression of anti-CD19 CAR on the cell surface (**Figure 5.1a**). The presence of anti-CD19 CAR was confirmed by the FITC signal of CD19 protein attached to the cell's surface. Additionally, the expression of CXCR4-tGFP was confirmed by the visualization of tGFP on the cell's surface (**Figure 5.1b**). These results provide evidence that the synthesized mRNAs are capable of producing anti-CD19 CAR and CXCR4 modified immune cells.

To test the ability of Phe(m)-Fab' to generate anti-CD19 CAR T cells, primary cytotoxic $CD8^+$ mouse T cells were transfected with anti-CD19 CAR mRNA using Phe(m) or Phe(m)-Fab'. The expression of CAR was confirmed by staining the cells with CD19-FITC protein. **Figure 5.2a,b** shows the successful generation of anti-CD19 CAR T cells indicated by the increased binding of CD19-FITC to their surface. While Phe(m)-Fab' can generate CAR T cells, Phe(m) without targeting ligand expresses significantly lower anti-CD19 CAR proteins on the surface, highlighting the importance of the Fab' targeting ligands to transfect T cells.

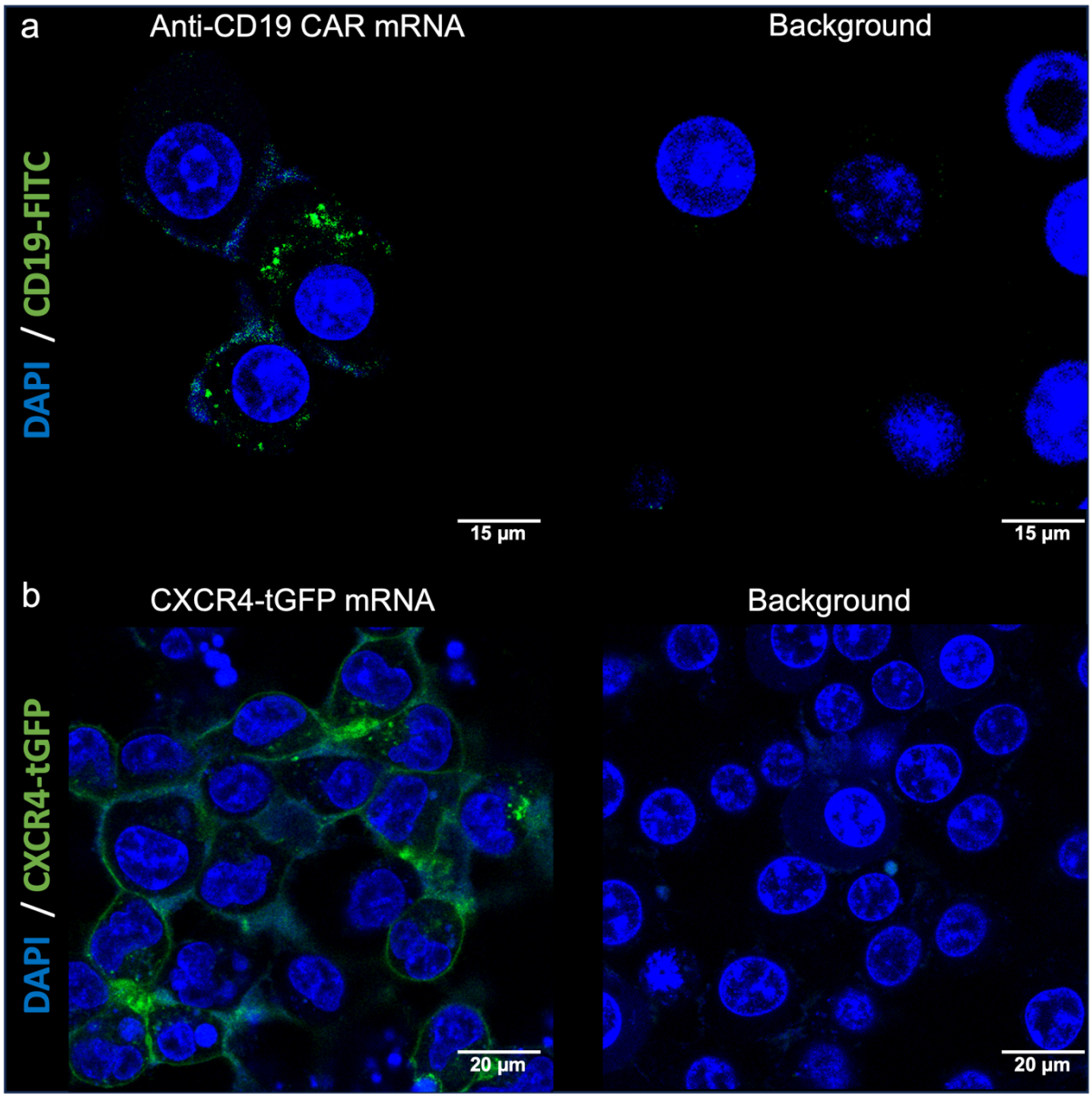


**Figure 5.1** CLSM images 24 hours after *in vitro* transfection with a) anti-CD19 CAR mRNA and b) CXCR4-tGFP mRNA in RAW 264.7 cells using Lipofectamine MessengerMAX as a transfecting reagent.

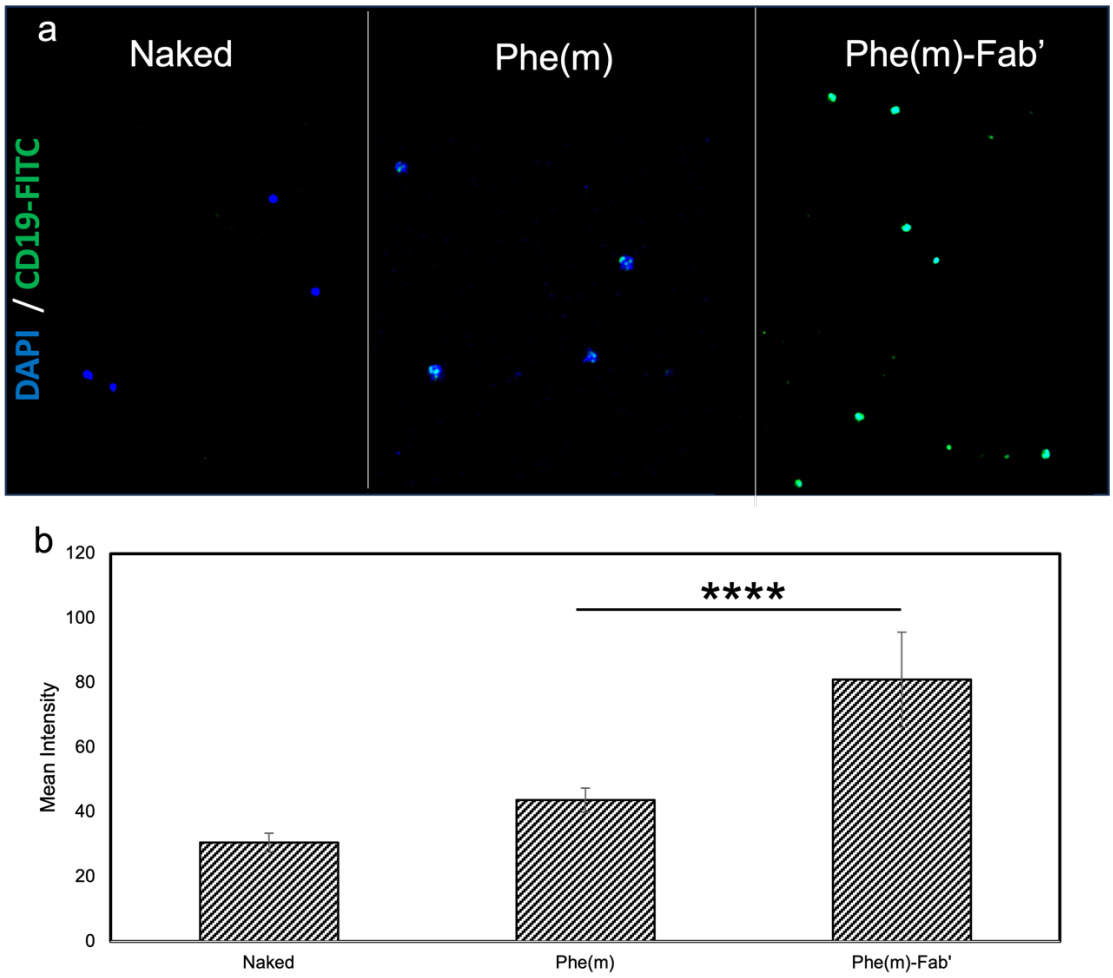


**Figure 5.2** Expression of anti-CD19 CAR protein on the surface of $CD8^+$ T cells detected by CLSM. a) CLSM images of T cells after incubation with naked mRNA, Phe(m), or Phe(m)' for 24 hours. b) Mean intensity of FITC on T cells after transfection of anti-CD19 CAR mRNA and staining with CD19-FITC protein cells based on CLSM measurements. Data is presented as the mean ± S.D. (n = 20). Statistical analysis *via* two-sided unpaired t-test (* $p < 0.05$, ** $p < 0.01$, *** $p < 0.001$, ****$p < 0.0001$)

The duration of protein expression is a crucial factor in RNA-based technologies. Therefore, the expression of anti-CD19 CAR on primary cytotoxic $CD8^+$ mouse T cells has been monitored over several days using jetMESSENGER transfecting reagent and anti-CD19 CAR mRNA. At several time points the expression of CAR was measured using CLSM after staining the cells with DAPI solution and CD19-FITC protein (**Figure 5.3**)

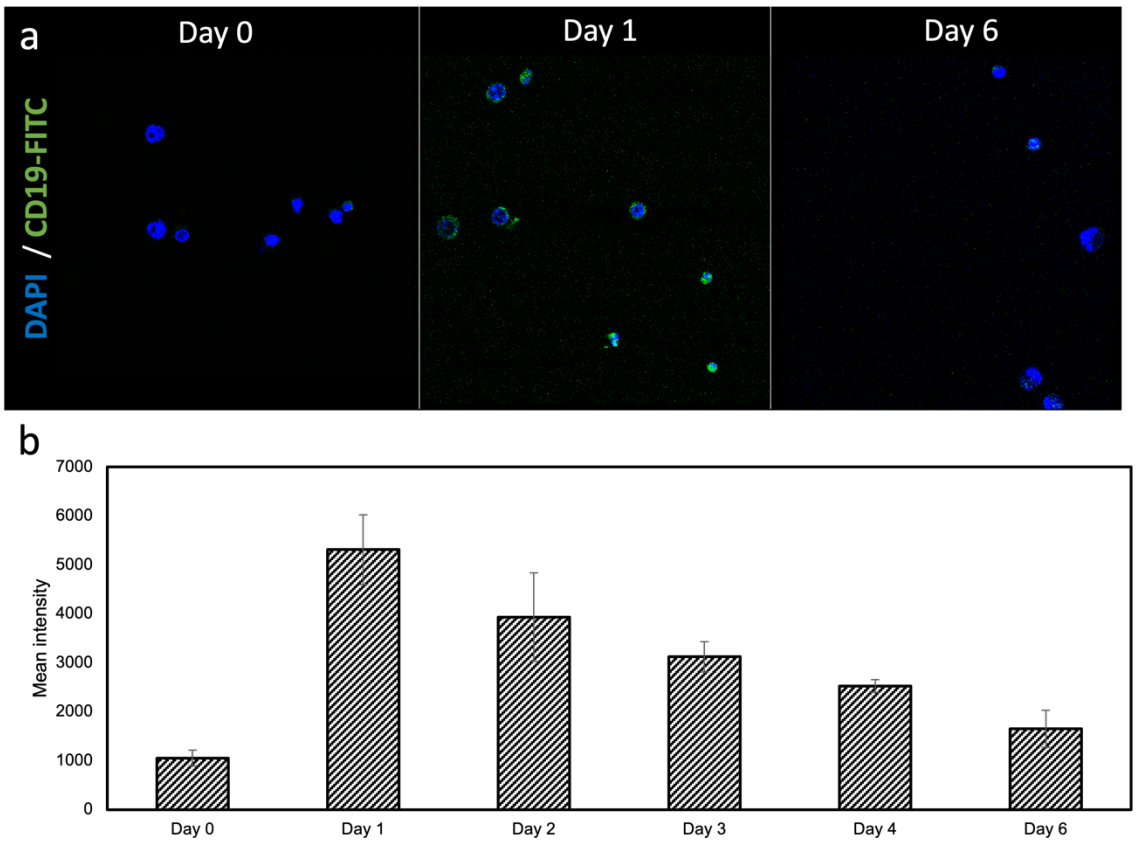


**Figure 5.3** Expression profile of anti-CD19 CAR on primary cytotoxic $CD8^+$ T cells over several days. a) CLSM images of cytotoxic $CD8^+$ T cells after transfection with antiCD19-CAR mRNA. CAR was stained with CD19-FITC. b) The mean intensity of FITC on T cells after transfection with anti-CD19 CAR mRNA and staining with CD19-FITC protein based on CLSM measurements. Data is presented as the mean ± S.D. (n = 20).

As expected with mRNA delivery systems, CAR protein expression lasts for several days after transfection, with a maximum after 24 hours. A similar expression profile of CARs on T cells generated by mRNA has been reported by other groups (Y. Zhao et al. 2010; Neha N. Parayath and Stephan 2021) which provides valuable information about the timing of eventual booster administrations for clinical applications. The data suggests that boosters to maintain a high number of CAR T cells may be effective when administered several days after the initial treatment, as the expression of CAR proteins has significantly decreased at that point.

The cytotoxic potential of *in vitro* generated anti-CD19 chimeric antigen receptor (CAR) T cells against A20 cells, a mouse lymphoma cell line overexpressing CD19. Following the generation of CAR T cells, they were co-incubated with A20 cells for 24 hours. Subsequently, the viability of the A20 cells was assessed using the CCK-8 kit (**Figure 5.4**). The results were then normalized to a control group in which untreated $CD8^+$ T cells were added to the A20 cells. The findings revealed that CAR T cells transfected with Phe(m)-Fab' exhibited a reduced number of viable A20 cells compared to the control group. This observation suggests that the CAR T cells effectively targeted and eliminated a greater proportion of A20 cells compared to both regular T cells and CAR T cells transfected with Phe(m) lacking the targeting ligand. Consequently, these results indicate the potential efficacy of Phe(m)-Fab in enhancing the cytotoxic activity of CAR T cells, thereby demonstrating their capacity to combat cancer in an *in vitro* setting.

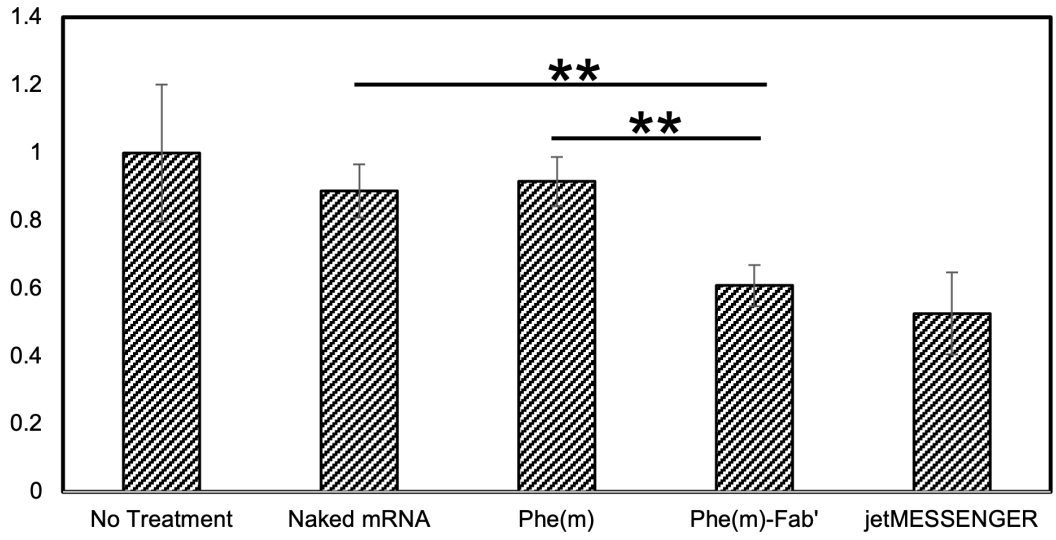


**Figure 5.4** Killing assay of anti-CD19 CAR T cells against A20 cells. Viable A20 cells were detected after 24 hours of incubation with anti-CD19 CAR T cells *via* CCK-8 kit. The measurements were normalized against A20 cells incubated with untreated T cells. Data are presented as the mean ± S.D. (n = 5). Statistical analysis *via* two-sided unpaired t-test (* $p < 0.05$, ** $p < 0.01$, *** $p < 0.001$)

On top of T cells targeting $CD19^+$ cancer cells, T cells expressing the chemokine receptor CXCR4 to increase the migration of T cells to solid tumors were investigated. First, we confirmed the expression of CXCR4-tGFP using Phe(m)-Fab' and the CXCR4-tGFP mRNA synthesized in Chapter 2. $CD8^+$ T cells were incubated with Phe(m)-Fab' encapsulating CXCR4-tGFP mRNA for 24 h, then the cell nuclei were stained with DAPI, and the CXCR4-tGFP expression was determined by using CLSM. **Figure 5.5** shows a significant increase of signal in the T cells that were transfected with Phe(m)-Fab' compared to the ones transfected with naked mRNA. This confirms that Phe(m)-Fab' successfully generates CXCR4 T cells.

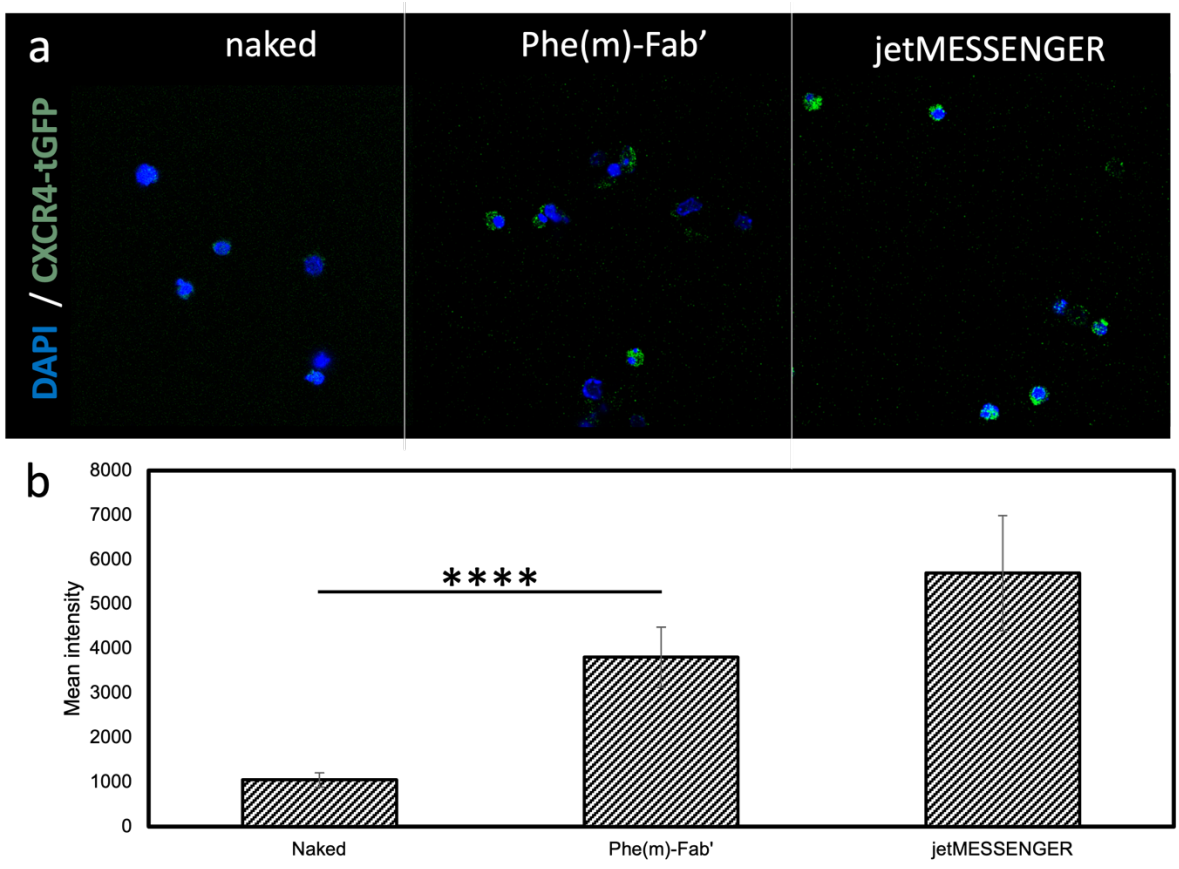


**Figure 5.5** Expression of CXCR4-tGFP on cytotoxic $CD8^+$ T cells. a) CLSM images of T cells after incubation with CXCR4-tGFP mRNA. b) Mean intensity of tGFP signal in T cells from CLSM measurement. The data is presented as the mean ± S.D. (n = 20). Statistical analysis *via* two-sided unpaired t-test (* $p < 0.05$, ** $p < 0.01$, *** $p < 0.001$, ****$p < 0.0001$)

The expression of CXCR4-tGFP on primary cytotoxic $CD8^+$ mouse T cells has been monitored over several days in primary cytotoxic $CD8^+$ mouse T cells using jetMESSENGER transfecting reagent and CXCR4-tGFP mRNA. At several time points the expression was measured using CLSM after staining the cells with DAPI solution (**Figure 5.6a,b**)

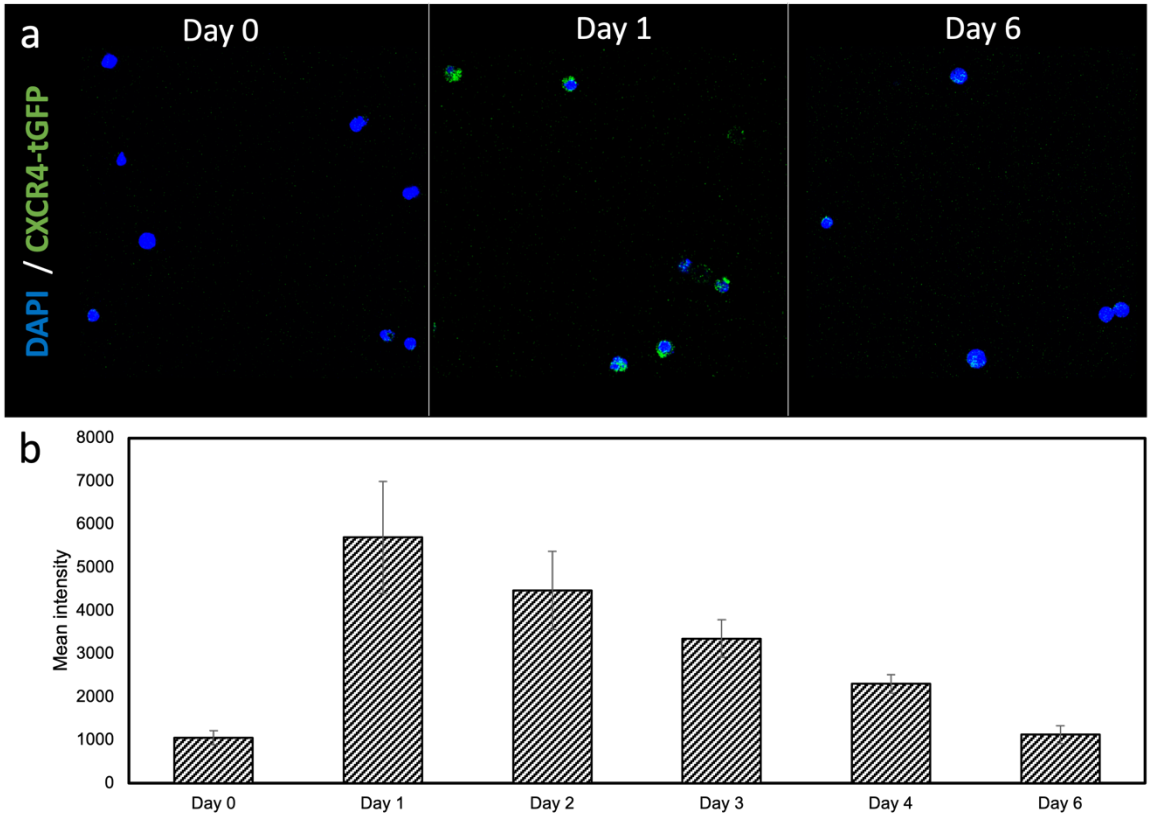


**Figure 5.6** Expression profile of CXCR4-tGFP on primary cytotoxic $CD8^+$ T cells over several days. a) CLSM images of cytotoxic $CD8^+$ T cells after transfection with CXCR4-tGFP mRNA at different time points. b) The mean intensity of tGFP on T cells after transfection with CXCR4-tGFP based on CLSM measurements at different time points. Data is presented as the mean ± S.D. (n = 20).

Similarly to anti-CD19 CAR in **Figure 5.3**, CXCR4-tGFP protein expression lasts for several days after transfection, with a maximum after 24 hours, which indicates that booster injections would likely be necessary for *in vivo* applications treating cancer after several days to keep the concentration of CXCR4 expressing T cells high.

Next, to assess the enhanced ability of CXCR4 T cells to infiltrate tumors expressing the corresponding CXCL12 ligand, an invasion assay was conducted. The migration of T cells through Matrigel simulates the migration of T cells into tissues towards the CXCL12-expressing tumor. After 24 hours, the number of T cells that migrated to the bottom well was counted (**Figure 5.7**).

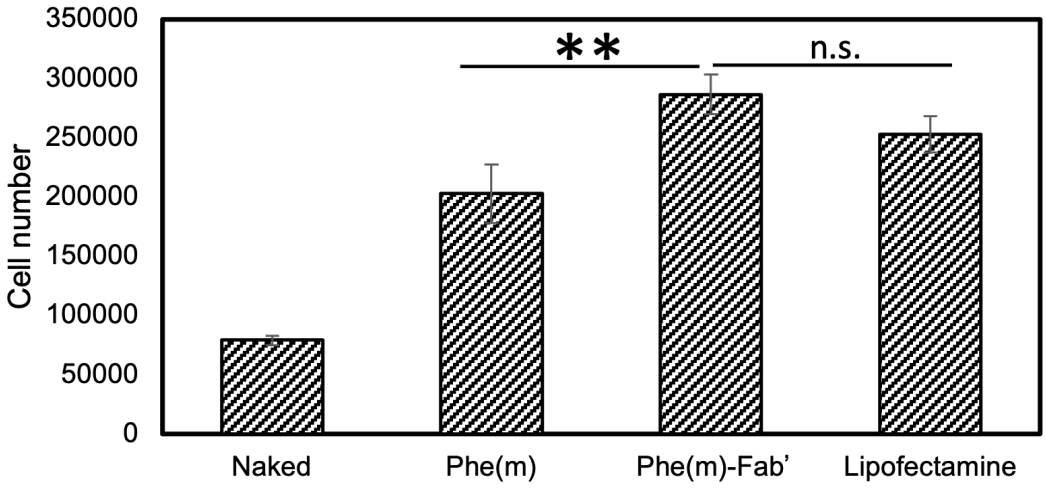


**Figure 5.7** Invasion assay of *in vitro* transfected CXCR4 T cells (top well) against 4T1 cancer cells (bottom well) through Matrigel. The bars represent the number of cells in the supernatant of the bottom well presented as the mean ± S.D. (n = 3). Statistical analysis *via* two-sided unpaired t-test (* $p < 0.05$, ** $p < 0.01$, *** $p < 0.001$)

The results show that T cells transfected with Phe(m)-Fab' migrated through the Matrigel towards the CXCL12 expressing 4T1 cells most effectively out of all the groups, even outperforming the commercial transfecting reagent Lipofectamine MessengerMAX. The Matrigel invasion assay is particularly valuable for studying three-dimensional invasion, as it allows cells to invade through the Matrigel matrix, closely resembling the *in vivo* invasion process. Traditionally, in an invasion assay, cells stay attached to the membrane on the bottom of the Matrigel between the top and the bottom well. However, due to the small size of T cells, and the chosen membrane diameter of 8 μm, this likely caused T cells to migrate into the

bottom well after infiltrating the Matrigel to the bottom. Nonetheless, this is a promising indicator for the enhanced migration and infiltration of CXCR4 T cells towards cancer masses.

*In vivo* experiments were conducted to assess the luciferase expression of the reporter protein Fluc in a small sample number of mice following intratumoral (i.t.) injection near a 4T1-HA tumor. The 4T1-HA tumor is known to recruit immune cells, leading to an increased population of T cells in the tumor environment. The results depicted in **Figure 5.8** demonstrate an elevated protein expression in the mouse treated with Phe(m)-Fab'. While these findings are compelling, further investigations are necessary to determine the specific type of cells that are transfected. This is crucial to ascertain whether the observed increase in expression is due to enhanced T cell uptake or if other cell types are also being transfected. Although *in vitro* results have indicated highly specific ligand-specific transfection, it is important to recognize that the biological environment *in vivo* is significantly more complex and challenging to predict. Therefore, additional experiments focusing on the determination of the transfected cell type are warranted.

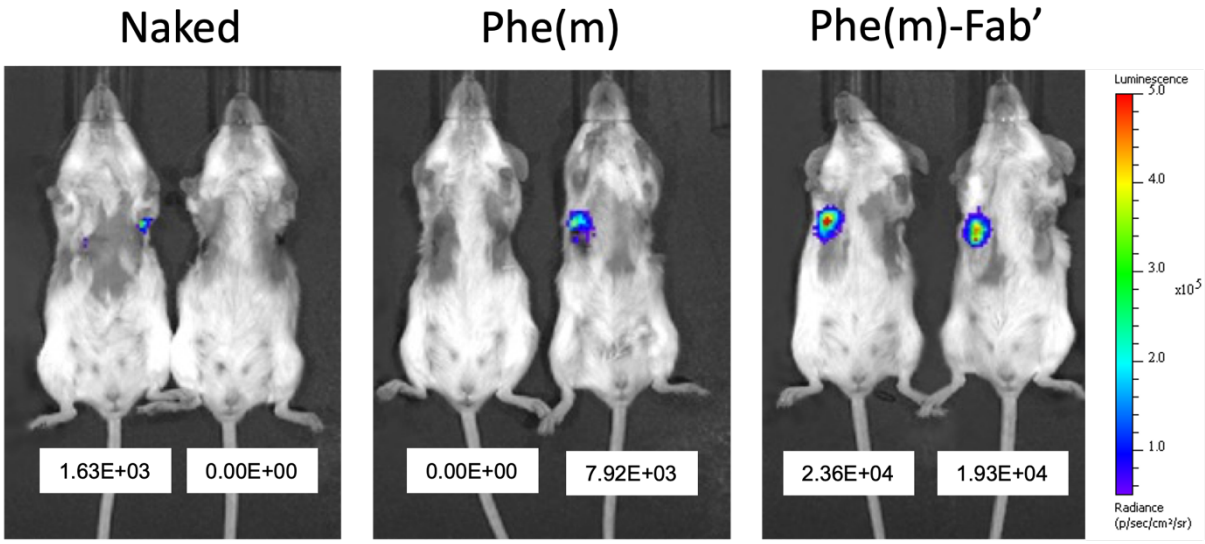


**Figure 5.8** *in vivo* firefly luciferase expression after i.t. injection of micelles in mice bearing 4T1-HA tumors. The average radiance of the area is given in [p/s/cm≤/sr]

The *in vivo* generation of chemokine-modified immune cells was investigated in a study involving the administration of naked CXCR4-tGFP or CXCR4-tGFP encapsulating Phe(m) or Phe(m)-Fab' *via* subcutaneous (s.c.) injection in 4T1-tumor bearing mice. This administration route was chosen because it has been demonstrated that s.c. injection close to the lymph node results in high uptake in the lymph nodes due to the drainage *via* lymphatic vessels (Richter, Bhansali, and Morris 2012), which contain a high number of T cells. The particle size of Phe(m)-Fab’ is especially suitable for s.c. administration to target lymph nodes, as particles larger than 100 nm struggle to pass the interstitium, whereas smaller particles can migrate through the channel of the interstitium to gain access to the lymphatic system (Christien Oussoren and Storm 2001; C. Oussoren et al. 1997).

The resulting expression of CXCR4-tGFP was quantified using an *in vivo* imaging system (IVIS) 30 hours post-injection. A control group consisting of mice without injection was included to account for background fluorescence (**Figure 5.9a,b**). Remarkably, the mice receiving the treatment exhibited elevated GFP expression at the tumor site, indicating successful expression of CXCR4 and subsequent migration from the transfection site to the tumor site. These observations are encouraging indicators of the successful *in situ* generation of CXCR4-tGFP T cells and their ability to migrate from the transfection site to the tumor.

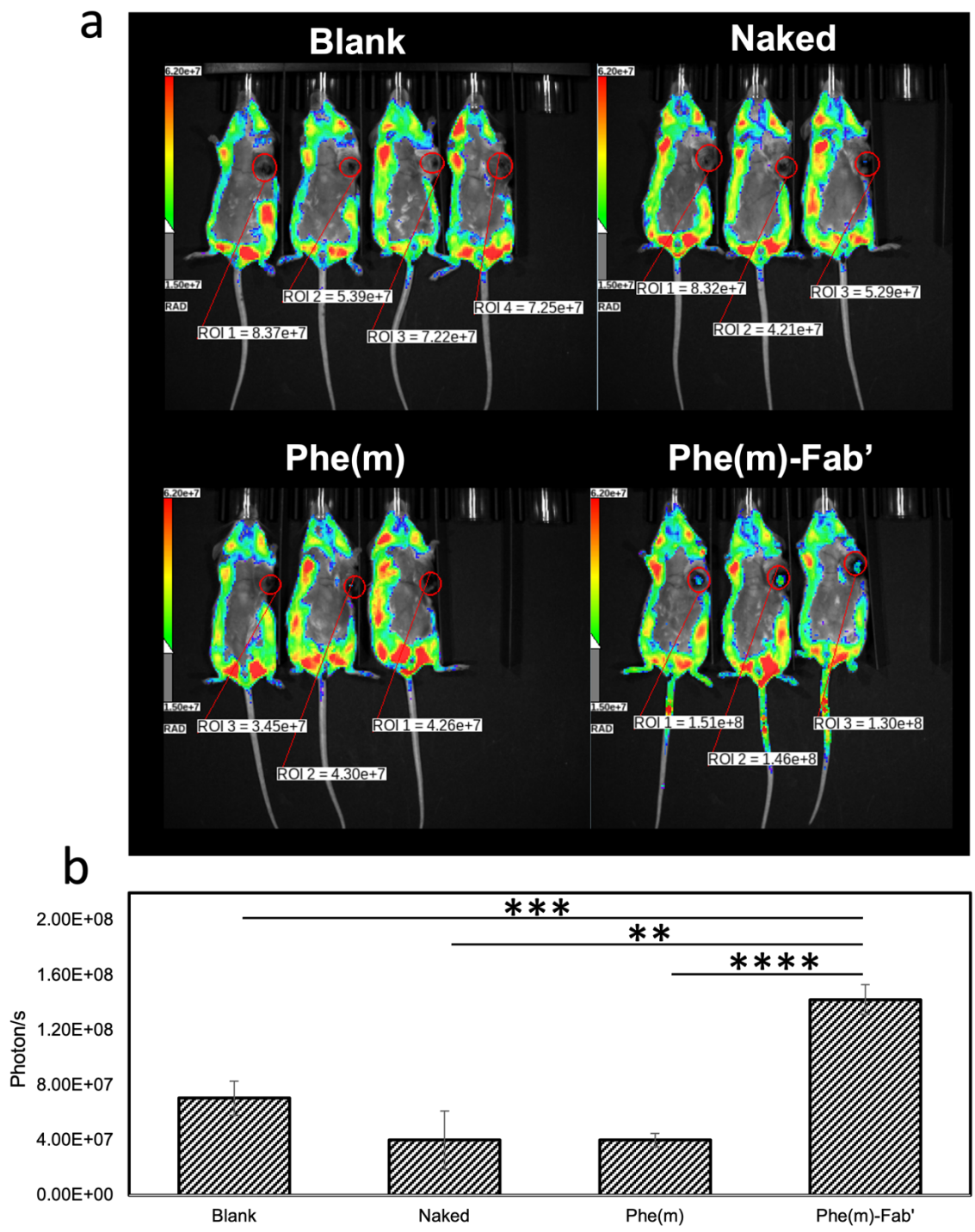


**Figure 5.9** IVIS of 15-week-old mice bearing 4T1-tumors 30 hours after s.c. injection of CXCR4-tGFP mRNA *via* Phe(m)-Fab' (n = 3) or untreated mice (n = 4). a) IVIS images of mice 48 hours after injection or CXCR4-tGFP mRNA. b) Quantification of GFP signal based on IVIS measurements. Statistical analysis *via* two-sided unpaired t-test (* $p < 0.05$, ** $p < 0.01$, *** $p < 0.001$, **** $p < 0.0001$)

To identify *in situ* generated CXCR4-modified cells, 4T1 tumor-bearing mice were injected with CXCR4-tGFP mRNA encapsulated in various delivery vehicles. 24 hours after subcutaneous injection, mice were sacrificed, and the spleen, lymph nodes, and tumors were analyzed by flow cytometry to identify immune cells expressing CXCR4-tGFP (**Figure 5.10**). However, none of the treatment groups displayed GFP signals, including the commercial *in vivo* jetPEI.

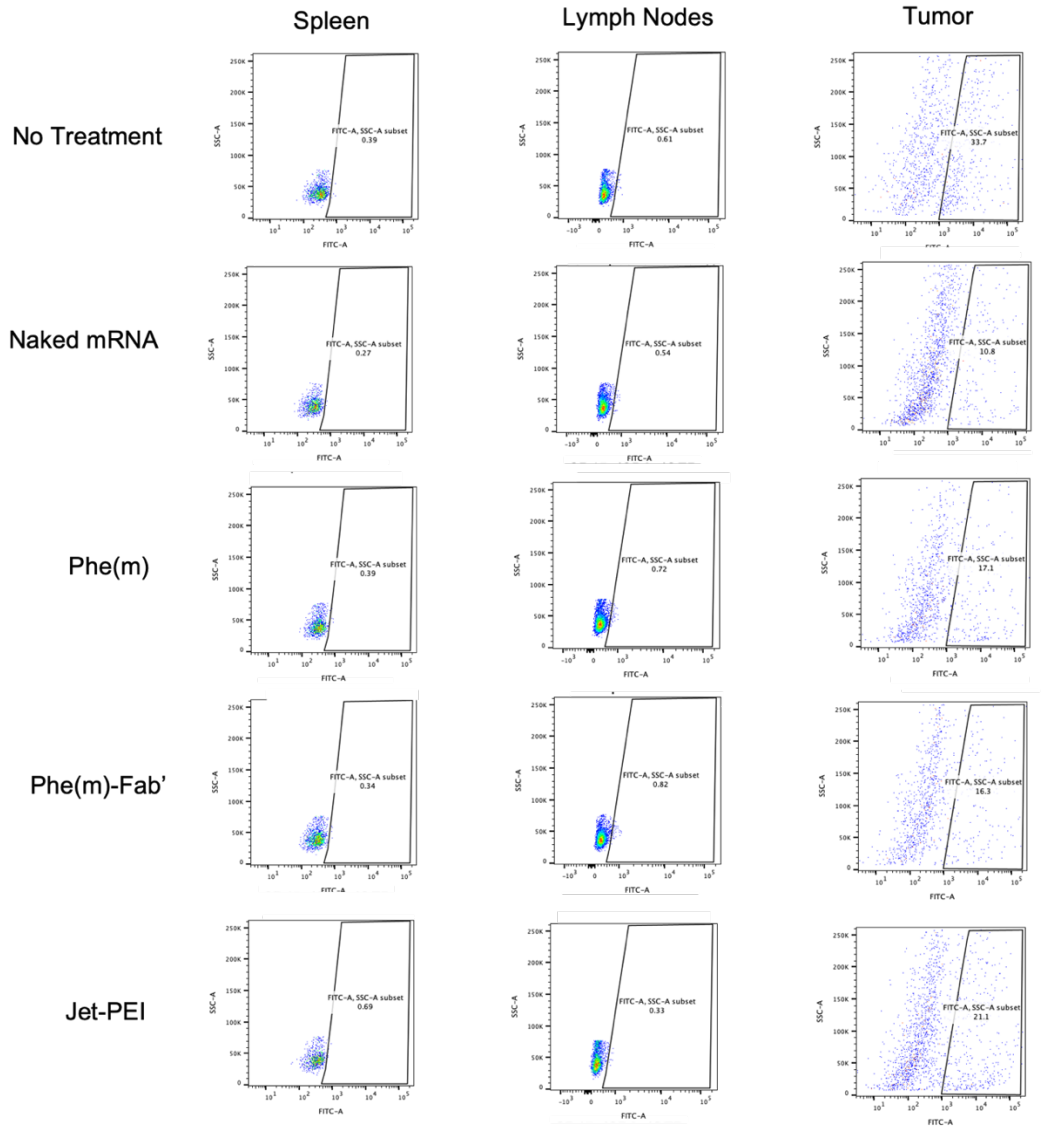


**Figure 5.10** Flow cytometry of $CD8^+$ T cells from organs and tumor samples 24 hours after s.c. injection of 5 μg CXCR4-tGFP mRNA *via* various delivery vehicles.

Possible reasons for this might include, that the dose or injection rate needs to be adjusted to get robust expression *in vivo*. In this experiment, a single dose of 5 µg mRNA per mouse was injected, but higher doses are commonly reported in studies about *in situ* generation of T cells. For example, in a study where polymeric nanoparticles were used to deliver mRNA to T cells *in vivo*, doses of 50 µg mRNA were injected three consecutive days in their *in vivo* experiment (N. N. Parayath et al. 2020). Also, the total number of CAR T cells in mice might be small, making them difficult to detect within tissues without increasing the dose.

Furthermore, the interferon response induced by *in vitro* transcribed mRNA in cells can significantly impact the expression of proteins, which might also make detection difficult. Unmodified IVT mRNA has been shown to elicit robust type I interferon responses, which can activate protein kinase R (PKR) and 2′-5′-oligoadenylate synthetase (OAS), leading to reduced transfection efficiency (Loomis et al. 2018)(Loomis et al. 2018) . Experiments have demonstrated that the use of nucleoside-modified IVT mRNA, along with improved purification protocols, eliminates immune activation by mRNA and increases its translation, thus opening therapeutic applications

Another way to enhance the protein expression and the generation of CAR T cells, it is common to implement N1-methyl-pseudouridine (N1-methyl-Ψ) in place of uridine (Morais, Adachi, and Yu 2021a; Andries et al. 2015). Ψ is a rotational isomer of uridine, in which the N-C glycosidic bond is substituted with the C-C bond. The isomerization reaction also creates an extra hydrogen bond donor (-N1H). Ψ can be further methylated at the N1 position by Nep1 (an N1-specific Ψ methyltransferase) to generate N-methyl-Ψ. d, hydrogen bond donor; a, hydrogen bond acceptor. N1-methyl-Ψ provides enhanced mRNA stability and reduces inflammatory responses, thereby improving translational efficiency. The significance of m1Ψ in mRNA therapeutics has been underscored in various studies and has been implemented in Covid-19 vaccines including the ones from BioNTech and Moderna Therapeutics (comirnaty®

and spikevax®, respectively), emphasizing its critical contribution to mRNA vaccines (Nance and Meier 2021; Morais, Adachi, and Yu 2021a). For this reason, Gluc mRNA replacing uridine with N1-methyl-Ψ was synthesized by IVT and transfection in HEK-293 cells was compared to unmodified Gluc mRNA formulated with Lipofectamine MessengerMAX. However, we found that N1-methyl-Ψ modified Gluc mRNA could not outperform unmodified mRNA in our experiment (**Figure 5.11**).

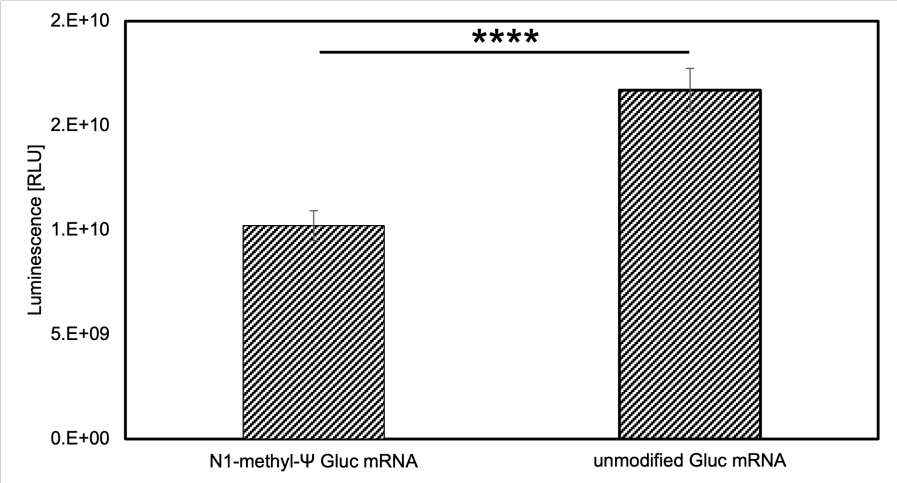


**Figure 5.11** Luminescence of Gluc in the supernatant of HEK-293 cells measured by Luminometer. Data are presented as the mean ± S.D. (n = 10). Statistical analysis *via* two-sided unpaired t-test (* $p < 0.05$, ** $p < 0.01$, *** $p < 0.001$, **** $p < 0.0001$)

It is possible that inefficient cleanup resulted in the low expression of protein with the mRNA incorporating N1-methyl-Ψ. It has been shown that contamination of double-stranded RNA (dsRNA) in IVT products, which is sensed as a viral invader, activating dsRNA-dependent enzymes, such as oligoadenylate synthetase (OAS), RNA- specific adenosine deaminase (ADAR), and RNA-activated protein kinase (PKR), results in the inhibition of protein synthesis (Baiersdörfer et al. 2019). For this reason, more elaborate cleanup processes, such as HPLC may be able to lead to enhanced protein expression making it viable to improve the efficacy of the treatment in the future.

## 5.4 Conclusion

In the field of *in situ* cell therapy, the generation of functional cancer-targeting T cells is crucial for therapeutic success. In this chapter, we confirmed the expression of anti-CD19 CAR mRNA and CXCR4-tGFP using Phe(m)-Fab' and assessed the efficacy of the resulting T cells in targeting cancer cells. The findings demonstrated sustained protein expression over several days in T cells, with anti-CD19 CAR T cells generated using Phe(m)-Fab' showing comparable efficacy to those generated by the commercial transfection reagent jetMESSENGER in decreasing the viability of A20 lymphoma cells *in vitro*.

Furthermore, the study investigated the efficacy of CXCR4 T cells in enhancing migration towards tumors expressing CXCL12. In an invasion assay, *in vitro* transfected CXCR4 T cells exhibited migration through a Matrigel-coated membrane towards 4T1 cancer cells, indicating their potential for tumor targeting. Subsequently, *in vivo* experiments involving the subcutaneous injection of Phe(m)-Fab' loaded with CXCR4-tGFP mRNA in mice bearing 4T1 tumors provided strong evidence of the generation of functional CXCR4 T cells. These transfected cells migrated towards the solid tumor site, as detected *via* IVIS measurements.

However, this chapter also revealed challenges in detecting modified T cells *in vivo*, as the presence of CXCR4 T cells in the tumor could not be confirmed by flow cytometry as of yet. Higher dosages, refined mRNA formulations or multiple boosters may be necessary to improve the therapeutic efficacy, and to successfully detect *in situ* engineered T cells in the future.

# Chapter 6.

# Conclusions and Future Perspectives

## 6.1 Conclusions

The treatment of malignant tumors remains a global concern, with conventional methods such as surgery, chemotherapy, and radiotherapy often associated with severe side effects. In contrast, immunotherapy has emerged as a promising approach in cancer treatment, leveraging activated immune cells to specifically target and attack tumor cells while minimizing adverse effects. One of the key strategies in cancer immunotherapy is adoptive cell therapy, also known as tumor immune cell therapy, which involves extracting immune cells from the body, amplifying the desired immune cells, and reintroducing them into the body to elicit an immune response against tumor cells.

However, the complex manufacturing processes, high costs, and limited efficacy in treating solid tumors have constrained the widespread adoption of adoptive cell therapy. Nevertheless, the challenges associated with adoptive cell therapy have spurred the development of innovative strategies that integrate immunology, cell biology, and biomaterials to overcome these obstacles and enable *in vivo* preparation. This transformation has the potential to shift CAR-T therapy from personalized, cell-based products to off-the-shelf drugs, thereby addressing some of the existing limitations.

In this thesis, a targeted mRNA delivery system was developed to specifically deliver mRNA for the generation of engineered immune cells relevant to cancer treatment. The system utilized a block ionomer to stabilize mRNA in a PIC micelle, incorporating a flexible polymer backbone with phenylalanine sidechains to enhance mRNA interaction through π-π stacking and facilitate endosomal escape due to its ionizable nature. The resulting micelle demonstrated significant improvements in transfection and could be modified by attaching targeting ligands on its surface to facilitate specific mRNA delivery to immune cells.

Furthermore, the thesis highlights the successful attachment of Fab' antibody fragments targeting CD8 to the surface of the PIC micelles, on, enabling highly specific mRNA delivery to T cells and the generation of anti-CD19 CAR T cells. This approach demonstrated the potential of Fab' to induce targeted mRNA delivery to T cells, holding promise for the implementation of Phe(m)-Fab' to generate T cells with chimeric receptors for enhanced cancer therapy. The versatility of the system was further demonstrated by the enhanced transfection of macrophages through the use of mannose targeting ligands, showcasing the adaptability of the system based on the specific targeting ligand employed.

The engineering of functional CAR T cells and chemokine receptor T cells using Phe(m)-Fab' as a sophisticated polymeric carrier for mRNA has been highlighted by several *in vitro* experiments, demonstrating enhanced anticancer effects of Phe(m)-Fab' transfected T cells. Furthermore, the expression and migration of *in situ* generated CXCR4-expressing cells shows the potential to guide immune cells to solid tumor sides more effectively in the future.

The desire for *in situ* engineered T cells has been highlighted by recent attempts by various groups to generate CAR T cells *in vivo* (C. Wang et al. 2023; Neha N. Parayath and Stephan 2021). Among them is a polymeric delivery system based on the research findings of Parayath et al. (N N Parayath et al. 2020), which was recently acquired by the company Sanofi. In their study, they reported a particle size of 106.9 ± 7.2 nm, while Phe(m)-Fab' has a particle size of approximately 55 nm. Additionally, the zeta potential of their system positive, whereas the zeta potential of our system is neutral. It is noteworthy that positively charged particles tend to accumulate in the lung, and PBAE-based nanoparticles, such as those used in the Sanofi system, have been shown to primarily accumulate in the lung and liver following intravenous injection (Rui et al. 2022; Yuan et al. 2023).

The smaller particle size of Phe(m)-Fab' can lead to preferential drainage to the lymph nodes after subcutaneous administration, as smaller particles have been shown to exhibit this behavior (Hawley, Davis, and Illum 1995). Furthermore, neutral or negatively charged particles also tend to drain to the lymph nodes. The fate of the particle after intravenous injections, as well as the stability and protection of mRNA in harsh *in vivo* conditions, were also not adequately addressed in the study by Parayath et al. For example, the effect of anion-exchange with the mRNA in their core was not discussed, despite the addition of polyanions to the polyplex in their formulation.

Although they demonstrated CAR expression on T cells *in vivo*, this was achieved through the administration of extremely high dosages of 50 μg mRNA per injection for three consecutive days, raising concerns about the efficiency of their delivery system. In contrast, our current micelle system has shown *in vivo* protein expression with as little as 5 μg mRNA in a single injection. Additionally, while Parayath et al. demonstrated improved targeting of $CD8^+$ cells within CD45+ immune cells, further investigation into the off-targeting delivery in other cells is not fully described.

While the system acquired by Sanofi is in a mature stage and has extensive pre-clinical *in vivo* data, Phe(m)-Fab' has demonstrated promising *in vitro* results for targeted mRNA delivery and for the generation of functional modified T cells, combined with rigorous particle characterization. While more *in vivo* studies will be necessary in the future to compare Phe(m)-Fab' with more mature treatments in the pre-clinical phase, most recent *in vivo* data shows potential to deliver mRNA *in vivo* and for the implementation of Phe(m)-Fab' to generate T cells with chimeric receptors *in situ*.

Despite these advancements in the *in situ* generation of CAR T cells, challenges persist in the application of CAR immunotherapy, particularly in the context of solid tumors. Major hurdles include CAR T cell manufacturing, the lack of tumor-specific antigens, inefficient CAR T cell trafficking and infiltration into tumor sites, and the lag in the development of CAR immunotherapy for solid tumors compared to anti-CD19 CAR T cells. However, the thesis also presented the successful generation of immune cells expressing the chemokine receptor CXCR4 by exchanging the encapsulated mRNA without the need to adjust the micelle formulation. This approach leverages chemokines to signal cell migration and guide transfected immune cells to their target sites, offering potential solutions to the challenges associated with CAR immunotherapy in solid tumors.

In conclusion, the thesis contributes to the advancement of cancer immunotherapy by developing a targeted mRNA delivery system that holds promise for the *in situ* generation of modified immune cells relevant to cancer treatment. The findings underscore the potential of this system to address the limitations of current adoptive cell therapy approaches and pave the way for enhanced cancer therapy through the generation of immune cells with chimeric receptors. Furthermore, the successful generation of immune cells expressing CXCR4 highlights the adaptability and potential of the system to address challenges in CAR immunotherapy, particularly in the context of solid tumors.

## 6.2 Future perspectives

The field of immunotherapy faces a significant challenge in generating a sufficient number of modified immune cells to achieve a therapeutic anticancer effect, particularly when utilizing mRNA due to its transient expression profile. This limitation may necessitate multiple administrations to achieve the desired anticancer effect. To address this challenge, several strategies can be employed to improve the expression of proteins on immune cells. One approach involves tuning the mRNA, for example, by incorporating pseudouridine into its structure or by employing GPC purification to remove impurities. These modifications can potentially lead to a more robust generation of chimeric antigen receptor (CAR) T cells, thereby enhancing therapeutic outcomes.

Optimization of the CAR domains might also result in CAR T cells that proliferate CAR T cells *in vivo* while preventing exhaustion. For instance, the intracellular CAR region featuring stimulatory and costimulatory domains like CD3 and CD28 plays an important role in initiating T cell proliferation upon interaction with the targeted antigen (Mehrabadi et al. 2022). Various stimulatory and costimulatory domains have been studied for their impact on T cell proliferation and persistence. However, it is crucial to note that excessive CAR signaling might induce strong proliferation, but is linked to rapid T cell exhaustion (Majzner et al. 2020). Most recent CAR designs integrate transgenes for cytokine release, such as IL-2 cytokines, preventing T cell exhaustion and promoting proliferation upon activation. Incorporating these immunostimulatory cytokines, enhances CAR-T cells' resistance to the immunosuppressive tumor microenvironment, improving function and growth.

In addition to optimizing mRNA, the careful selection of antigen receptors and chemokine receptors is crucial for the development of more advanced CAR structures and specific immune cell homing. This is essential for successful recognition and infiltration of tumors. Furthermore, the versatility of mRNA technology allows for its exchange to address

various diseases, such as regulating the balance of helper T cells through mRNA delivery.

Moreover, efforts to simplify the design of nanocarriers are desirable for the advancement of immunotherapy. It is noteworthy that the simplicity of construction and ease of repeat preparation are key features of US FDA-approved nanomaterials-related drugs. However, many of the nanomaterials used for CAR-T treatment are complex in design and contain a wide variety of chemical or bioactive components, making it challenging to regulate their quality and efficacy. The complexity of biomaterial constructs may also pose difficulties in mass production on a clinical scale. Therefore, a comprehensive understanding of the biomaterials used for CAR-T therapy is essential to provide guidelines for the development of safe and cost-effective biomaterials to enhance immunotherapy. It is crucial to emphasize that all aspects of biomaterial design should be carefully considered to meet their intended applications. For instance, the complex composition and physical properties of liposome nanoparticles, including size, morphology, surface charge, drug or gene loading, ligand type, and density, can unexpectedly alter the characteristics of CAR-T cells.

In conclusion, the future outlook for *in situ* generated immune cells in immunotherapy is promising, with ongoing efforts focused on optimizing mRNA, selecting appropriate receptors, and simplifying nanocarrier design. These advancements hold great potential for improving the efficacy and safety of immunotherapy, ultimately benefiting patients with various diseases, including cancer. Further research and development in this area will undoubtedly contribute to the evolution of immunotherapy and its widespread clinical application.

# Acknowledgments

I would like to express my heartfelt appreciation to Associate Professor Horacio Cabral for accepting me in his lab and for his excellent supervision during my time as a PhD student. Thanks to his support I was able to grow as a scientist and acquire valuable skills for my future.

I am also very grateful to Professor Satoshi Uchida, Professor Yasuyuki Sakai, Professor Satoru Nagatoishi, and Professor Tsutomu Suzuki, for their critical input and kind suggestions. Engaging in meaningful discussions with them not only broadened my perspective as a researcher but also significantly enhanced the quality of my work.

Also, I would like to express my gratitude to the people of Kataoka Lab at the Innovation Center of NanoMedicine (iCONM), especially Professor Hiroaki Kinoh and Dr. Xueying Liu.

Also, a big thank you to all the members at Cabral Lab for their great support during my time here. In particular, I would like to convey my deepest gratitude to Dr. Eger Rigte Boonstra for his tireless support, mentorship, and the countless lunches we shared. Also, special thanks to Dr. Shang-Wei Li for his assistance and great friendship during our time together. I also want to thank Mr. Okajima Hiroki and Mr. Yuki Nakashima who I consider my companions from the RNA group, and Mr. Guanghao Hu, who helped me greatly in the final months of my PhD. And finally, special thanks to Mrs. Hiroko Koyama for her tireless support and assistance.

I also want to express my love and gratitude to my mother and my sister, who always encouraged and supported me, not only during my time here but throughout my whole life.

Thanks also to Dr. Thahomina Tareque Khan, whom I shared an apartment and many amazing travel stories with, for her companionship and great advice throughout my PhD life.

And finally, I want to thank my friends and family in Japan and abroad, who have been an amazing support to me on this journey and who I feel lucky to have.

# Achievements

## I. Original Articles:

1. **Lucas Mixich**, Eger Boonstra, Keita Masuda, Shang-Wei Li, Yuki Nakashima, Fanlu Meng, Momoko Sakata, Tatsuro Goda, Satoshi Uchida, Horacio Cabral Ionizable polymeric micelles with phenylalanine moieties enhance intracellular delivery of self-replicating RNA for long-lasting protein expression *in vivo*, Biomacromolecules January 5, 2024, xxxx, xxx, xxx-xxx https://doi.org/10.1021/acs.biomac.3c01102

2. Wenqian Yang, Takuya Miyazaki, Yasuhiro Nakagawa, Eger Boonstra, **Lucas Mixich**, Akira Matsumoto, Peng Mi, Satoshi Uchida & Horacio Cabral *et al.* Block catiomers with flanking hydrolyzable tyrosinate groups enhance *in vivo* mRNA delivery *via* π–π stacking-assisted micellar assembly, Science and Technology of Advanced Materials, 24:1 (2023)

3. Yang W, **Mixich L**, Boonstra E, Cabral H. Polymer-Based mRNA Delivery Strategies for Advanced Therapies. Adv Healthc Mater. 2023 Feb 13

## II. Conferences:

- **Domestic presentations:**

1. **L. Mixich**, T. Miyazaki, E. Boonstra, W. Yang, S. Uchida and H. Cabral, Polymer-Based Polyion Complex Micelles with Controlled Chain Flexibility Boost mRNA Delivery NIMS WEEK Tokyo, Japan 2022 Nov (Poster).

- **International Presentations:**

1. **L. Mixich**, T. Miyazaki, E. Boonstra, W. Yang, S. Uchida and H. Cabral, Polymeric Nanocarriers for Enhanced Delivery of mRNA. 5th Stockholm-Tokyo Workshop "Towards a Sustainable Future - the University and the Wider World" Tokyo, Japan, 2023 Feb (Oral).

2. **L. Mixich**, T. Miyazaki, H. Cabral, Polyion complex micelles based on flexible catiomers for mRNA delivery. The University of Tokyo & Tsinghua University PhD-Students Online Workshop on Health Biotechnology and Engineering 2021 Dec. (online; Oral).

# References

Adachi, Hironori, Martin Hengesbach, Yi-Tao Yu, and Pedro Morais. 2021. “From Antisense RNA to RNA Modification: Therapeutic Potential of RNA-Based Technologies.” *Biomedicines* 9 (5): 550. https://doi.org/10.3390/biomedicines9050550.

Akbay, Esra A, Shohei Koyama, Yan Liu, Ruben Dries, Lauren E Bufe, Michael Silkes, Md Maksudul Alam, et al. 2017. “Interleukin-17A Promotes Lung Tumor Progression through Neutrophil Attraction to Tumor Sites and Mediating Resistance to PD-1 Blockade.” *Journal of Thoracic Oncology : Official Publication of the International Association for the Study of Lung Cancer* 12 (8): 1268–79. https://doi.org/10.1016/j.jtho.2017.04.017.

Allen, Theresa M. 2002. “Ligand-Targeted Therapeutics in Anticancer Therapy.” *Nature Reviews Cancer* 2 (10): 750–63. https://doi.org/10.1038/nrc903.

Andries, Oliwia, Séan Mc Cafferty, Stefaan C De Smedt, Ron Weiss, Niek N Sanders, and Tasuku Kitada. 2015. “N1-Methylpseudouridine-Incorporated MRNA Outperforms Pseudouridine-Incorporated MRNA by Providing Enhanced Protein Expression and Reduced Immunogenicity in Mammalian Cell Lines and Mice.” *Journal of Controlled Release* 217: 337-44. https://doi.org/10.1016/j.jconrel.2015.08.051.

Baiersdörfer, Markus, Gábor Boros, Hiromi Muramatsu, Azita Mahiny, Irena Vlatkovic, Ugur Sahin, and Katalin Karikó. 2019. “A Facile Method for the Removal of DsRNA Contaminant from In Vitro-Transcribed MRNA.” *Molecular Therapy - Nucleic Acids* 15 (April): 26–35. https://doi.org/10.1016/j.omtn.2019.02.018.

Barnes, Tristan A., and Eitan Amir. 2017. “HYPE or HOPE: The Prognostic Value of Infiltrating Immune Cells in Cancer.” *British Journal of Cancer* 117 (4): 451–60.

https://doi.org/10.1038/bjc.2017.220.

Bernstein, P, S W Peltz, and J Ross. 1989. “The Poly(A)-Poly(A)-Binding Protein Complex Is a Major Determinant of mRNA Stability in Vitro.” *Molecular and Cellular Biology* 9 (2): 659–70. https://doi.org/10.1128/mcb.9.2.659-670.1989.

Bessis, N., F. J. GarciaCozar, and M. C. Boissier. 2004. “Immune Responses to Gene Therapy Vectors: Influence on Vector Function and Effector Mechanisms.” *Gene Therapy* 11: 10–17. https://doi.org/10.1038/sj.gt.3302364.

Billingsley, Margaret M, Alex G Hamilton, David Mai, Savan K Patel, Kelsey L Swingle, Neil C Sheppard, Carl H June, and Michael J Mitchell. 2021. “Orthogonal Design of Experiments for Optimization of Lipid Nanoparticles for MRNA Engineering of CAR T Cells.” *Nano Letters* 22 (1) :533-542. https://doi.org/10.1021/acs.nanolett.1c02503.

Billingsley, Margaret M, Nathan Singh, Pranali Ravikumar, Rui Zhang, Carl H June, and Michael J Mitchell. 2020. “Ionizable Lipid Nanoparticle-Mediated MRNA Delivery for Human CAR T Cell Engineering.” *Nano Letters* 20 (3): 1578-1589. https://doi.org/10.1021/acs.nanolett.9b04246.

Bingle, L, N J Brown, and Claire E Lewis. 2002. “The Role of Tumour-Associated Macrophages in Tumour Progression: Implications for New Anticancer Therapies.” *The Journal of Pathology* 196 (3): 254–65. https://doi.org/10.1002/path.1027.

Blumenthal, Daniel S, Linara Gabitova, Brett Menchel, Patricia Reyes-Uribe, Andrew Best, Michael Lynch, Sotheavy Chhum, Maggie Schmierer, Sascha Abramson, and Michael Klichinsky. 2021. “104 Development and Characterization of Human Chimeric Antigen Receptor Monocytes (CAR-Mono), a Novel Cell Therapy Platform.” *Journal for Immunotherapy of Cancer* 9 (3): 114. https://doi.org/10.1136/jitc-2021-sitc2021.104.

Brown, Christine E, Darya Alizadeh, Renate Starr, Lihong Weng, Verena Wagner, Araceli

Naranjo, Ostberg, et al. 2016. “Regression of Glioblastoma After Chimeric Antigen Receptor T-Cell Therapy.” *New England Journal of Medicine* 375 (26): 2561-9. https://doi.org/10.1056/nejmoa1610497.

Bulcha, Jote T., Yi Wang, Hong Ma, Phillip W.L. Tai, and Guangping Gao. 2021. “Viral Vector Platforms within the Gene Therapy Landscape.” *Signal Transduction and Targeted Therapy* 6 (1): 53. https://doi.org/10.1038/s41392-021-00487-6.

Burugu, Samantha, Karama Asleh-Aburaya, and Torsten O. Nielsen. 2017. “Immune Infiltrates in the Breast Cancer Microenvironment: Detection, Characterization and Clinical Implication.” *Breast Cancer* 24 (1): 3–15. https://doi.org/10.1007/s12282-016-0698-z.

Cabral, Horacio, Kanjiro Miyata, Kensuke Osada, and Kazunori Kataoka. 2018. “Block Copolymer Micelles in Nanomedicine Applications.” *Chemical Reviews* 118 (14): 6844–92. https://doi.org/10.1021/acs.chemrev.8b00199.

Carlile, Thomas M, Maria F Rojas-Duran, Boris Zinshteyn, Hakyung Shin, Kristen M Bartoli, and Wendy V Gilbert. 2014. “Pseudouridine Profiling Reveals Regulated MRNA Pseudouridylation in Yeast and Human Cells.” *Nature* 515 (7525): 143–46. https://doi.org/10.1038/nature13802.

Carrasco, Manuel J., Suman Alishetty, Mohamad Gabriel Alameh, Hooda Said, Lacey Wright, Mikell Paige, Ousamah Soliman, et al. 2021. “Ionization and Structural Properties of MRNA Lipid Nanoparticles Influence Expression in Intramuscular and Intravascular Administration.” *Communications Biology* 4 (1): 1–15. https://doi.org/10.1038/s42003-021-02441-2.

Challener. 2023. “C.A. Technology for In Vivo CAR T-Cell Therapy Advances.” *BioPharm International* 36 (2): 14–17.

Chanmee, Theerawut, Pawared Ontong, Kenjiro Konno, and Naoki Itano. 2014. “Tumor-

Associated Macrophages as Major Players in the Tumor Microenvironment." *Cancers* 6 (3): 1670–90. https://doi.org/10.3390/cancers6031670.

Chen, Qixian, Kensuke Osada, Zhishen Ge, Satoshi Uchida, Theofilus A Tockary, Anjaneyulu Dirisala, Akitsugu Matsui, et al. 2017. "Polyplex Micelle Installing Intracellular Self-Processing Functionalities without Free Catiomers for Safe and Efficient Systemic Gene Therapy through Tumor Vasculature Targeting." *Biomaterials* 113: 253–65. https://doi.org/https://doi.org/10.1016/j.biomaterials.2016.10.042.

Chen, Shaoyi, Stelios Florinas, Abigail Teitgen, Ze Qi Xu, Changshou Gao, Herren Wu, Kazunori Kataoka, Horacio Cabral, and R. James Christie. 2017. "Controlled Fab Installation onto Polymeric Micelle Nanoparticles for Tuned Bioactivity." *Science and Technology of Advanced Materials* 18 (1): 666-680. https://doi.org/10.1080/14686996.2017.1370361.

Chen, Yu-Hsi, Ruoyu Jiang, and Abraham P Lee. 2023. "Titering of Chimeric Antigen Receptors on CAR T Cells Enabled by a Microfluidic-Based Dosage-Controlled Intracellular MRNA Delivery Platform." https://doi.org/10.1101/2023.03.14.532624.

Curren Smith, Evita Weagel. 2015. "Macrophage Polarization and Its Role in Cancer." *Journal of Clinical & Cellular Immunology* 06 (04): 1–8. https://doi.org/10.4172/2155-9899.1000338.

Deshayes, Stephanie, Horacio Cabral, Takehiko Ishii, Yutaka Miura, Shutaro Kobayashi, Takashi Yamashita, Akira Matsumoto, Yuji Miyahara, Nobuhiro Nishiyama, and Kazunori Kataoka. 2013. "Phenylboronic Acid-Installed Polymeric Micelles for Targeting Sialylated Epitopes in Solid Tumors." *Journal of the American Chemical Society* 135 (41): 15501-7. https://doi.org/10.1021/ja406406h.

Di, Jiaxing, Zhili Du, Kangzeng Wu, Shanshan Jin, Xun Wang, Tonglei Li, and Yuhong Xu.

2022. “Biodistribution and Non-Linear Gene Expression of MRNA LNPs Affected by Delivery Route and Particle Size.” *Pharmaceutical Research* 39 (1): 105–14. https://doi.org/10.1007/s11095-022-03166-5.

Dirisala, Anjaneyulu, Satoshi Uchida, Theofilus A Tockary, Naoto Yoshinaga, Junjie Li, Shigehito Osawa, Lahari Gorantla, Shigeto Fukushima, Kensuke Osada, and Kazunori Kataoka. 2019. “Precise Tuning of Disulphide Crosslinking in MRNA Polyplex Micelles for Optimising Extracellular and Intracellular Nuclease Tolerability.” *Journal of Drug Targeting* 27 (5–6): 670–80. https://doi.org/10.1080/1061186X.2018.1550646.

Duh, Yulander, Yu Yuan Hsiao, Chia Lung Li, Jason C. Huang, and Hanna S. Yuan. 2015. “Aromatic Residues in RNase T Stack with Nucleobases to Guide the Sequence-Specific Recognition and Cleavage of Nucleic Acids.” *Protein Science* 24 (12): 1934–41. https://doi.org/10.1002/pro.2800.

Esfahani, Khashayar, Liya Roudaia, Najwa Buhlaiga, Sonia V d. Rincón, Neha Papneja, and Wilson H Miller. 2020. “A Review of Cancer Immunotherapy: From the Past, to the Present, to the Future.” *Current Oncology*. 27 (2): 87-97 https://doi.org/10.3747/co.27.5223.

Fitzgerald, Julie C, Scott L Weiss, Shannon L Maude, David M Barrett, Simon F Lacey, J Joseph Melenhorst, Pamela Shaw, et al. 2017. “Cytokine Release Syndrome After Chimeric Antigen Receptor T Cell Therapy for Acute Lymphoblastic Leukemia.” *Critical Care Medicine* 45 (2): e124–31. https://doi.org/10.1097/CCM.0000000000002053.

Foster, Jessica, Crystal Griffin, Jo Lynne Rokita, Allison Stern, Cameron Brimley, Komal S Rathi, Maria Lane, et al. 2021. “Development of GPC2-Directed Chimeric Antigen Receptors Using MRNA for Pediatric Brain Tumors.” 10 (9): e004450. https://doi.org/10.1101/2021.07.06.451385.

Fukuda, Ichiki, Seibu Mochizuki, and Kazuo Sakurai. 2015. “Macrophage-Targeting Gene Delivery Using a Micelle Composed of Mannose-Modified Lipid With Triazole Ring and Dioleoyl Trimethylammonium Propane.” *Biomed Research International*. 2015: 350580 https://doi.org/10.1155/2015/350580.

Gallie, D R. 1991. “The Cap and Poly(A) Tail Function Synergistically to Regulate MRNA Translational Efficiency.” *Genes & Development* 5 (11): 2108–16. https://doi.org/10.1101/gad.5.11.2108.

Geall, Andrew J, Christian W Mandl, and Jeffrey B Ulmer. 2013. “RNA: The New Revolution in Nucleic Acid Vaccines.” *Seminars in Immunology* 25 (2): 152–59. https://doi.org/10.1016/j.smim.2013.05.001.

Gosecki, Mateusz, Mariusz Gadzinowski, Monika Gosecka, Teresa Basinska, and Stanislaw Slomkowski. 2016. “Polyglycidol, Its Derivatives, and Polyglycidol-Containing Copolymers-Synthesis and Medical Applications.” *Polymers* 8 (6): 1–25. https://doi.org/10.3390/polym8060227.

Havel, Jonathan J, Diego Chowell, and Timothy A Chan. 2019. “The Evolving Landscape of Biomarkers for Checkpoint Inhibitor Immunotherapy.” *Nature Reviews Cancer*. 19 (3): 133-150. https://doi.org/10.1038/s41568-019-0116-x.

Hawley, A. E., S. S. Davis, and L. Illum. 1995. “Targeting of Colloids to Lymph Nodes: Influence of Lymphatic Physiology and Colloidal Characteristics.” *Advanced Drug Delivery Reviews* 17 (1): 129–48. https://doi.org/10.1016/0169-409X(95)00045-9.

Henze, Anne-Theres, and Massimiliano Mazzone. 2016. “The Impact of Hypoxia on Tumor-Associated Macrophages.” *The Journal of Clinical Investigation* 126 (10): 3672–79. https://doi.org/10.1172/JCI84427.

Houseley, Jonathan, and David Tollervey. 2009. “The Many Pathways of RNA Degradation.”

*Cell* 136 (4): 763–76. https://doi.org/10.1016/j.cell.2009.01.019.

Hu, Jianfei, Zuwei Wang, Cheng-yu Liao, Zhiwen Chen, Feng-ping Kang, Cai-feng Lin, Tian-Sheng Lin, Long Huang, Yuan Tian, and Shi Chen. 2022. "Induced Expression of CCL19 Promotes the Anti-Tumor Ability of CAR-T Cells by Increasing Their Infiltration Ability." *Frontiers in Immunology*. 13: 958960 https://doi.org/10.3389/fimmu.2022.958960.

Jalkanen, Aimee L., Stephen J. Coleman, and Jeffrey Wilusz. 2014. "Determinants and Implications of MRNA Poly(A) Tail Size - Does This Protein Make My Tail Look Big?" *Seminars in Cell and Developmental Biology* 34: 24–32. https://doi.org/10.1016/j.semcdb.2014.05.018.

Jarak, Ivana, Miguel Pereira-Silva, Ana Cláudia Santos, Francisco Veiga, Horacio Cabral, and Ana Figueiras. 2021. "Multifunctional Polymeric Micelle-Based Nucleic Acid Delivery: Current Advances and Future Perspectives." *Applied Materials Today* 25: 101217. https://doi.org/10.1016/j.apmt.2021.101217.

Jemielity, Jacek, Tolvert Fowler, Joanna Zuberek, Janusz Stepinski, Magdalena Lewdorowicz, Anna Niedzwiecka, Ryszard Stolarski, Edward Darzynkiewicz, and Robert E Rhoads. 2003. "Novel 'Anti-Reverse' Cap Analogs with Superior Translational Properties." *RNA (New York, N.Y.)* 9 (9): 1108–22. https://doi.org/10.1261/rna.5430403.

Johnson, Laura A, John Scholler, Takayuki Ohkuri, Akemi Kosaka, Prachi Patel, Shannon E McGettigan, Arben Nace, et al. 2015. "Rational Development and Characterization of Humanized Anti–EGFR Variant III Chimeric Antigen Receptor T Cells for Glioblastoma." *Science Translational Medicine*. 7 (275): 275ra22. https://doi.org/10.1126/scitranslmed.aaa4963.

Kainthan, Rajesh K, Johan Janzen, E J Levin, Dana V Devine, and Donald E Brooks. 2006. "Biocompatibility Testing of Branched and Linear Polyglycidol." *Biomacromolecules*. 7

(3): 703-9. https://doi.org/10.1021/bm0504882.

Kamel, Yasser Mostafa. 2021. “CAR-T Therapy, the End of a Chapter or the Beginning of a New One?” *Cancers*. 13 (4): 853. https://doi.org/10.3390/cancers13040853.

Kanapathipillai, Mathumai, Amy Brock, and Donald E. Ingber. 2014. “Nanoparticle Targeting of Anti-Cancer Drugs That Alter Intracellular Signaling or Influence the Tumor Microenvironment.” *Advanced Drug Delivery Reviews* 79: 107–18. https://doi.org/10.1016/j.addr.2014.05.005.

Kargaard, Anna, Joost P G Sluijter, and Bert Klumperman. 2019. “Polymeric SiRNA Gene Delivery - Transfection Efficiency versus Cytotoxicity.” *Journal of Controlled Release : Official Journal of the Controlled Release Society* 316 (December): 263–91. https://doi.org/10.1016/j.jconrel.2019.10.046.

Karikó, Katalin, Hiromi Muramatsu, János Ludwig, and Drew Weissman. 2011. “Generating the Optimal MRNA for Therapy: HPLC Purification Eliminates Immune Activation and Improves Translation of Nucleoside-Modified, Protein-Encoding MRNA.” *Nucleic Acids Research* 39 (21): e142. https://doi.org/10.1093/nar/gkr695.

Kataoka, Kazunori, Atsushi Harada, and Yukio Nagasaki. 2001. “Block Copolymer Micelles for Drug Delivery: Design, Characterization and Biological Significance.” *Advanced Drug Delivery Reviews* 47: 113–31. https://doi.org/10.1016/j.addr.2012.09.013.

Khaleghpour, K, Y V Svitkin, A W Craig, C T DeMaria, R C Deo, S K Burley, and N Sonenberg. 2001. “Translational Repression by a Novel Partner of Human Poly(A) Binding Protein, Paip2.” *Molecular Cell* 7 (1): 205–16. https://doi.org/10.1016/s1097-2765(01)00168-x.

Klichinsky, Michael, Marco Ruella, Olga Shestova, Saad S Kenderian, Miriam Y Kim, Roddy O’Connor, John Scholler, Carl June, and Saar Gill. 2017. “Abstract 4575: Chimeric

Antigen Receptor Macrophages (CARMA) for Adoptive Cellular Immunotherapy of Solid Tumors." *Cancer Research* 77 (13_Supplement): 4575. https://doi.org/10.1158/1538-7445.AM2017-4575.

Kochenderfer, James N, Mark E Dudley, Sadik H Kassim, Robert Somerville, Robert O Carpenter, Maryalice Stetler-Stevenson, James Chih-Hsin Yang, et al. 2015. "Chemotherapy-Refractory Diffuse Large B-Cell Lymphoma and Indolent B-Cell Malignancies Can Be Effectively Treated With Autologous T Cells Expressing an Anti-Cd19 Chimeric Antigen Receptor." *Journal of Clinical Oncology*. 33 (6): 540-9. https://doi.org/10.1200/jco.2014.56.2025.

Kochenderfer, James N, Wyndham H Wilson, John E Janik, Mark E Dudley, Maryalice Stetler-Stevenson, Steven A Feldman, Irina Maric, et al. 2010. "Eradication of B-Lineage Cells and Regression of Lymphoma in a Patient Treated with Autologous T Cells Genetically Engineered to Recognize CD19." *Blood* 116 (20): 4099–4102. https://doi.org/10.1182/blood-2010-04-281931.

Kohli, Karan, Venu G. Pillarisetty, and Teresa S. Kim. 2022. "Key Chemokines Direct Migration of Immune Cells in Solid Tumors." *Cancer Gene Therapy* 29 (1): 10–21. https://doi.org/10.1038/s41417-021-00303-x.

Kongkatigumjorn, Nachnicha, Samuel A Smith, Moore Chen, Katie Fang, Shenglin Yang, Elizabeth R Gillies, Angus P R Johnston, and Georgina K Such. 2018. "Controlling Endosomal Escape Using PH-Responsive Nanoparticles with Tunable Disassembly." *ACS Applied Nano Materials* 1 (7): 3164–73. https://doi.org/10.1021/acsanm.8b00338.

Kryczek, Ilona, Shuang Wei, Evan T Keller, Rebecca Liu, and Weiping Zou. 2007. "Stroma-Derived Factor (SDF-1/CXCL12) and Human Tumor Pathogenesis." *Ajp Cell Physiology* 292 (3): C987-95. https://doi.org/10.1152/ajpcell.00406.2006.

Ladányi, Andrea. 2015. “Prognostic and Predictive Significance of Immune Cells Infiltrating Cutaneous Melanoma.” *Pigment Cell and Melanoma Research* 28 (5): 490–500. https://doi.org/10.1111/pcmr.12371.

Lane, Kirk B, Brian Egan, Sherell Vick, Rasul Abdolrasulnia, and Virginia L Shepherd. 1998. “Characterization of a Rat Alveolar Macrophage Cell Line That Expresses a Functional Mannose Receptor.” *Journal of Leukocyte Biology* 64 (3): 345-50. https://doi.org/10.1002/jlb.64.3.345.

Lang, Jiayan, Xiao Zhao, Yingqiu Qi, Yinlong Zhang, Xuexiang Han, Yanping Ding, Jiajing Guan, Tianjiao Ji, Ying Zhao, and Guangjun Nie. 2019. “Reshaping Prostate Tumor Microenvironment to Suppress Metastasis via Cancer-Associated Fibroblast Inactivation With Peptide-Assembly-Based Nanosystem.” *Acs Nano* 13 (11): 12357-12371. https://doi.org/10.1021/acsnano.9b04857.

Levine, Bruce L, James Miskin, Keith Wonnacott, and Christopher Keir. 2017. “Global Manufacturing of CAR T Cell Therapy.” *Molecular Therapy - Methods & Clinical Development* 4: 92–101. https://doi.org/https://doi.org/10.1016/j.omtm.2016.12.006.

Li, Hong Jun, Zejun Wang, Edikan Archibong, Qing Wu, Guojun Chen, Quanyin Hu, Tianyuan Ci, et al. 2021. “Scattered Seeding of CAR T Cells in Solid Tumors Augments Anticancer Efficacy.” *National Science Review* 9 (3): nwab172. https://doi.org/10.1093/nsr/nwab172.

Li, Mengjun, Linye He, Jing Zhu, Peng Zhang, and Shufang Liang. 2022. “Targeting Tumor-Associated Macrophages for Cancer Treatment.” *Cell and Bioscience* 12 (1): 1–13. https://doi.org/10.1186/s13578-022-00823-5.

Lima, Sarah Azoubel, Laura B. Chipman, Angela L. Nicholson, Ying Hsin Chen, Brian A. Yee, Gene W. Yeo, Jeff Coller, and Amy E. Pasquinelli. 2017. “Short Poly(A) Tails Are a Conserved Feature of Highly Expressed Genes.” *Nature Structural and Molecular*

*Biology* 24 (12): 1057–63. https://doi.org/10.1038/nsmb.3499.

Loomis, Kristin, Kevin E Lindsay, Chiara Zurla, Sushma M Bhosle, Daryll Vanover, Emmeline L Blanchard, Jonathan L Kirschman, Ravi V Bellamkonda, and Philip J Santangelo. 2018. "in Vitro Transcribed MRNA Vaccines With Programmable Stimulation of Innate Immunity." *Bioconjugate Chemistry* 29 (9): 3072-3083. https://doi.org/10.1021/acs.bioconjchem.8b00443.

Lovejoy, Alexander F, Daniel P Riordan, and Patrick O Brown. 2014. "Transcriptome-Wide Mapping of Pseudouridines: Pseudouridine Synthases Modify Specific MRNAs in S. Cerevisiae." *PloS One* 9 (10): e110799. https://doi.org/10.1371/journal.pone.0110799.

Maalej, Karama Makni, Maysaloun Merhi, Varghese Inchakalody, S Mestiri, Majid Alam, Cristina Maccalli, Honar Cherif, et al. 2023. "CAR-Cell Therapy in the Era of Solid Tumor Treatment: Current Challenges and Emerging Therapeutic Advances." *Molecular Cancer* 22 (1): 20. https://doi.org/10.1186/s12943-023-01723-z.

Majzner, Robbie G., Skyler P. Rietberg, Elena Sotillo, Rui Dong, Vipul T. Vachharajani, Louai Labanieh, June H. Myklebust, et al. 2020. "Tuning the Antigen Density Requirement for Car T-Cell Activity." *Cancer Discovery* 10 (5): 702–23. https://doi.org/10.1158/2159-8290.CD-19-0945.

Mehrabadi, Ali Zarezadeh, Reza Ranjbar, Mahdieh Farzanehpour, Alireza Shahriary, Ruhollah Dorostkar, Mohammad Ali Hamidinejad, and Hadi Esmaeili Gouvarchin Ghaleh. 2022. "Therapeutic Potential of CAR T Cell in Malignancies: A Scoping Review." *Biomedicine and Pharmacotherapy* 146: 112512. https://doi.org/10.1016/j.biopha.2021.112512.

Mi, Peng, Horacio Cabral, and Kazunori Kataoka. 2020a. "Ligand-Installed Nanocarriers toward Precision Therapy." *Advanced Materials* 32 (13): 1–29. https://doi.org/10.1002/adma.201902604.

———. 2020b. “Ligand-Installed Nanocarriers toward Precision Therapy.” *Advanced Materials* 32 (13): 1902604. https://doi.org/https://doi.org/10.1002/adma.201902604.

Mixich, Lucas, Eger Boonstra, Keita Masuda, Shang-Wei Li, Yuki Nakashima, Fanlu Meng, Momoko Sakata, Tatsuro Goda, Satoshi Uchida, and Horacio Cabral. 2024. “Ionizable Polymeric Micelles with Phenylalanine Moieties Enhance Intracellular Delivery of Self-Replicating RNA for Long-Lasting Protein Expression In Vivo.” *Biomacromolecules*, January. https://doi.org/10.1021/acs.biomac.3c01102.

Miyazaki, Takuya, Satoshi Uchida, Satoru Nagatoishi, Kyoko Koji, Taehun Hong, Shigeto Fukushima, Kouhei Tsumoto, Kazuhiko Ishihara, Kazunori Kataoka, and Horacio Cabral. 2020. “Polymeric Nanocarriers with Controlled Chain Flexibility Boost MRNA Delivery In Vivo through Enhanced Structural Fastening.” *Advanced Healthcare Materials* 9 (16): 2000538. https://doi.org/https://doi.org/10.1002/adhm.202000538.

Moffett, H. F., M. E. Coon, S. Radtke, S. B. Stephan, L. McKnight, A. Lambert, B. L. Stoddard, H. P. Kiem, and M. T. Stephan. 2017. “Hit-and-Run Programming of Therapeutic Cytoreagents Using MRNA Nanocarriers.” *Nature Communications* 8 (1): 389. https://doi.org/10.1038/s41467-017-00505-8.

Morais, Pedro, Hironori Adachi, and Yi-Tao Yu. 2021a. “The Critical Contribution of Pseudouridine to MRNA COVID-19 Vaccines.” *Frontiers in Cell and Developmental Biology* 9: 789427. https://doi.org/10.3389/fcell.2021.789427.

Morais, Pedro, Hironori Adachi, and Yi Tao Yu. 2021b. “The Critical Contribution of Pseudouridine to MRNA COVID-19 Vaccines.” *Frontiers in Cell and Developmental Biology* 9 (November): 1–9. https://doi.org/10.3389/fcell.2021.789427.

Morrissey, Meghan A, Adam P Williamson, Adriana M Steinbach, Edward W Roberts, Nadja Kern, Mark B Headley, and Ronald D Vale. 2018. “Chimeric Antigen Receptors That

Trigger Phagocytosis." *ELife* 7 (June): e36688. https://doi.org/10.7554/eLife.36688.

Müller, Nadja, Susanne Michen, Stefanie Tietze, Katrin Töpfer, Alexander Schulte, Katrin Lamszus, Marc Schmitz, Gabriele Schackert, Ira Pastan, and Achim Temme. 2015. "Engineering NK Cells Modified With an EGFRvIII-Specific Chimeric Antigen Receptor to Overexpress CXCR4 Improves Immunotherapy of CXCL12/SDF-1α-Secreting Glioblastoma." *Journal of Immunotherapy (Hagerstown, Md. : 1997)* 38 (5): 197–210. https://doi.org/10.1097/CJI.0000000000000082.

Murad, John P, Dileshni Tilakawardane, Anthony K Park, Lupita S Lopez, Cari A Young, Jackson Gibson, Yukiko Yamaguchi, et al. 2021. "Pre-Conditioning Modifies the TME to Enhance Solid Tumor CAR T Cell Efficacy and Endogenous Protective Immunity." *Molecular Therapy* 29 (7): 2335-2349. https://doi.org/10.1016/j.ymthe.2021.02.024.

Murdoch, Craig, Athina Giannoudis, and Claire E Lewis. 2004. "Mechanisms Regulating the Recruitment of Macrophages into Hypoxic Areas of Tumors and Other Ischemic Tissues." *Blood* 104 (8): 2224–34. https://doi.org/10.1182/blood-2004-03-1109.

Nagarsheth, Nisha, Max S Wicha, and Weiping Zou. 2017. "Chemokines in the Cancer Microenvironment and Their Relevance in Cancer Immunotherapy." *Nature Reviews Immunology* 17 (9): 559-572. https://doi.org/10.1038/nri.2017.49.

Nance, Kellie D, and Jordan L Meier. 2021. "Modifications in an Emergency: The Role of N1-Methylpseudouridine in COVID-19 Vaccines." *ACS Central Science* 7 (5): 748–56. https://doi.org/10.1021/acscentsci.1c00197.

Ndeupen, Sonia, Zhen Qin, Sonya Jacobsen, Aurélie Bouteau, Henri Estanbouli, and Botond Z. Igyártó. 2021. "The MRNA-LNP Platform's Lipid Nanoparticle Component Used in Preclinical Vaccine Studies Is Highly Inflammatory." *IScience* 24 (12): 103479 . https://doi.org/10.1016/j.isci.2021.103479.

Ni, Jiahong, Suddham Singh, and Lai-Xi Wang. 2002. “Synthesis of Maleimide-Activated Carbohydrates as Chemoselective Tags for Site-Specific Glycosylation of Peptides and Proteins.” *Bioconjugate Chemistry* 4 (1): 232-8. https://doi.org/10.1021/bc025617f.

Ohtani, Yumi, Kayleigh C Ross, Aditya Dandekar, Rashid Gabbasov, and Michael Klichinsky. 2020. “128 Development of an M1-Polarized, Non-Viral Chimeric Antigen Receptor Macrophage (CAR-M) Platform for Cancer Immunotherapy.” *Journal for ImmunoTherapy of Cancer* 8 (3): A141-A141 https://doi.org/10.1136/jitc-2020-sitc2020.0128.

Oussoren, C., J. Zuidema, D. J.A. Crommelin, and G. Storm. 1997. “Lymphatic Uptake and Biodistribution of Liposomes after Subcutaneous Injection. II. Influence of Liposomal Size, Lipid Composition and Lipid Dose.” *Biochimica et Biophysica Acta - Biomembranes* 1328 (2): 261–72. https://doi.org/10.1016/S0005-2736(97)00122-3.

Oussoren, Christien, and Gert Storm. 2001. “Liposomes to Target the Lymphatics by Subcutaneous Administration.” *Advanced Drug Delivery Reviews* 50 (1–2): 143–56. https://doi.org/10.1016/S0169-409X(01)00154-5.

Oyewumi, Moses O, Robert A Yokel, Michael Jay, Tricia Coakley, and Russell J Mumper. 2004. “Comparison of Cell Uptake, Biodistribution and Tumor Retention of Folate-Coated and PEG-Coated Gadolinium Nanoparticles in Tumor-Bearing Mice.” *Journal of Controlled Release : Official Journal of the Controlled Release Society* 95 (3): 613–26. https://doi.org/10.1016/j.jconrel.2004.01.002.

Pan, Kevin, Hizra Farrukh, Veera Chandra Sekhar Reddy Chittepu, Huihong Xu, Chong xian Pan, and Zheng Zhu. 2022. “CAR Race to Cancer Immunotherapy: From CAR T, CAR NK to CAR Macrophage Therapy.” *Journal of Experimental and Clinical Cancer Research* 41 (1): 1–21. https://doi.org/10.1186/s13046-022-02327-z.

Parayath, N N, S B Stephan, A L Koehne, P S Nelson, and M T Stephan. 2020. “In Vitro-Transcribed Antigen Receptor MRNA Nanocarriers for Transient Expression in Circulating T Cells in Vivo.” *Nature Communications* 11 (1): 6080. https://doi.org/10.1038/s41467-020-19486-2.

Parayath, Neha N., and Matthias T. Stephan. 2021. “In Situ Programming of CAR T Cells.” *Annual Review of Biomedical Engineering* 23: 385–405. https://doi.org/10.1146/annurev-bioeng-070620-033348.

Pascolo, Steve. 2004. “Messenger RNA-Based Vaccines.” *Expert Opinion on Biological Therapy* 4 (8): 1285–94. https://doi.org/10.1517/14712598.4.8.1285.

Peng, Zheng-Hong, Vivek Sharma, Scott F Singleton, and Paul D Gershon. 2002. “Synthesis and Application of a Chain-Terminating Dinucleotide MRNA Cap Analog.” *Organic Letters* 4 (2): 161–64. https://doi.org/10.1021/ol0167715.

Rajan, Thangavelu Soundara, Placido Bramanti, and Emanuela Mazzon. 2020. “In Vitro-Transcribed MRNA Chimeric Antigen Receptor T Cell (IVT MRNA CAR T) Therapy in Hematologic and Solid Tumor Management: A Preclinical Update.” *International Journal of Molecular Sciences* 21 (18): 6514. https://doi.org/10.3390/ijms21186514.

Rehman, Zia ur, Inge S Zuhorn, and Dick Hoekstra. 2013. “How Cationic Lipids Transfer Nucleic Acids into Cells and across Cellular Membranes: Recent Advances.” *Journal of Controlled Release : Official Journal of the Controlled Release Society* 166 (1): 46–56. https://doi.org/10.1016/j.jconrel.2012.12.014.

Richter, Wolfgang F., Suraj G. Bhansali, and Marilyn E. Morris. 2012. “Mechanistic Determinants of Biotherapeutics Absorption Following SC Administration.” *AAPS Journal* 14 (3): 559–70. https://doi.org/10.1208/s12248-012-9367-0.

Riley, Rachel, Carl H June, Robert Langer, and Michael J Mitchell. 2019. “Delivery

Technologies for Cancer Immunotherapy." *Nature Reviews Cancer* 18 (3): 175-196. https://doi.org/10.1038/s41573-018-0006-z.

Rosenberg, Steven A, and Nicholas P Restifo. 2015. "Adoptive Cell Transfer as Personalized Immunotherapy for Human Cancer." *Science (New York, N.Y.)* 348 (6230): 62–68. https://doi.org/10.1126/science.aaa4967.

Rui, Yuan, David R. Wilson, Stephany Y. Tzeng, Hannah M. Yamagata, Deepti Sudhakar, Marranne Conge, Cynthia A. Berlinicke, Donald J. Zack, Anthony Tuesca, and Jordan J. Green. 2022. "High-Throughput and High-Content Bioassay Enables Tuning of Polyester Nanoparticles for Cellular Uptake, Endosomal Escape, and Systemic in Vivo Delivery of MRNA." *Science Advances* 8 (1): eabk2855. https://doi.org/10.1126/sciadv.abk2855.

Rurik, Joel G, István Tombácz, Amir Yadegari, Pedro O Méndez Fernández, Swapnil V Shewale, Li Li, Toru Kimura, et al. 2022. "CAR T Cells Produced in Vivo to Treat Cardiac Injury." *Science (New York, N.Y.)* 375 (6576): 91–96. https://doi.org/10.1126/science.abm0594.

Schmaljohann, Dirk. 2006. "Thermo- and PH-Responsive Polymers in Drug Delivery." *Advanced Drug Delivery Reviews* 58 (15): 1655–70. https://doi.org/https://doi.org/10.1016/j.addr.2006.09.020.

Schulz, Olga, Swantje I. Hammerschmidt, G. Leandros Moschovakis, and Reinhold Förster. 2016. "Chemokines and Chemokine Receptors in Lymphoid Tissue Dynamics." *Annual Review of Immunology* 34: 203–42. https://doi.org/10.1146/annurev-immunol-041015-055649.

Schwartz, Schraga, Douglas A Bernstein, Maxwell R Mumbach, Marko Jovanovic, Rebecca H Herbst, Brian X León-Ricardo, Jesse M Engreitz, et al. 2014. "Transcriptome-Wide Mapping Reveals Widespread Dynamic-Regulated Pseudouridylation of NcRNA and

MRNA.” *Cell* 159 (1): 148–62. https://doi.org/10.1016/j.cell.2014.08.028.

Shi, Tao, Yanyu Ma, Lingfeng Yu, Jiaxuan Jiang, Shihao Shen, Yinglong Hou, and Tingting Wang. 2018. “Cancer Immunotherapy: A Focus on the Regulation of Immune Checkpoints.” *International Journal of Molecular Sciences* 19 (5): 1389. https://doi.org/10.3390/ijms19051389.

Shima, Fumiaki, Takami Akagi, and Mitsuru Akashi. 2014. “Synthesis and Preparation of Nanoparticles Composed of Amphiphilic Poly(γ-Glutamic Acid) with Different Hydrophobic Side Chains and Their Potential of Membrane Disruptive Activity.” *Colloid and Polymer Science* 292 (10): 2663–71. https://doi.org/10.1007/s00396-014-3303-z.

Shinchi, Hiroyuki, Masaharu Yuki, Takayoshi Yamauchi, Mayumi Niimura, Masahiro Wakao, Howard B Cottam, Tomoko Hayashi, Dennis A Carson, Toshiro Moroishi, and Yasuo Suda. 2021. “Glyco-Nanoadjuvants: Sugar Structures on Carriers of a Small Molecule TLR7 Ligand Affect Their Immunostimulatory Activities.” *Acs Applied Bio Materials* 4 (3): 2732-2741. https://doi.org/10.1021/acsabm.0c01639.

Sivasakthi, V., Anand Anbarasu, and Sudha Ramaiah. 2013. “π-π Interactions in Structural Stability: Role in RNA Binding Proteins.” *Cell Biochemistry and Biophysics* 67 (3): 853–63. https://doi.org/10.1007/s12013-013-9573-0.

Smith, Samuel A., Laura I. Selby, Angus P.R. Johnston, and Georgina K. Such. 2019. “The Endosomal Escape of Nanoparticles: Toward More Efficient Cellular Delivery.” *Bioconjugate Chemistry* 30 (2): 263–72. https://doi.org/10.1021/acs.bioconjchem.8b00732.

Srivastava, Shivani, and Stanley R Riddell. 2015. “Engineering CAR-T Cells: Design Concepts.” *Trends in Immunology* 36 (8): 494–502. https://doi.org/10.1016/j.it.2015.06.004.

Sterner, Robert C, and Rosalie M Sterner. 2021. “CAR-T Cell Therapy: Current Limitations and Potential Strategies.” *Blood Cancer Journal* 11 (4): 69. https://doi.org/10.1038/s41408-021-00459-7.

Tchou, Julia, Yangbing Zhao, Bruce L Levine, Paul J Zhang, Megan M Davis, J Joseph Melenhorst, Irina Kulikovskaya, et al. 2017. “Safety and Efficacy of Intratumoral Injections of Chimeric Antigen Receptor (CAR) T Cells in Metastatic Breast Cancer.” *Cancer Immunology Research* 5 (12): 1152-1161. https://doi.org/10.1158/2326-6066.cir-17-0189.

Thalla, Maharshi, Jagadeeshkumar Gangasani, Pritam Saha, Srikanth Ponneganti, Roshan M Borkar, V G M Naidu, U S N Murty, and Subham Banerjee. 2020. “Synthesis, Characterizations, and Use of O-Stearoyl Mannose Ligand-Engineered Lipid Nanoarchitectonics for Alveolar Macrophage Targeting.” *Assay and Drug Development Technologies* 18 (6): 249-260. https://doi.org/10.1089/adt.2020.999.

Thomas, Anja, Sophie S Müller, and Holger Frey. 2014. “Beyond Poly(Ethylene Glycol): Linear Polyglycerol as a Multifunctional Polyether for Biomedical and Pharmaceutical Applications.” *Biomacromolecules* 15 (6): 1935-54. https://doi.org/10.1021/bm5002608.

Uchida, Satoshi, Keiji Itaka, Hirokuni Uchida, Kentaro Hayakawa, Toru Ogata, Takehiko Ishii, Shigeto Fukushima, Kensuke Osada, and Kazunori Kataoka. 2013. “In Vivo Messenger RNA Introduction into the Central Nervous System Using Polyplex Nanomicelle.” *PLOS ONE* 8 (2): e56220. https://doi.org/10.1371/journal.pone.0056220.

Umoja Biopharma. n.d. “Umoja Biopharma Presents New Preclinical Data on Its Integrated In Vivo CAR T and Engineered Induced Pluripotent Stem Cell Platform Technologies at the Society for Immunotherapy of Cancer(SITC) 37th Annual Meeting. Press Release, Nov. 10, 2022.”

Varkouhi, Amir K, Marije Scholte, Gert Storm, and Hidde J Haisma. 2011. “Endosomal Escape Pathways for Delivery of Biologicals.” *Journal of Controlled Release : Official Journal of the Controlled Release ¥ Society* 151 (3): 220–28. https://doi.org/10.1016/j.jconrel.2010.11.004.

Velmurugan, Ramraj, Dilip K. Challa, Sripad Ram, Raimund J. Ober, and E. Sally Ward. 2016. “Macrophage-Mediated Trogocytosis Leads to Death of Antibody-Opsonized Tumor Cells.” *Molecular Cancer Therapeutics* 15 (8): 1879–89. https://doi.org/10.1158/1535-7163.MCT-15-0335.

Vilgelm, Anna E, and Ann Richmond. 2019. “Chemokines Modulate Immune Surveillance in Tumorigenesis, Metastasis, and Response to Immunotherapy.” *Frontiers in Immunology* 10: 333. https://doi.org/10.3389/fimmu.2019.00333.

Wang, Chang, Siyu Wang, Diana D. Kang, and Yizhou Dong. 2023. “Biomaterials for in Situ Cell Therapy.” *BMEMat* 1 (3): 1–14. https://doi.org/10.1002/bmm2.12039.

Wang, Tao, Leon M Larcher, Lixia Ma, and Rakesh N Veedu. 2018. “Systematic Screening of Commonly Used Commercial Transfection Reagents towards Efficient Transfection of Single-Stranded Oligonucleotides.” *Molecules (Basel, Switzerland)* 23 (10): 2564. https://doi.org/10.3390/molecules23102564.

Weill, Laure, Eulàlia Belloc, Felice Alessio Bava, and Raúl Méndez. 2012. “Translational Control by Changes in Poly(A) Tail Length: Recycling MRNAs.” *Nature Structural and Molecular Biology* 19 (6): 577–85. https://doi.org/10.1038/nsmb.2311.

Weinkove, Robert, P J M George, Nathaniel Dasyam, and Alexander D McLellan. 2019. “Selecting Costimulatory Domains for Chimeric Antigen Receptors: Functional and Clinical Considerations.” *Clinical & Translational Immunology* 8 (5): e1049. https://doi.org/10.1002/cti2.1049.

Weissman, Drew, Norbert Pardi, Hiro Muramatsu, and Katalin Karikó. 2013. “HPLC Purification of in Vitro Transcribed Long RNA.” *Methods in Molecular Biology (Clifton, N.J.)* 969: 43–54. https://doi.org/10.1007/978-1-62703-260-5_3.

White, Karen L, Thomas Rades, Richard H Furneaux, Peter C Tyler, and Sarah Hook. 2006. “Mannosylated Liposomes as Antigen Delivery Vehicles for Targeting to Dendritic Cells.” *Journal of Pharmacy and Pharmacology* 58 (6): 729-37. https://doi.org/10.1211/jpp.58.6.0003.

Wilson, Katie A., Devany J. Holland, and Stacey D. Wetmore. 2016. “Topology of RNA-Protein Nucleobase-Amino Acid π-π Interactions and Comparison to Analogous DNA-Protein π-π Contacts.” *Rna* 22 (5): 696–708. https://doi.org/10.1261/rna.054924.115.

Wilson, Katie A., Ryan W. Kung, Simmone D’Souza, and Stacey D. Wetmore. 2021. “Anatomy of Noncovalent Interactions between the Nucleobases or Ribose and π-Containing Amino Acids in RNA-Protein Complexes.” *Nucleic Acids Research* 49 (4): 2213–25. https://doi.org/10.1093/nar/gkab008.

Wolf, Hans, Yvonne Müller, Sibylle Salmen, Wolfgang Wilmanns, and Gundram Jung. 1994. “Induction of Anergy in Resting Human T Lymphocytes by Immobilized Anti-CD3 Antibodies.” *European Journal of Immunology* 24 (6): 1410-7. https://doi.org/10.1002/eji.1830240626.

Yang, Wenqian, Lucas Mixich, Eger Boonstra, and Horacio Cabral. 2023. “Polymer-Based MRNA Delivery Strategies for Advanced Therapies.” *Advanced Healthcare Materials* 12 (15): e2202688. https://doi.org/10.1002/adhm.202202688.

Yang, Wenqian, Takuya Miyazaki, Yasuhiro Nakagawa, Eger Boonstra, Keita Masuda, Yuki Nakashima, Pengwen Chen, et al. 2023. “Block Catiomers with Flanking Hydrolyzable Tyrosinate Groups Enhance in Vivo MRNA Delivery via π–π Stacking-Assisted Micellar

Assembly." *Science and Technology of Advanced Materials* 24 (1): 2170164. https://doi.org/10.1080/14686996.2023.2170164.

Yip, Amy, and Rachel M Webster. 2018. "The Market for Chimeric Antigen Receptor T Cell Therapies." *Nature Reviews. Drug Discovery* 17 (3): 161-162. https://doi.org/10.1038/nrd.2017.266.

Yu, Shengnan, Ming Yi, Shuang Qin, and Kongming Wu. 2019. "Next Generation Chimeric Antigen Receptor T Cells: Safety Strategies to Overcome Toxicity." *Molecular Cancer* 18 (1): 125. https://doi.org/10.1186/s12943-019-1057-4.

Yuan, Mujie, Zeyu Han, Yan Liang, Yong Sun, Bin He, Wantao Chen, and Fan Li. 2023. "MRNA Nanodelivery Systems: Targeting Strategies and Administration Routes." *Biomaterials Research* 27 (1): 90. https://doi.org/10.1186/s40824-023-00425-3.

Zhang, Li, Lin Tian, Xiaoyang Dai, Hua Yu, Jiajia Wang, Anhua Lei, Mengmeng Zhu, et al. 2020. "Pluripotent Stem Cell-Derived CAR-Macrophage Cells with Antigen-Dependent Anti-Cancer Cell Functions." *Journal of Hematology & Oncology* 13 (1): 153. https://doi.org/10.1186/s13045-020-00983-2.

Zhao, Yangbing, Edmund K Moon, Carmine Carpenito, Chrystal M Paulos, Xiaojun Liu, Andrea Brennan, Anne Chew, et al. 2010. "Multiple Injections of Electroporated Autologous T Cells Expressing a Chimeric Antigen Receptor Mediate Regression of Human Disseminated Tumor." *Cancer Research* 70 (22): 9053-61. https://doi.org/10.1158/0008-5472.can-10-2880.

Zhao, Zhongwei, Weiqian Chen, Wen J Weng, Jingjing Shen, and Jiansong Ji. 2019. "Delivery Strategies of Cancer Immunotherapy: Recent Advances and Future Perspectives." *Journal of Hematology & Oncology* 12 (1): 126. https://doi.org/10.1186/s13045-019-0817-3.

Zhou, Zhuxian, Xiangrui Liu, Dingcheng Zhu, Yue Wang, Zhen Zhang, Xuefei Zhou, Nasha

Qiu, Xuesi Chen, and Youqing Shen. 2017. “Nonviral Cancer Gene Therapy: Delivery Cascade and Vector Nanoproperty Integration.” *Advanced Drug Delivery Reviews* 115 (June): 115–54. https://doi.org/10.1016/j.addr.2017.07.021.